NOLTR 64-99

CHARACTERISTICS OF THE TURBULENT BOUNDARY LAYER WITH HEAT AND MASS TRANSFER AT M=6.7

19 OCTOBER 1964

NOL

UNITED STATES NAVAL ORDNANCE LABORATORY, WHITE OAK, MARYLAND

NOLTR 64-99

NOLTR 64-99

Aerodynamics Research Report No. 228

CHARACTERISTICS OF THE TURBULENT BOUNDARY LAYER WITH HEAT AND MASS TRANSFER AT M=6.7

by
James E. Danberg

ABSTRACT: Transpiration from a porous surface into a turbulent boundary layer is a possible technique for protecting aerodynamic surfaces from the severe heating rates associated with hypersonic speeds. The effects of air transpiration and wall temperature on skin friction drag, heat transfer, and other pertinent boundary layer characteristics were determined from measurements on a porous flat plate in the U. S. Naval Ordnance Laboratory's Hypersonic Wind Tunnel No. 4 at a Mach number of 6.7.

The effects of heat and mass transfer on the distribution of Mach number, static and total temperature, and velocity were measured, from which various boundary layer parameters were determined such as: skin friction coefficient; Stanton number; total, momentum, displacement, and energy boundary layer thicknesses. Lowering the wall temperature decreased the total and displacement thicknesses and increased the momentum and energy

U. S. NAVAL ORDNANCE LABORATORY
WHITE OAK, MARYLAND

thicknesses. All the boundary layer thicknesses increased approximately linearly with increasing injection rate.

Velocity distributions in the fully turbulent layer are adequately described by a Prandtl mixing length analysis in which the velocity profile is transformed into a form similar to the semi-logarithmic profile of incompressible flow. Unlike incompressible flow, the constant of integration of the mixing length velocity profile is found to increase with heat transfer rate and decrease with increasing mass transfer rate. These effects are related to changes in the laminar sublayer thickness.

A modified Crocco equation adequately describes the relationship between the temperature and velocity distributions. Based on these semi-empirical equations, the skin friction was numerically calculated as a function of momentum thickness Reynolds number, and the results agreed with the measurements. The skin friction calculations can be extended to the evaluation of heat transfer through the use of Reynolds' analogy which was experimentally verified with and without air transpiration.

Characteristics of the Turbulent Boundary Layer with Heat and Mass Transfer at M=6.7

This report is based on a thesis of identical title submitted by the author to the Catholic University of America in partial fulfillment of the requirements for the degree of Doctor of Engineering.

The investigation was carried out as part of the Aeroballistics Research Program of the U. S. Naval Ordnance Laboratory and was sponsored by the Bureau of Naval Weapons under Task No. RMGA-42-034/212-1/F009-10-001.

The author is greatly indebted to his faculty advisor Dr. Paul K. Chang for encouragement and stimulating discussions leading to the completion of the research. The dissertation was approved for the Faculty of the School of Engineering by Drs. P. K. Chang, G. D. Boehler, and Eva M. Winkler.

In addition, the author wishes to acknowledge the support and assistance of the staff of the Aeroballistics Department of the

U. S. Naval Ordnance Laboratory, and, in particular, Dr. Eva M. Winkler for her guidance from the very beginning of the research; Mrs. A. P. Jackson who helped obtain and reduce the data; and Mr. F. J. Brown who operated the wind tunnel and prepared the model.

R. E. ODENING
Captain, USN
Commander

K. R. ENKENHUS
By direction

TABLE OF CONTENTS

LIST OF ILLUSTRATIONS

LIST OF TABLES

LIST OF SYMBOLS

A	Area
B	A Constant
C	A Constant
c_f	Skin Friction Coefficient = $\tau_w/\frac{1}{2}\rho_\delta u_\delta^2$
c_p	Specific Heat at Constant Pressure
c_q	Mass Transfer Coefficient = $\rho_w v_w/\rho_\delta u_\delta$
D	A Constant
E	Energy Flux per Unit Area = $-q + u\tau$
K	Permeability of the Porous Material
k	Universal Constant
M	Mach Number
n	Exponent in Power-Law Velocity Relation
p	Pressure
q	Heat Flux per Unit Area
R	Gas Constant
Re_x	Reynolds Number = $\rho_\delta u_\delta x/\mu_\delta$
Re_θ	Reynolds Number = $\rho_\delta u_\delta \theta/\mu_\delta$
r_f	Recovery Factor
St	Stanton Number
T	Temperature
t	Thickness of Porous Material
u	Velocity Component in the x-Direction
u_τ	Shear Velocity = $\sqrt{\tau_w/\rho_w}$
u^+	Nondimensional Velocity = u/u_τ

u^{++}	Transformed Nondimensional Velocity (see equation (42))
v	Velocity Component in y-Direction
w	Mass Flow per Unit Area of Porous Material = $\rho_w v_w$
x	Distance from the Leading Edge of the Plate in the Direction of the Free-Stream Velocity
y	Distance Normal to the Plate Surface
y^+	Nondimensional Distance from the Surface = $u_\tau y/\nu_w$
α	Angle of Flow Deflection Because of Displacement Effect of the Boundary Layer
β	A Parameter = $(T_e - T_w)/(T_{t\delta} - T_w)$
γ	Ratio of Specific Heats
Δ	Distance from the Wall to the Maximum Static Temperature
δ	Total Boundary Layer Thickness
δ_n	Total Boundary Layer Thickness Appropriate to the Power-Law Velocity Relation
δ^*	Displacement Thickness
κ	A Constant
μ	Dynamic Viscosity
ν	Kinematic Viscosity = μ/ρ
Θ	Energy Thickness
θ	Momentum Thickness
ρ	Density
τ	Shear Stress

SUBSCRIPTS

a	Tip Temperature of Equilibrium Temperature Probe
b	Base Temperature of Equilibrium Temperature Probe
c	Conditions on Surface of Cone of the Equilibrium Temperature Probe
e	Adiabatic Wall Temperature
o	Conditions of Zero Mass Transfer
t	stagnation Conditions
u	Conditions on Underside of Porous Material
w	Conditions on Top Surface of Porous Plate
δ	Conditions at Outer Edge of the Boundary Layer
∞	Conditions in the Free-Stream Ahead of Plate Leading Edge Shockwave

SUPERSCRIPTS

$\overline{\quad}$	Average Conditions

INTRODUCTION

This particular study is concerned with the effects of mass and heat transfer on a hypersonic turbulent boundary layer on a flat plate. Information obtained from the present investigation has possible future use in the design of high speed missiles, satellite re-entry vehicles, and rocket nozzle cooling problems because mass transfer cooling provides a method for protecting aerodynamic surfaces from high heating rates. Transpiration will probably be most practical when used to cool relatively small areas of high heating such as control surfaces or in changing the thermal radiative or electromagnetic properties of the boundary layer. In addition, information on the transpiration process will shed light on the heat blocking effects of ablation products. In any case, before such systems can be effectively designed, it is necessary to establish the parameters which govern the phenomenon and the magnitude of these parameters associated with efficient transpiration cooling.

Fundamentally, the purpose of the present research is to provide new experimental data which extends the Mach number range of the available mass transfer data. The ultimate objective is to provide additional evidence from which the analysis and theories can be checked, improved, or on which new analyses can be based.

In approaching this objective, it is the intention to obtain more than the overall or gross effect but also to investigate how the effect is produced in more detail. In this way the more fundamental assumptions inherent in the theories can be examined and suggestions for improvements are then more apparent.

Unfortunately, with the status of today's knowledge, it is not possible to examine the effects of heat and mass transfer on the physical mechanism of turbulence. If the exact solutions of the conservation equations for mass, momentum, and energy could be obtained, boundary layer profiles of velocity and temperature would be the result from which the skin friction and heat transfer would follow directly. At the present time, however, such solutions are not available and analyses are based on generalized velocity and temperature profiles determined from experimental data. These profiles are then used with simplified and integrated momentum and energy equations. The results are formulas of heat transfer and skin friction which are only as good and general as the approximate profiles initially assumed.

The specific objectives of this research are:

1. To obtain new experimental data on both skin friction and heat transfer with and without mass transfer at a Mach number of 6.7 on a flat plate

2. To establish the Reynolds analogy under the above conditions
3. To measure and analyze the velocity and temperature profiles over a range of conditions of mass transfer, heat transfer and Reynolds number

Review of Theory

Since exact solutions of the conservation equations have not yet been found, most analyses are based on an approach first suggested by L. Prandtl. The analysis is called the mixing length theory which is in some ways analogous to the mean-free-path concept of the kinetic theory of gases. Although the mixing length theory has never been fully accepted, it has produced quite general and useful results. However, before discussing the mixing length theory some alternate theories will be mentioned.

A method for predicting mass-, momentum-, and energy-, transfer rates has been developed by Knuth[1] in which a semi-empirical skin-friction coefficient Reynolds number relation for a fluid of constant properties is derived. The effects of mass transfer are included in this constant property solution. Compressibility, heat transfer, and composition of the injected gas are accounted for by evaluating the constant property equations at a reference temperature and a reference composition derived from laminar flow results.

A similar empirical method has been suggested by Spalding[2] in which a functional relationship between skin-friction coefficient and Reynolds number is assumed. Empirical factors are introduced which modify the skin-friction coefficient and the Reynolds number in the incompressible friction law to account for compressibility, heat transfer, etc. These factors are then considered as functions of the boundary layer parameters, such as Mach number, wall-to-free stream temperature ratio, and mass transfer. The functional dependence is determined from experimental data.

Although both of these methods have the advantage of being simple and relatively easy to apply, they are not very satisfying from a theoretical point of view because they do not relate the skin friction to conditions in the physical boundary layer.

Rott[3] and Persh[4] have attempted to derive theories for mass transfer into a compressible turbulent boundary layer employing different assumptions than those used in the mixing length theory. The assumptions employed are, however, just as arbitrary as those in the mixing length theory.

In all of these theories, considerably more experimental data will be required before a positive judgment can be made concerning the various assumptions employed. Because of the empiricism in all theories of turbulence, it is not possible to

extrapolate, with confidence, beyond conditions where data already exists.

Mixing Length Theory

Prandtl's[5] incompressible mixing length theory and a closely related one by von Karman[6,7] have been extended to adiabatic compressible flow by Van Driest[8] and Wilson[9]. The theory was further extended to include: heat transfer by Harkness[10] and Moore[11]; roughness in incompressible flow by Prandtl and Schlichting[12]; roughness in compressible flow by Fenter[13]; and mass transfer by Rubesin[14], Dorrance and Dore[15] and Lapin[16]. Several authors have extended the basic theory to include injection of gases other than air and including the effects of chemical reactions. For further discussion on the latter theories, see reference 17.

All of these theories are based on a suggestion by Prandtl that the turbulent shear stress in the boundary layer could be written as follows

$$\tau = \rho \overline{v'u'} = \rho \ell^2 \frac{du}{dy} \left| \frac{du}{dy} \right| \qquad (1)$$

Essentially, the formulation is based on dimensional reasoning and a very simplified physical model of turbulence. Prandtl found from experimental data that the mixing length, ℓ, was

$$\ell = k y \qquad (2)$$

Theoretical arguments proposed by von Karman lead to the following mixing length equation

$$\ell = k \frac{du}{dy} \Big/ \frac{d^2u}{dy^2} \tag{3}$$

When one or the other mixing length is employed in equation (1), and then equation (1) is inserted into the momentum equation, the result is a very complicated differential equation for the velocity profile. Since the equation derived in this way cannot be solved, a major assumption is made at this point in order to obtain a velocity profile. It is assumed that all the terms in the momentum equation and the continuity equation containing derivatives with respect to x, the stream direction, are small compared to the remaining terms. In other words, the flow is reduced to that of a Couette flow where x affects the local profile only through the wall shear stress. This assumption has been shown to be untrue except as an approximation in a region very near the wall. Nevertheless, the assumption allows the computation of a nearly correct velocity profile, and although the x terms are not negligible everywhere in the boundary layer, the resulting equation is a reasonably good approximation except in the laminar sublayer and at the very outer edge of the boundary layer.

Compressibility and heat transfer affect these equations only through the local density which appears in equation (1). It is on this point that the differences between the Prandtl

and von Karman mixing length enter the problem. In incompressible flow, both forms of the mixing length give the same velocity distribution. When the density within the boundary layer is not constant, the resulting velocity distributions are somewhat different depending on which formula is used. It can be shown that Prandtl's equation gives a slightly higher velocity profile slope, but the difference is slight. Therefore, it is not surprising that many theories which are based on von Karman's mixing length give essentially the same answer as would be obtained from Prandtl's when terms of secondary importance are dropped. No critical experiment has been performed to determine which of the two formulations is more correct. In fact, in view of the uncertainty in the mixing length theory as a whole, it may be doubted whether a distinction is possible at all.

Because there is little with which to justify choosing either equation (2) or (3), Prandtl's mixing length will be used in analyzing the experimental velocity profiles mainly because it is simpler to work with when mass transfer is involved. The constant of proportionality, k, will be taken as equal to its incompressible value of .4. This assumption is made because k = .4 is well established in incompressible flow and not contradicted by any compressible data. Exact determination of k depends on the derivative of experimental data which is very difficult to obtain with any degree of accuracy.

If the density and τ are assumed known, then equation (1) can be solved for the velocity in the region of the boundary layer where the theory applies, provided a constant of integration is evaluated from experimental data. An objective in analyzing the present data will be to determine how heat and mass transfer affect the constant of integration.

It should be pointed out that all theories of transpiration consider that mass is transferred uniformly across a plane which is identified as the surface of the porous body, but no such porous surface exists. The porous plate model developed for the present tests has a finite number of pores distributed uniformly on the surface so that mass is transferred as small jets of non-uniform strength and direction. None of the theories have so far taken into account the destabilizing effect of mass transfer on the laminar sublayer. Results from the present experiments show that increased mass transfer acts on the sublayer in a way similar to surface roughness. It may be possible under some circumstances, for example, low Reynolds number and small injection rate, that the skin friction coefficient increases because of the destabilizing effect of blowing.

Reynolds Analogy

In the mixing length theory, it is necessary to know the distribution of density across the boundary layer, and most of the analyses which were cited earlier make use of the simple Crocco integral[18] where total temperature is proportional to

velocity. The constants in the relationship are determined from the temperature and velocity at the wall and outer edge of the boundary layer. The temperature is related to density by assuming the perfect gas equation of state and that the pressure is a constant. Restated, the fundamental assumptions are:

1. At every point in the boundary layer the transport of momentum (i.e., the shear stress) is proportional to the flux of energy.

2. The constant of proportionality is the same at every point within the boundary layer.

3. The pressure in the boundary layer is a constant. The consequences of these assumptions are important because first, they imply a Prandtl number equal to one everywhere, even in the laminar flow at the wall which is obviously incorrect. Second, it is implied that the Stanton number is equal to one half of the skin-friction coefficient which is a form of Reynolds analogy for Prandtl number equal to one.

Insufficient experimental data exists on which to base improvements in the above simple theory. Some attempts to improve the theories have been made, but one of the main deficiencies is that no measurements have been made of both skin friction and heat transfer. Furthermore, very few experiments in compressible flow have included temperature and velocity profiles and none exist with mass transfer. It is, therefore, the objective of these experiments to provide skin friction and

heat transfer data at the same conditions which can be used to check the validity of Reynolds analogy. In addition, since temperature and velocity profiles were obtained for the same conditions, a direct investigation of the Crocco relationship will also be made.

Skin Friction Law

Once velocity and temperature profiles have been determined theoretically, a skin friction law can be calculated. The integral momentum equation for the local skin friction coefficient for a flat plate is

$$\frac{c_f}{2} + c_q = \frac{d\theta}{dx} \tag{4}$$

where

$$\theta = \int_0^\delta \frac{\rho u}{\rho_\delta u_\delta}\left(1 - \frac{u}{u_\delta}\right) dy \tag{5}$$

Mixing length theory applies only in the fully turbulent layer, whereas a laminar region is generally assumed near the wall with a mixed laminar and turbulent transitional layer between them. At the outer edge, on the other hand, there is another transitional region where the turbulence becomes intermittent and disappears completely when the free stream is reached. Four regions are listed in the following table with their approximate incompressible y location.

Included is the percentage contribution that each layer makes to the momentum thickness at a $Re_\theta = 2 \times 10^3$

TABLE I

Layer	Location	Percentage Contributions to Momentum Thickness
Laminar Sublayer	$0 \leq y \leq 5\nu_w/u_\tau$	0.6%
Buffer Layer	$5\nu_w/u_\tau \leq y \leq 30\nu_w/u_\tau$	6.8%
Turbulent Layer	$30\nu_w/u_\tau \leq y \leq .2\delta$	50.0%
Velocity Defect Layer	$.2\delta \leq y \leq \delta$	42.6%

The table shows that the turbulent layer and the defect layer are most important, and it can be shown that the fully turbulent region increases with increasing Reynolds numbers. The laminar sublayer and buffer layer are also important because they determine the lower limit of the fully turbulent region, but otherwise they contribute relatively little to the momentum thickness. The velocity defect layer is physically a large part of the boundary layer thickness (80 percent) but is approximated rather well by extrapolating the fully turbulent profile except near the outer edge.

The principal equations needed to obtain a skin friction law have been presented as well as the principle assumptions involved. It can be concluded that the fully turbulent layer is the single most important part of the boundary layer, and when the momentum integral approach is used, it is the velocity

and temperature profiles in this region which mainly determine the skin-friction law. Consequently, analysis of the present data is aimed at determining the effect of heat and mass transfer on the fully turbulent layer when it is correlated in the manner suggested by the mixing length theory.

Although approximate analytical equations can be derived for the velocity and temperature profiles within the assumptions outlined above, it is still impossible to obtain an exact analytical solution for the momentum thickness equation (5) because of its complicated integrand. Normally a mathematical approximation is made involving a repeated integration by parts where only the first nonzero term is retained. The procedure can be performed independently of any specific profile assumption as follows

$$\theta = \int_0^\delta \frac{\rho u}{\rho_\delta u_\delta}\left(1-\frac{u}{u_\delta}\right)dy = \frac{\rho u}{\rho_\delta u_\delta}\left(1-\frac{u}{u_\delta}\right)y\Big|_0^\delta - \frac{d}{dy}\left[\frac{\rho u}{\rho_\delta u_\delta}\left(1-\frac{u}{u_\delta}\right)\right]\frac{y^2}{2}\Big|_0^\delta + \cdots + \int_0^\delta \frac{y^n}{n!}\frac{d^n}{dy^n}\left[\frac{\rho u}{\rho_\delta u_\delta}\left(1-\frac{u}{u_\delta}\right)\right]dy \tag{6}$$

The assumed boundary conditions are

$$y=0,\ \frac{u}{u_\delta}=0,\ \frac{\rho}{\rho_\delta}=\frac{\rho_w}{\rho_\delta}$$
$$y=\delta,\ \frac{u}{u_\delta}=1,\ \frac{\rho}{\rho_\delta}=1 \text{ and } \left(\frac{du}{dy}\right)_\delta \text{ is finite} \tag{7}$$

Therefore, the first nonzero term is equal to

$$\theta \cong \left(\frac{d(u/u_\delta)}{dy}\right)_\delta \frac{\delta^2}{2} \tag{8}$$

Van Driest, Rubesin, Lapin and others have used essentially the same type of approximation. It is only a first approximation as can be seen from the following figure which gives a geometric interpretation to equation (8) where the shaded area is equal to $\left(d\frac{u}{u_\delta}\right)_\delta \cdot \delta \cdot \frac{\delta}{2}$.

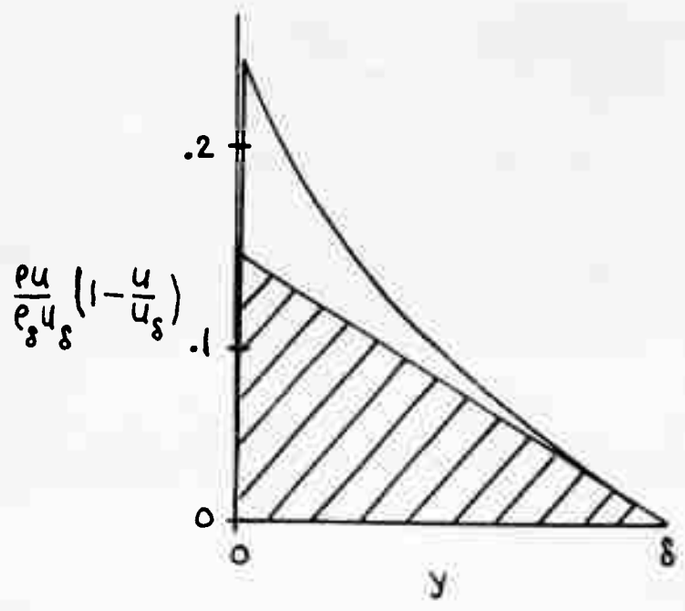

Many of the details of the profile are neglected, but equation (8) does show some of the basic features and, therefore, it may be expected to indicate the correct trend for θ with the principal parameters. It is, however, only coincidence if the magnitude should turn out to be correct.

As a consequence of the above discussion, it is apparent that a closed form analytical result employing the above

approximation to the momentum thickness may be in error due to a number of factors as, for example, the error in truncating the expansion or neglecting certain regions of the profile. Therefore, no attempt will be made to obtain analytical skin-friction laws from the profile correlations. Modern numerical computers can, of course, be used with the generalized profiles to obtain practically exact integration of the momentum thickness and integral momentum equations. Thus, the principle objectives are to determine the effect of heat and mass transfer on the velocity and temperature profiles and then to numerically compute the skin-friction law based on generalizations of these profiles.

EXPERIMENTAL FACILITY

The experiments described herein have been conducted in the U. S. Naval Ordnance Laboratory's Hypersonic Wind Tunnel No. 4, the basic components of which are described in reference 19, 20, and 21. This wind tunnel is capable of operating continuously at Mach numbers from 5 to 10 with supply temperatures from 300°K to 800°K and supply pressures from 1 to 50 atmospheres. During the present experiments, a Mach number 6.7 uniform flow, two-dimensional nozzle was used with a supply temperature of 550°K and supply pressures between 15.2 and 38.0 atmospheres, which is the maximum possible at Mach number 6.7. Automatic controls held the supply conditions constant during the measurements with an average deviation of $\pm$ 1°C in supply temperature and $\pm$ 0.1 atmosphere in supply pressure.

A special test section for the tunnel was used for the porous flat plate experiments. The model spanned the test section from side wall to side wall with its testing surface on the plane of symmetry of the two-dimensional nozzle and with the leading edge located approximately at the nozzle exit. Provision was made in the test section wall for mounting the traversing mechanism which held the various boundary layer probes.

MODEL DESIGN CONSTRUCTION AND CALIBRATION

The porous flat plate model has two main parts, the holder and the porous insert. The holder consists of a sharp leading edge section followed by a flat surface with provision in the center for the porous insert and a plenum chamber underneath. The porous insert is designed for uniform gas injection into the boundary layer and is instrumented for measuring pressures and temperatures.

Holder

Figures 1 and 2 show the two parts of the holder. Figure 2 in particular shows the plenum chamber and the recess for the porous insert. On the right-hand side in figure 1 is the top plate which holds down the insert after it is in place and provides the sharp leading edge and continuous smooth (measured roughness of 11 $\pm$ 4 micro inches) surface around the insert. The leading edge radius is about .015 mm, and the underside of the plate diverges at a 10^{o} angle to the upper surface. Overall model dimensions are: length, 59.06 cm; maximum thickness, 3.302 cm; and width, 25.40 cm at the leading edge; it is wider at the trailing edge because the tunnel walls are tapered .015 cm/cm to account for the tunnel boundary layer growth. Figure 4 shows a sketch of the holder and the porous insert.

Injected gas is brought into the plenum chamber through the side wall of the test section along the entire length of the porous insert. Provision is also made here for bringing

out the thermocouple wires and static pressure tubing from the plenum chamber.

Near the leading and trailing edges, the holder contains manifolds for the porous insert cooling system. These manifolds are soldered to stainless steel tubes imbedded in the porous material. Low temperature oil is circulated as a coolant entering through the test section wall directly into the trailing edge manifold and leaving from the leading edge manifold.

The back of the holder is exposed to high temperatures caused by a complicated shock wave system behind the plate. A cooling system using circulating water was installed on the back of the plate to prevent the injected gas in the plenum chamber from being heated and thereby preventing any conduction from the high temperature gas passing over the back of the holder to the colder test surface of the model.

The top surface plate clamps the porous insert down on continuous seals and thereby prevents any leakage around the porous material. As an added precaution, cement was put into the fine gap between the top plate and the insert. Measurements indicate the maximum discontinuity between surfaces before the cement was applied was less than .051 mm.

Porous Insert

The porous insert is a plate 48.85 cm long, 17.78 cm wide, and 1.067 cm thick. The material is sintered 316 stainless steel powder composed of spheres 40 microns and smaller in

diameter. The resulting density is 42.7 percent of solid 316 stainless steel which is 8.028 g/cm^3. The testing surface is flat within $\pm$ .127 mm, and its surface roughness is 60 to 70 micro inches.

Temperature of the insert is controlled by circulating a low viscosity oil through 15 equally spaced stainless steel tubes sintered into the bottom surface during manufacture of the plate. The axis of each tube (.343 cm outside diameter) is parallel with the long dimension of the model.

Nine static pressure orifices, .635 mm in inside diameter, are located on the testing surface. The first orifice is located 5.08 cm from the start of the porous insert and .556 cm to one side of the plate centerline. The remaining pressure orifices are 5.08 cm apart in the flow direction and alternate on either side of the center coolant tube. Stainless steel tubing cemented into the porous material connect the orifices with the read-out system.

Nine thermocouple stations with four thermocouples at each station are located on the opposite side of the center coolant tube from the corresponding pressure orifice. The thermocouples are made from .254 mm iron and constantan wire. At a given station, the thermocouples are located as shown in figure 4. A view of the underside of the porous insert exposing the coolant tubes and manifolds is shown in figure 3.

Thermal conductivity--Knowledge of certain properties of the

porous material is necessary in order to evaluate the data obtained from the porous plate. For example, one method to measure the heat transfer into the plate depends on measuring the temperature distribution through the insert wall and the thermal conductivity of the material. Therefore, a sample of the material was sent to the National Bureau of Standards for thermal conductivity tests. The results of these tests are reported in reference 22, and, for comparison, the results of similar tests for solid 316 stainless steel are reported in reference 23. The conductivity of the porous material averages about 10 to 12.5 percent of solid stainless steel and has the same temperature dependence. At low temperatures (-140°C), the conductivity is 2.5×10^{-4} kcal/m sec°C or about the same as glass, and, at room temperature, the conductivity of the porous material corresponds to that of granite.

Average mass flow--During the wind tunnel experiments, the mass flow through the porous material was held constant at one of three selected values by regulating the total flow of air into the system. Although the mass flow was held constant, the temperature of the porous material was varied considerably during operation, and this has a pronounced effect on the pressure drop which was also measured. In order to distinguish the effects of changing the temperature level from increased contamination of the pores, the relation between pressure drop, temperature distribution, and mass flow has been derived and used

to reduce all the data to common conditions. The resulting mass flow per unit area is:

$$(\rho v)_w = \frac{K(p_u^2 - p_w^2)}{2RA}\left[\frac{1}{t}\int_0^t \mu T \, dy\right]^{-1} \qquad (9)$$

This equation is derived from Darcy's law[24]. If the mass flow through the plate is held constant, but the temperature is changed by varying the temperature of the fluids in the cooling tubes, then the pressure drop term decreases as the average of μT decreases. Since the maximum temperature difference between some tests was as much as 20 percent, the pressure drop across the porous insert changed by 35 to 40 percent. All the data obtained during calibration and during wind tunnel tests are shown in figure 5 where each value has been adjusted by the above equation to a common temperature of 20°C. Since the data were accumulated from all of the wind tunnel tests and from the calibration before and after about 200 hours of testing, it is concluded that there is no appreciable uniform contamination.

The calibration tests covered the same range of mass flow and of $p_u^2 - p_w^2$ as during the wind tunnel testing, but the pressure ratios, p_w/p_u, were quite different. During the calibration, the pressure ratio was between .936 and 1.000, and during the wind tunnel tests, it was between .022 and .033. Despite the large difference in conditions, the data form a single curve. This indicates that compressibility has very little effect on

the flow through the pores for this material.

Local mass flow calibration--Comparison of experimental results with theoretical analyses is considerably simplified by having uniform injection into the boundary layer and, therefore, the porous insert has been designed to produce uniform injection. In order to verify that the injection was actually uniform over the surface, the local mass flow distribution was measured. In figure 6 the local measurements on the plate centerline where the boundary layer surveys were made, and 5.08 cm each side of the centerline, are shown as fractions of the mean mass flow. Local mass flow deviates nine percent from its mean value. Note that the mass flow is nearly uniform across the plate.

Calibration tests were performed before and again at the end of the wind tunnel tests. The measurements did not change in form or magnitude. The maximum deviation in the second calibration was less than one percent. This confirmed that very little contamination of the porous material occurred even after 200 hours of operation.

INSTRUMENTATION

The results presented herein are based on boundary layer surveys made with Pitot pressure probes and equilibrium temperature probes. Combined with surface pressure and temperature measurements, the data from these probes are sufficient to describe the Mach number, total and static temperature, and velocity boundary layer profiles.

Pitot Pressure Probes

The Pitot pressure probes used were made from circular stainless steel tubing of .559 mm outside diameter and an inlet diameter of .254 mm with a 10^{o} beveled lip. Pressures were measured with a Statham pressure transducer with a range of 0-1 atmosphere (in some cases a similar transducer in the range 0-300 mm Hg was used) and recorded on a variable span, strip chart recorder. The transducer and recording system were calibrated before and after each survey against a mercury manometer with $\pm$ .1 mm measuring accuracy.

All probes used in the boundary layer surveys were supported in the tunnel by a micrometer-traversing mechanism which allowed positioning of the probe with an accuracy of .025 mm. Each traverse was made from the free stream toward the plate, and maximum probe movement was about 7.5 cm. The point of wall contact, needed to evaluate absolute wall distances, was indicated by the completion of an electric circuit at surface contact.

Several factors which affect the accuracy of Pitot probe measurements are discussed in Appendix I where it is concluded that probe-wall interference is probably the major cause of error in the measurements taken near and at the point of wall contact. Turbulent fluctuations also cause some inaccuracies in the same data and, therefore, wall contact points were usually disregarded when describing the region near the wall. Compared to most of the data, less emphasis was given to the points within one probe diameter of the wall because of possible wall interference.

Pressure Data Reduction

The Rayleigh formula[25] was used to compute the Mach number from the measured Pitot pressure and the static pressure which was assumed constant in the boundary layer and equal to the wall static pressure. Wall static pressure was measured by orifices in the plate surface.

The surface shear stress was calculated by taking the slope of the Mach number distribution interpolated between the probe measurements and zero Mach number at the plate surface, and multiplying this by the calculated local velocity of sound and the viscosity of the air at the surface (the viscosity was obtained from reference 26). Both the viscosity and the velocity of sound just depend on the surface temperature of the plate which was indicated by the thermocouples installed in the porous material.

Temperature Measurement in Hypersonic Boundary Layers

Static temperatures within hypersonic wind tunnel boundary layers must be obtained indirectly. This is because the presence of any probe tends to convert, through shock waves and viscosity effects, the translational energy of the flow into thermal energy in the immediate vicinity of the instrument. Thus, probes tend to indicate the total temperature of the flow, i.e., the total energy. Fortunately, the total temperature is simply related to the static temperature and therefore is an adequate measurement when combined with measurements of the flow Mach number.

The conventional total temperature probe[27-31] is the instrument most frequently adapted for hypersonic boundary layer work. Such a probe operates by adiabatically compressing a sample of the flow by passing it through a normal shock wave. This sample enters the probe and passes over a temperature sensing element (e.g., a thermocouple) at relatively low speeds. Ideally, the sample is at total temperature, and the sensing element immersed in this flow ideally would indicate total temperature. Practically, in a low density or low absolute pressure, high-speed and high-temperature flow, the heat losses from the sensing element due to conduction and radiation combined with the small heating potential of the sample causes large deviations in element temperature from the ideal.

Equilibrium Temperature Probe

In fact, as the size of the total temperature probe is decreased or the flow density is decreased, the sensing element temperature tends to indicate the external surface temperature of the probe, which is nearly the adiabatic wall temperature associated with the external boundary layer on the probe. This suggests that by designing a probe of suitable geometry where the relationship between adiabatic wall temperature and total temperature is known, the measurement of that adiabatic wall temperature would be sufficient for boundary layer work. Such a probe might be called an adiabatic wall temperature probe. Unfortunately, some conduction and radiation effects are also present in any practical design and, therefore, the sensing element does not indicate adiabatic wall temperature but a temperature associated with equilibrium between the heat losses and the aerodynamic heating. Therefore, such a probe is called an equilibrium temperature probe.

Theory of Equilibrium Temperature Probe

A possible configuration for an equilibrium temperature probe might be a sharp, small-angled cone made from low emmissivity metal and supported by a thermal insulator (see fig. 7). The cone is mounted in the flow with its axis parallel to the flow direction. A thermocouple measures the temperature of the cone (T_a). An additional thermocouple (T_b) is provided in the

insulating support to facilitate evaluation of the conduction losses effect on T_a.

Ideally, the primary thermocouple (T_a) indicates the adiabatic wall temperature (T_e) which is a property of the basic flow, the cone geometry, and the type of boundary layer on the cone. Cone adiabatic wall temperatures are directly proportional to local total temperature, all other conditions being equal.

$$T_o = A T_e \tag{10}$$

where

$$A = 1/[r_f (1-T/T_o)_c + (T/T_o)_c] \tag{11}$$

$(T/T_o)_c$ is the ratio of static to total temperature in the flow just outside the cone boundary layer, and it can be determined from the Mach number ahead of the cone and the cone geometry through use of conventional cone relations[25]. The recovery factor (r_f) is approximately a constant because it depends only on the Prandtl number which varies only slightly with temperature under wind tunnel operating conditions. If the local cone Reynolds number does not exceed the Reynolds number of transition, then the recovery factor equals the square root of the Prandtl number.

Data Reduction for Equilibrium Temperature Probe

Equilibrium temperature probes were held in the tunnel by the same mechanism as used for the Pitot probe. The temperatures

indicated by the probe thermocouples were recorded on strip chart recorders. Wall contact was indicated by the conical tip completing an electrical circuit when it first touched the wall. Tunnel supply temperatures were recorded during all surveys. Thus, a recovery factor for the probe was computed for each survey when the probe was in the free stream and assumed constant for that survey. Local total temperatures through the boundary layer were calculated by (a) interpolating between the Mach number data to obtain values corresponding to the same position as the temperature data, (b) calculating the factor A in equation (11) from the cone Mach number (obtained from ref. 25) and the constant recovery factor and (c) calculating T_o from equation (10).

Heat transfer rates were calculated from the slope of the total temperature distribution at the model surface (equal to the slope of the static temperature at the surface) and the thermal conductivity of air[26] at the surface temperature. This procedure supplements the heat transfer obtained from the tempera ure distribution within the model wall.

In forming Stanton numbers, the adiabatic wall temperature is required. For the zero mass transfer cases, the adiabatic wall temperatures were calculated assuming a recovery factor equal to the Prandtl number raised to the one third power, where wall temperature was used to evaluate the Prandtl number. The effect of mass transfer on the recovery factor has been measured

by Leadon and Bartle[32]. Their value of recovery factor ratio (i.e., recovery factor with mass transfer divided by the zero mass transfer recovery factor) shown in figure 8 was used to obtain the recovery factor for the various mass transfer cases.

Static temperature distributions through the boundary layer were calculated from total temperature and Mach number distributions. Compressible flow tables[25] were used to obtain the required temperature ratio at the corresponding Mach number. With static temperatures known, local velocities of sound can be calculated, and this times the Mach number gives the local velocity.

TEST CONDITIONS

All of the experiments reported herein were performed in the U. S. Naval Ordnance Laboratory's Hypersonic Tunnel No. 4.

Flow Conditions

The Hypersonic Tunnel No. 4 was equipped with a fixed block uniform flow nozzle of nominal exit Mach number of 6.7. This nominal exit Mach number varied slightly with exit Reynolds number per unit length. However, the resulting changes were small, as were the nonuniformities in the nozzle's axial flow. Both the effect of Reynolds number on the Mach number and the uniformity of the flow are described in reference 21.

Throughout all tests the supply temperature was held constant at 275°C, while the supply pressure was varied between 15 and 38 atmospheres. The Reynolds number per unit length varied from 8×10^6 to 19×10^6 per meter.

Model Conditions

Four locations on the plate were investigated, 37.78, 42.86, 47.94, and 53.02 cm from the leading edge. These stations were presumed to have fully developed turbulent flow for the following reasons: the Mach number and velocity profiles were characteristic of supersonic turbulent profiles; the measured wall temperatures were characteristic of completed transition, i.e., a local maximum at, or before station 5 (32.7 cm from the leading edge); and profiles obtained nearer the leading edge than station 5 were characteristically laminar. The transition

Reynolds number without air injection was 2.6×10^6. A relatively small decrease was observed to occur with air injection, indicating that free stream turbulence probably controlled the location of transition more than any other factor. Thus, natural turbulent boundary layers were obtained at the last four stations, and boundary layer trips were not required.

The ratio of wall temperature to free stream temperature varied somewhat with mass transfer; the average values were 4.1, 5.2, and 7.6. Because of the change in heat transfer rate in the transition region, a variation in the wall temperature occurred in that region which could not be controlled by the cooling system. It was most pronounced for the zero mass transfer and highest pressure conditions and decreased, along with the overall temperature level, as the mass transfer rate increased. Figure 9 shows the temperature distribution which had the greatest variation. It amounted to 25°C or about 10 percent of the driving potential $T_e - T_w$ for heat transfer.

The boundary layer on the plate was investigated without air injection and at three mass transfer rates. These corresponded to .09, .17, and .25 percent of free stream mass flow per unit area.

STATIC PRESSURE DISTRIBUTION

Figure 10 shows the wall static pressures as measured by an oil manometer for the runs of 15 atmosphere supply pressure. The static pressure in the undisturbed free stream was 3.65 mm Hg corresponding to a Mach number of 6.7. It was observed during all the testing that the model surface pressure was considerably higher than free stream static pressure. The amount of the excess in pressure can be seen from figure 10. In the downstream region where most of the testing was performed, the increase was due to the displacement effect of the boundary layer. That is to say, the boundary layer was so thick that its effect on the external flow could not be neglected.

In the zero injection case, there was a slight favorable pressure gradient in the flow direction of -4×10^{-4} mm Hg/mm. The effect produced on the skin friction coefficients compared with the ideal flat plate can be calculated from the integral momentum equation which can be written[33] as

$$c_f = 2\frac{d\theta}{dx} - \frac{2\theta}{\rho_\delta u_\delta^2}\frac{\partial p}{\partial x}\left(2 + \frac{\delta^*}{\theta} - M_\delta^2\right) \qquad (12)$$

The last term in equation (12) represents the pressure gradient effect. The second term on the right is approximately the difference between the friction relation for the flat plate and the two-dimensional body which is

$$c_f = 2\frac{d\theta}{dx} \qquad (13)$$

A value computed for a typical station is:

$$\frac{2\theta}{\rho_\delta u_\delta^2}\frac{dp}{dx}\left(2+\frac{\delta^*}{\theta}-M_\delta^2\right) = .2\times10^{-4} \qquad (14)$$

or about 1.5 percent of the average skin friction coefficient ($c_f = 14 \times 10^{-4}$). Although the wall shear stress obtained from the Mach number curves should be corrected for the pressure gradient effect, the inaccuracy in the determination of c_f is much larger than 1.5 percent (10 to 15 percent based on repeatability of the measurements) and, hence, no correction was made in the data.

Free Stream Static Pressure

In figure 10 for the mass transfer cases, wall static pressures are seen to rise sharply near the start of the porous material. The high pressure in this region may be attributed to a rapid change in displacement thickness where the injected air first influences the boundary layer. Changes in displacement thickness are so rapid that a shock wave is formed and propagates downstream essentially parallel to the leading edge shock wave. It can be clearly seen in figure 12 where static pressure probe surveys perpendicular to the plate are presented. The static pressure surveys were made for each station and with and without mass transfer using a 1.14 mm diameter static pressure probe with the orifices 7.62 cm behind the sharp tip. In the zero injection case, there is a distinct peak in each

survey which can be correlated with the downstream propagation of a weak leading edge shock wave. In the mass transfer cases there are two peaks. The first is the leading edge shock wave, and the second is a stronger wave emanating from near the start of the porous section. It should be noted that whenever the probe penetrates the shock wave, there will be shock-induced boundary layer separation on the probe, and the pressure readings are not correct local static pressures. Nevertheless, the maximum pressures are associated with the passage of the shock wave over the probe orifices. Thus, the maximum pressure can be used to locate the shock waves.

The fact that the origin of the mass transfer induced shock wave is displaced from the beginning of the porous material is probably due to the flexibility of the long and slender static pressure probe. Unsymmetrical loading on the probe tended to bend it about 5 mm away from the wall, which accounts for the probe location data being apparently 5 mm too near the wall. The same effect shows up in locating the leading edge shock wave which appears more oblique than it should ' a free stream Mach number of 6.7.

The flat plate surface is shown full scale in figure 12 and at each station on the plate is shown the static pressure measurement divided by the free stream static pressure. This pressure ratio is plotted against distance from the wall which is also shown full scale. The total boundary thickness is

indicated by a dashed line for the last four stations where profile surveys were made. An expansion wave traceable to imperfect continuation of the nozzle contour into the test section can be seen interacting with the flow at the most rearward stations. The expansion wave, as can be seen in the figure, did not reach the boundary layer in these tests.

It is interesting to note that the measurements show a small pressure rise near the outer edge of the boundary layer. The higher pressure corresponds quite well with the wall static pressure and, therefore, supports the assumption that the static pressure is constant across the boundary layer. These results should be considered qualitative, however, because the forces on the flexible probe may have caused some unwanted deflections. In addition, the point where the shock waves reflected from the wall begin to interfere with the measurements was not determined although very near the wall (on the order of the probe diameter), it was possible to see some interference effects in the data. Nevertheless, there is a measurable increase in pressure near the boundary layer edge which might be explained by the effect of turbulence level on static pressure measurements. The pressure rise might also be related to the turning of the mean streamlines as they enter and penetrate into the boundary layer. At the high Mach numbers of the outer layers, the turning could account for the observed pressure increase. In any case, for

the purpose of data reduction, the static pressure was considered constant across the boundary layer and equal to the wall pressure.

Following the high pressure region near the start of the porous material, there is a minimum in pressure which can be seen in figure 10 in the mass transfer cases. The small pressure rise after the minimum is associated with the transition of the boundary layer from laminar to turbulent flow. A similar effect has been observed by Coles[39] in connection with supersonic turbulent boundary layer measurements. The pressure change is slight for the 15 atmosphere zero mass transfer cases shown in figure 10. Figure 11 shows a 38 atmosphere zero mass transfer case on an expanded scale. The transition region now extends from station 3 to 6 as indicated by wall temperature measurements. With mass transfer the boundary layer thickness is considerably larger, and the effect of transition produces a measurable pressure change.

Analysis of Displacement Thickness Effect

The displacement effect on surface pressures in the region where measurements were made can be analyzed in the following way. Consider a control volume of unit width, one side being the plate surface extending from the leading edge to a given station, a second side is identical and parallel to the first side but displaced away from the surface sufficiently to be entirely outside the boundary layer. All the mass that enters

the upstream face of the control volume must be accounted for as it leaves the volume. The total inflow cannot leave the downstream face of the volume since the effect of the boundary layer is to decrease the mass flow near the plate. Thus, the flow is displaced upward away from the plate; that is, it is given a component of velocity away from the wall and leaves the control volume through the upper surface. At supersonic speeds, a turning of the flow is accompanied by a change in pressure. As the flow turns in the boundary layer, it is compressed as in the case of flow through an oblique shock wave, and the larger the turning angle the higher the downstream pressure becomes. At hypersonic speeds only a very small turning angle is required to produce measurable amounts of compression.

Qualitatively, the displacement effect can be calculated from the following analyses. The continuity equation is:

$$\frac{\partial(\rho u)}{\partial x} + \frac{\partial(\rho v)}{\partial y} = 0 \tag{15}$$

This equation is integrated from the wall to the edge of the boundary layer, $y = \delta$, to obtain

$$\rho v \Big|_{y=0}^{y=\delta} = -\int_0^{\delta} \frac{\partial}{\partial x}(\rho u)\, dy \tag{16}$$

The limits can be written $\rho v = \rho_\delta v_\delta$ at $y = \delta$ and $\rho v = \rho_w v_w$ at $y = 0$. It can be assumed that $\rho_\delta u_\delta$ is constant, so that:

$$-\frac{\partial(\rho u)}{\partial x} = \frac{\partial}{\partial x}(\rho_\delta u_\delta - \rho u) \tag{17}$$

Therefore, equation (16) can be written as:

$$\rho_\delta v_\delta = \rho_w v_w + \int_0^\delta \frac{\partial}{\partial x}(\rho_\delta u_\delta - \rho u)\, dy \tag{18}$$

If equation (18) is divided by $\rho_\delta u_\delta$ one obtains

$$\frac{v_\delta}{u_\delta} = c_q + \frac{d\delta^*}{dx} \tag{19}$$

where

$$c_q = \rho_w v_w / \rho_\delta u_\delta \tag{20}$$

$$\delta^* = \int_0^\delta \left(1 - \frac{\rho u}{\rho_\delta u_\delta}\right) dy \tag{21}$$

if the angle of flow deflection due to the displacement effect of the boundary layer is equal to α, then

$$\frac{v_\delta}{u_\delta} = \tan\alpha \tag{22}$$

Equation (22) and (19) show that the flow at the boundary layer edge will turn in direct proportion to the mass transfer coefficient and the change in slope of the displacement thickness. The deflection of the flow is associated with a pressure rise, and the applicable relation is the same as that used to calculate deflection angles of oblique shock waves.[34]

$$\tan\alpha = \frac{p_\delta/p_\infty - 1}{\gamma M_\infty^2 - p_\delta/p_\infty + 1}\sqrt{\frac{2\gamma M_\infty^2 - (\gamma-1) - (\gamma+1)\,p_\delta/p_\infty}{(\gamma+1)\,p_\delta/p_\infty + (\gamma-1)}} \qquad (23)$$

This relation is more clearly understood if equation (23) is approximated by the more simple relation:

$$\tan\alpha \cong \left(\frac{p_\delta}{p_\infty} - 1\right) \Big/ \gamma M_\infty \qquad (24)$$

which holds for small pressure changes $p_\delta/p_\infty - 1 \ll \gamma M_\infty$ Combining equations (19) and (24), the final result is:

$$\frac{p_\delta}{p_\infty} = 1 + \gamma M_\infty \left(c_q + \frac{d\delta^*}{dx}\right) \qquad (25)$$

Equation (25) shows that the pressure rise is of the order of γM_∞ times the turning angle. For the present investigation, the percent pressure rise is about 1000 times the turning angle in radians ($\gamma M_\infty = 9.4$). A 10 percent increase in pressure is caused by a 0.6° turning angle.

A comparison is given in the following table between the experimental measurements and the pressure increase predicted by equations (19) and (23).

TABLE II

Comparison between Experimental and Calculated Surface Pressures

$c_q \times 10^4$	T_w/T_δ	$c_q + \frac{d\delta^*}{dx}$ (2)	p_δ/p_∞(1)	p_δ/p_∞(2)
0	4.2	.0091	1.09	1.08
0	7.6	.0184	1.17	1.12
9	4.2	.0191	1.19	1.10
17	4.2	.0220	1.23	1.18
25	4.2	.0304	1.32	1.30

(1) Calculated from equations (19) and (23)

(2) Measured data

The calculated values are also shown on figure 10. The calculations should only be compared with the pressures measured at the last four stations, 6, 7, 8, and 9, because the experimental displacement thickness slope (fig. 13) corresponds to the average of these last four stations.

EXPERIMENTAL RESULTS

The experimental results obtained from the boundary layer measurements are presented and discussed in the following section including descriptions of the Mach number, total and static temperature, and velocity profiles. The effects of heat and mass transfer on the boundary layer characteristics such as skin friction, Stanton number, total thickness, displacement thickness, and momentum thickness are also discussed based on the data contained in tables III through XIII which summarize the data from the present experiments.

Mach Number Profiles

A typical Mach number distribution through the boundary layer is shown in figure 14 for the zero mass transfer case, and on the same graph, for comparison, are three mass transfer cases of nearly identical Reynolds numbers and wall temperatures. Not all the data points that went into drawing the figure are shown. Zero mass transfer profiles were obtained for a relatively high heat transfer rate since the wall temperature is about half the adiabatic wall temperature. At the same wall temperature, the heat transfer rates are progressively smaller for the mass transfer cases.

The curves show a smooth monotonic decrease in Mach number from the free stream value to the wall. The linear region near the wall is roughly about 1 mm in thickness independent of the magnitude of the mass transfer and, hence, also the boundary

layer thickness. In addition, the slight increase in concaveness with mass transfer indicated the Mach number profiles cannot be made similar by any nondimensionalization of the distance from the wall by the boundary layer thickness.

Temperature Profiles

Temperature profiles are shown in figure 15 which corresponded to the Mach number profiles shown in figure 14. Total temperatures, nondimensionalized by the static temperature at the edge of the boundary layer, were obtained from equilibrium temperature probe measurements and show the strong influence mass transfer has on the total energy content in the air at a given distance from the wall. Although it is not very apparent from the figure, a slight increase in the total temperature exists at the outer edge of the boundary layer. Conduction of heat from relatively hot regions near the wall is greater than the transport of energy toward the wall near the outer edge, and as a result there is a slight accumulation of energy exceeding that of the free stream. High wall temperatures, i.e., low heat transfer rates into the wall, make the condition more pronounced.

The slope of the total temperature at each point of the boundary layer is an indication of the local transport of energy, kinetic as well as thermal. In an extended region (2 mm $< y <$ δ), the transport of energy is increased with mass transfer, as evidenced by an increase in slope although the absolute level

is decreased. Most of this energy is absorbed by the injected air and only a fraction penetrates through the boundary layer to the surface. Actually, a considerable decrease in heat transfer is indicated by the decrease in slope at the wall compared to the no mass transfer case. Immediately next to the wall, all the energy is thermal energy and is transferred into the wall by conduction.

Decreasing the wall temperature at a given mass transfer rate increases the heat transfer rate, and as a result a larger percentage of energy is taken out of the boundary layer. Figure 16 shows the effect wall temperatures have on the temperature profiles for zero mass transfer. As expected the total temperature level in the boundary layer is decreased as the wall temperature decreases, but the decrease is not large over most of the boundary layer (i.e., outer 80-90 percent). Most of the effect on the temperature distribution is within the 10 percent of the boundary layer nearest the wall.

Static temperature distributions were calculated from total temperature distributions using conventional compressible flow relations described previously. All static temperature curves approach unity at the outer edge of the boundary layer because they have been nondimensionalized by the free stream static temperature. The supply temperature of the tunnel was held constant during all experiments, and as a consequence the static

temperature in the free stream was essentially the same in all cases.

The static temperature curves have been connected to the value measured at the wall by a dotted line which goes through a maximum which was not experimentally observable. This can be shown to be true because at the wall the slope in temperature must be positive for conduction of heat into the surface, while at the last measured point the slope in static temperature is negative. It is interesting that this maximum occurs extremely close to the surface. Figure 17 shows the 20 percent of the boundary layer nearest to the surface for zero mass transfer, and the maximum can be seen to be about 0.1 mm from the wall or on the order of 1 percent of the boundary layer thickness. In the mass transfer cases, the location of the maximum is also extremely close to the wall.

Velocity Profiles

A local velocity of sound can be calculated from the static temperature at each distance from the wall corresponding to a Mach number measurement by interpolating between the measured temperature data. With the velocity of sound and the Mach number, the local velocity can be computed. Figure 18 shows the resulting velocity distribution through the boundary layer corresponding to temperature and Mach number curves shown previously. The velocity is nondimensionalized by the velocity at the outer edge of the boundary layer.

The curves have the typical turbulent boundary layer appearance with a sharp decrease in velocity near the wall, particularly in the zero mass transfer case. The velocity at the outer edge of the boundary layer is nearly 1000 m/sec, and the velocity at the last measured point, about .3 mm from the wall, is 420 m/sec. Thus, the velocity in this case decreases by 40 percent in the last 4 percent of the boundary layer.

As noted earlier, the skin friction was calculated from the slope of the Mach number profile rather than from the velocity profile in order not to introduce any inaccuracy from the temperature profile data. However, in every case the velocity slope at the wall was computed from the Mach number data and compared with the corresponding velocity curve. Agreement between the two procedures was always within 5 or 6 percent, which is less than the basic uncertainty in extrapolating either profile to zero at the wall.

Boundary Layer Parameters

Based on the boundary layer profiles as illustrated by figures 14, 15, and 18, certain properties of these profiles have been calculated, specifically:

δ = Distance from the wall corresponding to $u/u_\delta = .99$ = Total boundary layer thickness

$\delta^* = \int_0^\delta \left(1 - \frac{\rho u}{\rho_\delta u_\delta}\right) dy$ = Displacement thickness

$$\theta = \int_0^{\delta} \frac{\rho u}{\rho_\delta u_\delta}\left(1 - \frac{u}{u_\delta}\right) dy \quad = \text{Momentum thickness}$$

$$\Theta = \int_0^{\delta} \frac{\rho u}{\rho_\delta u_\delta}\left(\frac{T_{t\delta} - T_t}{T_e - T_w}\right) dy \quad = \text{Energy thickness}$$

The subscript δ refers to the asymptotic value that any variable tends toward near the outer edge of the boundary layer. Without mass transfer, each of these parameters increases roughly linearly with the distance from the leading edge as is shown in figure 19, 20, 21, and 22. The effect of lowering the wall temperature is to reduce δ and δ^* and to increase θ and Θ. The influence of δ^* on the apparent geometry already has been discussed.

Mass transfer also increases each thickness roughly linearly. The momentum thickness is affected the most, increasing by a factor of 3.5 at the maximum injection rate, and the total thickness is affected the least, only increasing 2.25 times.

The compressible form factor (displacement thickness divided by momentum thickness) is shown in figure 23 as a function of blowing rate. These results show that heat transfer has a significant influence on the form factor for low mass transfer rates, causing it to decrease by almost 40 percent when the temperature ratio changes from 7.6 to 4.1. The data show that the form factor tends to decrease slightly with mass

transfer with the decrease more pronounced at the higher wall temperatures.

Exponential Velocity Profile Correlation

One method of describing the velocity profiles, which has been employed since the earliest days of incompressible turbulent flow research, is the power-law relation

$$\frac{u}{u_\delta} = \left(\frac{y}{\delta}\right)^{\frac{1}{n}} \tag{26}$$

where δ is the total boundary layer thickness and n is a parameter which is, in general, a function of all the other parameters associated with the flow, i.e., Mach number, Reynolds number, wall temperature, and mass transfer. Total thickness data have been shown in figure 19 which correspond to a total thickness associated with a velocity ratio of .99.

Values of n for the zero mass transfer cases are plotted against length Reynolds number in figure 24. The n's were obtained by measuring the slope of the velocity profile plotted on log-log paper. A decrease of n from between 9 and 10 to about 7 was observed with increasing Reynolds number in the range 2.5×10^6 to 10×10^6.

The effect of mass transfer on the parameter is shown in figure 24. At the highest injection rate, n decreased to 25 percent of its value at zero injection.

The available published data on the profile exponent were compiled by Winkler[35] and presented along with some measurements

made in the NOL hypersonic wind tunnel. However, the data were presented without an explanation for why some n values were higher than others. The present data (fig. 24) shows the same trend as that found by Winkler, in which n decreases with increasing Reynolds number. A possible explanation of these observations is that the high n values were obtained in a transitional region even though the skin friction and wall temperature were a maximum upstream of the measuring location. Natural transition from laminar to turbulent flow is a highly unsteady process and in the case of the present tests, first breakdown of the disturbance waves in the laminar flow may o cur 15 or more centimeters ahead of station 6 at one instant, and in the next instant a laminar boundary layer may extend downstream of station 6. The percentage of time in which the boundary layer is turbulent increases with distance until the turbulent profile is fully established. The probe measures the mean properties and cannot detect the difference between the normal intermittancy of the outer layers of a turbulent boundary layer and the momentary existance of a laminar boundary layer, the outer edge of which may be closer to the wall than the probe. Therefore, near the edge of the measured boundary layer, the only difference is an increased percentage of the time in which the probe is in the uniform free stream.

Figure 24 shows an n of 7 at high Reynolds number, which is consistent with the average of all available high Reynolds

number data (see fig. 10 of ref. 35), while an n of 10 was observed at a Reynolds number of 3×10^6 in what otherwise appeared to be a turbulent profile. If a simple averaging is assumed between the time the probe is in the free stream and the time in a n = 7 turbulent boundary layer, then it can be estimated that the turbulent appearing boundary layer was still laminar as much as 30 percent of the time.

Skin Friction Coefficient

The local skin friction coefficients are summarized in tables III to XIII. Figure 25 shows the skin friction coefficient plotted against Reynolds number based on the distance from the leading edge.

$$c_f = f(Re_x) \tag{27}$$

where

$$c_f = \tau_w / \tfrac{1}{2} \rho_\delta u_\delta^2$$
$$Re_x = \rho_\delta u_\delta x / \mu_\delta \tag{28}$$

Some of the present low Reynolds number measurements are higher than might have been expected for the fully developed turbulent boundary layer. Calculations by the reference temperature procedure[36] and comparison with other available data[37] confirm this interpretation. The trend at the higher Reynolds numbers, however, suggests the fully turbulent condition is being rapidly approached.

As expected, heat transfer increases the Reynolds number at the end of transition. As can be seen in figure 25, the data at the highest wall temperature continuously increases with decreasing Reynolds number which indicates transition occurs at lower values of Reynolds number. However, at the lower wall temperature the data suggests c_f assumes a maximum value at the lowest Re_x which is characteristic of the end of the transition region. The maximum of c_f occurs between station 5 and 6.

In figure 25, the c_f data are plotted against length Reynolds number with the length equal to the distance from the leading edge. The maximum variation in Reynolds number is not only due to change in location on the plate, but in part it is due to a change in wind tunnel supply conditions. As a consequence, the variation of transition location is associated not only with the model wall temperature but is also associated with the changing supply pressure. Different supply pressure levels produce different free stream turbulence levels, which in turn influences the transition location. In order to present the data in such a way as to be independent of the transition location, the c_f data are plotted as a function of momentum thickness Reynolds number in figure 26. A unique relation is assumed to exist between c_f and Re_θ in the fully developed region, and the data are correlated by these parameters to about the same extent as in the c_f versus Re_x presentation.

Mass transfer decreases the skin friction by a considerable amount as shown in figure 27 where c_f divided by c_f at zero mass transfer (at constant length Reynolds number) is plotted as a function of c_q. The mass transfer parameter is twice the mass transfer coefficient divided by the zero mass transfer skin friction coefficient. The magnitude of the reduction in c_f is emphasized by noting that an injection parameter of 3.5 corresponds to a mass transfer rate of .25 percent of the free stream mass flow. Yet this relatively low mass transfer rate decreases the skin friction coefficient to 1/4 of its zero injection value.

The variation of momentum thickness with x provides a check on the consistency of the skin friction measurements obtained from the slope at the wall data. The rate of change of momentum thickness with x can be related to c_f through the integrated momentum equation. The relation is:

$$\frac{d\theta}{dx} = \frac{c_f}{2} + c_q \qquad (29)$$

Lines drawn in figure (28) have a slope determined from the measured c_q and the c_f obtained from extrapolation of the velocity profiles as previously explained. Slopes calculated in this way agree within the scatter of the data for all conditions tested. At high injection rates, the skin friction plays only a small part in determining the rate of change of θ because $c_f/2$ drops to only 6 percent of c_q.

Heat Transfer Coefficient

At hypersonic speeds, heat transfer is of greater interest than skin friction, and figure 29 contains the results of the heat transfer measurements. Both c_f and Stanton number (St) ratioed to their respective zero mass transfer data are plotted versus the mass transfer parameter. For the heat transfer data, the mass transfer parameter is formed by taking the ratio of mass transfer coefficient to the zero mass injection Stanton number.

Although there is considerable scatter in the data, the distribution of Stanton number with mass transfer is similar to the variation of skin friction coefficient. This leads to the conclusion that a direct correlation exists between Stanton number and skin friction coefficient, that is, a Reynolds Analogy relationship.

Reynolds Analogy

Since both skin friction and heat transfer rate were measured under the same conditions, a check is available on Reynolds analogy, where "Reynolds Analogy" means in one case the proportionality between c_f and S_t. In addition, since the velocity and temperature profile were obtained, the more fundamental aspects of Reynolds analogy, that is the analogy between momentum and energy transport at any point in the boundary layer, can also be investigated.

Figure 30 shows the Stanton number data plotted against corresponding skin friction coefficients. Zero injection points are generally highest in c_f (filled symbols), and the mass transfer points (open symbols) are the lowest. A straight line corresponding to an ideal Reynolds analogy ($S_t = c_f/2$) fits the data quite well, although the Colburn form of Reynolds analogy ($S_t = c_f/2Pr^{2/3}$) is only a little higher. The fact that the analogy has been demonstrated in a hypersonic turbulent boundary layer even with mass transfer is a most significant result.

The relationship between temperature and velocity can be used to investigate the local Reynolds analogy, where instead of considering the net flux of heat from the boundary layer into the wall with the shear stress on the wall, the flux of energy is compared with the flux of momentum at each point in the boundary layer. Since local heat and momentum fluxes are not measured in the boundary layer, the equations of motion and

energy neglecting the pressure gradient, i.e.,

$$\rho u \frac{\partial u}{\partial x} + \rho v \frac{\partial u}{\partial y} = \frac{\partial \tau}{\partial y} \tag{29}$$

$$\rho u \frac{\partial c_p T_t}{\partial x} + \rho v \frac{\partial c_p T_t}{\partial y} = \frac{\partial E}{\partial y} \tag{30}$$

are used to determine the coordinates of temperature and velocity that best show the effect of local Reynolds analogy. That is, if the flux of energy E were proportional to the flow of momentum τ, then from equations (29) and (30) it follows:

$$\rho u \frac{\partial}{\partial x}\left[c_p T_t - B u\right] + \rho v \frac{\partial}{\partial y}\left[c_p T_t - B u\right] = 0 \tag{31}$$

which is satisfied by the simple relation:

$$c_p T_t - B u = C \tag{32}$$

Hence, a linear relationship between T_t and u can be interpreted as demonstrating the existence of a local Reynolds analogy. The constants B and C can be evaluated in various ways. The simplest evaluation[18] assumes equation (32) is valid all across the boundary layer. A sufficient set of conditions on B and C can be obtained by using wall and free stream conditions. Such an assumption leads to the equation:

$$\frac{T_t - T_w}{T_{t_\delta} - T_w} = \frac{u}{u_\delta} \tag{33}$$

Equation (33) is not a realistic solution of the energy equation, but it does provide a convenient coordinate system with which to plot the profile data in order to show the degree of agreement or disagreement with Reynolds analogy. If perfect agreement is obtained, then Reynolds analogy exists everywhere in the boundary layer. Note that mass transfer is not an explicit function in equation (29) and (30) and enters only through the boundary conditions.

Figures 31 and 32 show the zero mass transfer profiles plotted as $(T_t-T_w)/(T_{t_\delta}-T_w)$ against u/u_δ. The data are correlated by the parameters suggested by equation (33), but there is still a systematic deviation which shows that a single linear relation will not describe the measurements. In fact, it is only reasonable that the temperature velocity distribution should be composed of parts, laminar sublayer, buffer layer, turbulent layer, etc., consistent with the normal picture of the turbulent velocity profile.

Nevertheless, the temperature velocity profile is represented quite well by equation (33), and a better approximation is given by the empirical equation (34)

$$\frac{T_t-T_w}{T_{t_\delta}-T_w}=\beta\left(\frac{u}{u_\delta}\right)+(1-\beta)\left(\frac{u}{u_\delta}\right)^2 \text{ where } \beta=\frac{T_e-T_w}{T_{t_\delta}-T_w} \qquad (34)$$

which is also shown on figures 31 and 32.

Figure 33 shows a set of temperature velocity profiles at different rates of mass transfer. Their general appearance is changed only in some minor details by the mass transfer. For example, the zero mass transfer profile has a change in slope at $u/u_\delta = .75$ which corresponds to the location of the laminar sublayer. With increasing mass transfer this point moves to lower values of u/u_δ consistent with the lower velocity at the sublayer outer edge. However, equation (34) approximates the mass transfer temperature velocity relation to the same degree of accuracy as in the zero mass transfer cases.

CORRELATION AND ANALYSIS OF THE VELOCITY PROFILES

Semi-empirical analyses of the turbulent boundary layer are usually based on correlations of velocity profile data. In these correlations, the profiles are somewhat arbitrarily divided into various layers where different flow mechanisms are assumed to dominate. Four main divisions of the profile are sometimes considered, namely, the laminar sublayer, buffer layer, fully turbulent region and the outer wake or velocity defect region. These regions are defined most simply in the nondimensional coordinate systems

$$1.\quad u^+ = \frac{u}{u_\tau}\ ,\quad y^+ = \frac{u_\tau\, y}{\nu} \qquad (35)$$

$$2.\quad u_\delta^+ - u^+\ ,\quad \frac{y}{\delta}$$

The laminar sublayer was originally thought of as a region immediately next to the surface where viscosity damps out the turbulent motion. Frequently the sublayer region is defined as extending from the wall to a y^+ of 5. In this region the velocity gradient is taken as the local shear stress divided by the local viscosity. Although the assumption of a purely laminar region has practical value, it is not consistent with measurements[38] which show a maximum in the turbulence level at a y^+ of about 5. Nevertheless, the region $0 < y^+ < 5$ is generally referred to as the laminar sublayer.

The buffer layer is the transition region between the laminar flow layer near the wall and the fully turbulent part of the boundary layer. Here the laminar and turbulent mechanisms are roughly of equal importance in determining the velocity distribution. Approximately the region extends from $y^+ = 5$ to $y^+ = 30$.

From $y^+ = 30$ to about $y/\delta = .2$, the velocity profile is assumed to be determined exclusively by the turbulence.

The turbulence does not extend uniformly to the edge of the boundary layer but becomes intermittent at large distances from the wall. There is a second transition region where the flow changes from fully turbulent to the uniform free stream conditions. This region has the characteristics of a wake propagating into the undisturbed flow. In incompressible flow, the wake or velocity defect region as it is called begins at y/δ of about .2. The wake region therefore constitutes the outer 80 percent of the total boundary layer thickness.

Figures 34 and 35 show the zero mass transfer velocity profiles from the present experiment in nondimensional coordinates u^+ versus y^+. The first figure contains data from the high heat transfer situation.

Figure 35 contains the data from a low heat transfer test. In both cases there is a consistent upward shift with Reynolds number in the fully turbulent region. This shift is due to the proximity of transition. The low Reynolds number data are in a

region where fully turbulent conditions are not yet established. A similar conclusion was reached in an earlier section in connection with the velocity profile exponent.

As a consequence of the transitional nature of the low Reynolds number data, attention will be exclusively focused on the highest Reynolds number tests in the discussion and analysis to follow. The profiles of main interest are shown in figures 36 and 37 where velocity profiles for low $\left(\frac{T_w}{T_\delta} \cong 7\right)$ and high $\left(\frac{T_w}{T_\delta} \cong 4\right)$ heat transfer rates are plotted in u^+ versus y^+ coordinates. Although the general level of all the profiles is the same, there is a definite increase in slope, which may be attributed to the increased mass transfer.

Mixing Length Theory of the Fully Turbulent Region

The fully turbulent region is the most significant part of the boundary layer and determines much of its appearance, even if it does not always constitute a physically large part of the profile. Prandtl proposed that the turbulent shear stress could be written as follows:

$$\tau = \rho \, l^2 \frac{du}{dy} \left|\frac{du}{dy}\right| \qquad (1)$$

Essentially, the formulation is based on dimensional reasoning and a very simplified physical model of turbulence. Furthermore, since the fully turbulent layer occurs close to the wall, it was assumed that the shear stress was constant and for all

practical purposes equal to the wall value. The value of the mixing length, ℓ, was evaluated not from theory but was based on observation of experimental data. The mixing length, it was suggested, was proportional to the distance from the wall, and the constant of proportionality was found to be a universal constant.

$$\ell = ky \tag{2}$$

In incompressible flow, these relations can be manipulated into the "log-law" velocity profile, the slope of which is given by

$$\frac{du}{dy} = \frac{\sqrt{\tau_w/\rho}}{ky} \tag{36}$$

or in nondimensional coordinates:

$$\frac{du^+}{dy^+} = \frac{1}{ky^+} \tag{37}$$

Equation (37) can be integrated to give the log-law which is

$$u^+ = \frac{1}{k} \ln y^+ + C \tag{38}$$

The constants k and C have been determined from experiments, as k = .4 and C = 5.5$\pm$ .5, for a smooth flat plate.

Effects of compressibility are generally accounted for in the shear stress equation (1) by using the local density.

Effects of Mass Transfer on Fully Turbulent Region

Mass transfer into the boundary layer changes the velocity gradient relations by adding a term to the local shear stress. The shear stress is not a constant but increases with velocity and mass transfer as can be shown by consideration of the momentum and continuity equations.

Momentum Equation

$$\rho u \frac{\partial u}{\partial x} + \rho v \frac{\partial u}{\partial y} = \frac{\partial \tau}{\partial y} \tag{29}$$

Continuity Equation

$$\frac{\partial(\rho u)}{\partial x} + \frac{\partial(\rho v)}{\partial y} = 0 \tag{15}$$

It has been shown by experiment that when the boundary layer is thin, the first term in equations (29) and (15) which contain derivatives with respect to x can be neglected when compared to the other terms. (See discussion on page 6.) The continuity equation (15) can then be integrated immediately to give $\rho v =$ constant. The constant is evaluated from the known condition at the wall where the mass flow is $(\rho v)_w$.

If the first term in equation (29) is neglected and the ρv in the second term is set equal to $(\rho v)_w$, then it can also be integrated from the wall ($y = 0$, $u = 0$, $\tau = \tau_w$) to an arbitrary point (y, u, τ).

$$(\rho v)_w u = \tau - \tau_w \tag{39}$$

or

$$\tau = \tau_w + (\rho v)_w u \tag{40}$$

Using equation (40), Prandtl's equation for the slope of the turbulent velocity profile including the effect of mass transfer becomes:

$$\frac{du^+}{dy^+} = \frac{\sqrt{\rho_w/\rho}}{k y^+} \sqrt{1 + 2 \frac{c_q}{c_f} \frac{u^+}{u_\delta^+}} \tag{41}$$

Transformation of Compressible Velocity Profile (with Heat and Mass Transfer) into the Incompressible Velocity Profile

The density ratio in equation (41) can be expressed in terms of the local velocity through the Crocco temperature-velocity relation, and, thus, it is convenient to transfer all velocity terms to the left hand side of the equation. A transformed velocity coordinate can then be introduced which satisfies the following equation:

$$du^{++} = \frac{\sqrt{\rho/\rho_w}}{\sqrt{1+2\frac{c_q}{c_f}\frac{u}{u_\delta}}}\,du^{+} \tag{42}$$

Equation (41) in terms of u^{++} and y^{+} has the same form as the incompressible zero mass transfer velocity slope and has the same solution.

$$u^{++} = \frac{1}{k}\ln y^{+} + C \tag{43}$$

Equation (43) applies only in the fully turbulent part of the profile and the constant, C, must be obtained from experiments. Results of the compressible but zero mass transfer analysis of Van Driest[8], Harkness[10], and Moore[11] can be produced from the above transformation. In each of these analyses, a density-velocity relationship was introduced, and equation (42) or its equivalent was integrated to obtain a complex expression in terms of the velocity for the left hand side of equation (43).

For example, Van Driest used the following form for the density ratio:

$$\frac{\rho_w}{\rho} = \frac{T}{T_w} = 1 + B\frac{u}{u_\delta} - A^2\left(\frac{u}{u_\delta}\right)^2 \qquad (44)$$

where

$$B = \frac{T_e - T_w}{T_w} \quad , \quad A^2 = \frac{T_e - T_\delta}{T_w}$$

Equation (42) can be integrated in this case to give

$$\frac{u_\delta^+}{A}\sin^{-1}\left[\frac{2A^2\frac{u}{u_\delta} - B}{(B^2+4A^2)^{1/2}}\right] + \frac{u_\delta^+}{A}\sin^{-1}\left[\frac{B}{(B^2+4A^2)^{1/2}}\right] = \frac{1}{k}\ln y^+ + C \qquad (45)$$

Although the right hand side implies the equation is valid only in the fully turbulent region, the left hand side has been integrated from the wall ($u/u_\delta = 0$) to some arbitrary point in the turbulent region.

Another example is the result obtained by Moore[11] which was originally derived starting from von Karman's equation. However, the same result can be arrived at through use of equation (42). Moore employed the following relation for the density ratio, which corresponds to equation (44) when the wall temperature equals the adiabatic wall temperature

$$\frac{\rho_w}{\rho} = \frac{T}{T_w} = 1 - \left(1 - \frac{T_\delta}{T_w}\right)\left(\frac{u}{u_\delta}\right)^2 \qquad (46)$$

Equation (42) and (43) become

$$\frac{u_\delta^+}{\sqrt{1-\frac{T_\delta}{T_w}}} \sin^{-1}\left[\sqrt{1-\frac{T_\delta}{T_w}}\,\frac{u}{u_\delta}\right] = \frac{1}{k}\ln y^+ + C \qquad (47)$$

The more general case including mass injection requires the integration of equation (42) combined with the density ratio given by equation (44). Such an integration has been performed by Rubesin[14] where equation (42) is put in the following form

$$u^{++} = \frac{1}{k}\ln y^+ + C = u_\delta^+\sqrt{\frac{c_f}{2c_q}} \int_0^{u/u_\delta} \frac{d\frac{u}{u_\delta}}{\sqrt{\left(1+B\frac{u}{u_\delta}-A^2\left(\frac{u}{u_\delta}\right)^2\right)\left(\frac{c_f}{2c_q}+\left(\frac{u}{u_\delta}\right)^2\right)}} \qquad (48)$$

The integration gives

$$u^{++} = \frac{2u_\delta^+\sqrt{\frac{c_f}{2c_q}}}{A\sqrt{D-E}} \left\{ F\left[k, \varphi\left(\frac{u}{u_\delta}=0\right)\right] - F\left[k, \varphi\left(\frac{u}{u_\delta}=1\right)\right] \right\} \qquad (49)$$

where

$$E = \left(B-\sqrt{B^2+4A^2}\right)/2A^2$$

$$D = \left(B-\sqrt{B^2-4A^2}\right)/2A^2$$

$$G = c_f/2c_q$$

$$F(k,\varphi) = \int_0^{\varphi} \frac{d\varphi}{\sqrt{1-k^2\sin^2\varphi}} = \text{Elliptical Integral of first kind}$$

(a) if $$k^2 = \frac{D+G}{D+E} < 1$$

then $$\sin^2\varphi\left(\frac{u}{u_\delta}\right) = \frac{D-\frac{u}{u_\delta}}{D-G}$$

(b) if $$k^2 = \frac{D - E}{D - G} < 1$$

then $$\sin^2 \varphi \left(\frac{u}{u_\delta}\right) = \frac{D - \frac{u}{u_\delta}}{D - E}$$

As pointed out above, the integration of equations (42) and (43) is restricted to the fully turbulent part of the boundary layer. Nevertheless, the equations cited of Van Driest and Moore were integrated from the wall, a point not in the turbulent part of the profile. Moore has even suggested that the right hand side of equation (43) be replaced by a law of the wall (e.g., Coles, ref. 39) with a term added to account for the variation of C with heat transfer. Since the added term cannot be just a function of the heat transfer rate and have the equations correctly transformed in the sublayer and at the wall, it appears that such a procedure is not completely sufficient to reduce the compressible profile with heat transfer to the incompressible profile. In the data reduction for the following analysis, it will be assumed that the velocity coordinate u^{++}

$$u^{++} \cong \int_0^{u^+} \frac{\sqrt{\rho/\rho_w}\, du^+}{\sqrt{1 + \frac{2 c_q}{c_f} \frac{u^+}{u^+_\delta}}} \qquad (50)$$

is a function of the y^+ coordinate, and it will be the objective to determine from the available data the variation of the profile parameter C with heat transfer, Mach number, and mass transfer.

Profile Constant Determination

There is insufficient understanding of the turbulent boundary layer to be able to calculate the profile constant in the "log-law" from theory. The value of the constant, C, may be considered as determined by the lower limit (of velocity and distance from the wall) of the fully turbulent region, or it may be considered as the upper boundary of the laminar sublayer-buffer layer regions. Near the wall, the velocity is determined by the distribution of laminar and turbulent shear stresses, and, therefore, the constant C is also determined by the distribution of these shear stresses. Some analyses have simplified this complex problem by neglecting the buffer region and only considering a laminar sublayer and a fully turbulent region where the flow changes from laminar to turbulent discontinuously. The problem of determining the location of the laminar-turbulent interface still remains, and various assumptions have been tried in the analyses. However, the interface location is not a physically real point in the flow, and, therefore, it can be questioned whether anything fundamental can be obtained by correlating data using that concept. The constant, C, on the other hand, provides a convenient way of correlating the data, and it may be thought of as referring to a physical location on the boundary layer profiles.

Incompressible Flow

The first measurements of the profile constant were obtained in incompressible pipe flow[40], and over the years a large amount of incompressible data has been accumulated. Despite the number of measurements, there is still a rather large uncertainty in the reported values. For example, Coles[39] in a review of selected incompressible flat plate boundary layer measurements has concluded that C has a value of $5.10 \pm .2$ at Reynolds numbers above 2000. Ross[41] investigated a large number of sources in which data were reported for various configurations (pipes, channels, flat plates, and airfoils) and found $C = 5.55 \pm .4$. Using much of the same data, Clauser[42] obtained $C = 4.9$. The fact that C has not been measured more precisely during the past 30 years gives some indication of the difficulty of performing these experiments. Even recent data show widely spread results. For example, Smith and Walker[43] determined a value of $C = 7.15$ fitted their data best at high Reynolds numbers, whereas Reynolds et al[44] obtained $C = 4.4$.

Compressible Adiabatic Flow

Coles[45] has shown that when the adiabatic compressible velocity profiles are transformed into coordinates similar to those presented here, they reduce approximately to the incompressible profiles. This is equivalent to saying the constant, C, has about the same value as in low speed flow. Figure 38 shows the few data points available for the adiabatic supersonic

case[37,45-48] as well as a few measurements of the incompressible boundary layer[39,41,43,44]. Most of this data falls between 4.5 and 6.5, and they are apparently independent of Mach number below M = 5. The only data at higher Mach numbers are those of Matting, et al[37], which were obtained in helium. However, because of the uncertainty in interpreting the results in helium and because of inconsistencies in those particular profiles, Matting's data were not included here.

Compressible Flow with Heat Transfer

Harkness[10] and Moore[11] have considered the effect of heat transfer on the compressible turbulent boundary layer. Although they employed the von Karman equation and presented the results in terms of the sublayer thickness, their conclusions apply equally well to the value of C. They determine the effect of heat transfer from the experimental data of Monaghan and Cooke[46], Lobb, Winkler and Persh[47], and Winkler and Cha[35]. From these experiments, it was found that C increases quite rapidly with heat transfer into the wall. The data used by Harkness and Moore has been reanalysized to obtain the profile constant and figure 39 shows C as a function of the nondimensional wall temperature, which is, of course, a direct indication of the heat transfer.

The highest Reynolds number profiles of the present experiments have been transformed through the use of equation (42), and the no blowing measurements are shown in figure 40. They

show the expected trend of increasing C with increasing heat transfer. The values of C obtained from these curves are also plotted in figure 39 and are generally consistent with the earlier results. It appears from the figure that the high heat transfer profile constant is a little high but still within the scatter of the available data. Since the data support an increase of C with decreasing wall temperature, it is interesting to speculate on the more fundamental reasons for such behavior. As indicated earlier, C is determined by the distribution of laminar and turbulent shear stresses in the sublayer and buffer layer. If the contribution of the turbulent shear were decreased, then laminar conditions would contribute more in determining the local velocity. Since the effect of turbulence is to decrease the velocity gradient from the higher laminar velocity gradient, it follows that a decrease in turbulence would result in a higher velocity gradient. Since the measured velocity at the lower edge of the fully turbulent region increased under conditions of heat transfer into the wall compared to the adiabatic case, it appears that removing energy from the boundary layer lowers the turbulence level near the wall, and conversely heat transfer away from the wall tends to increase the turbulence level.

As is well known, heat transfer produces just such an effect on the stability and transition of a laminar boundary layer[49].

Thus, there appears to be an analogous effect in fully turbulent flow.

It is not clear whether there is a change in the distribution of turbulence or whether there is an increased thickness of a purely laminar region or both. For example, if a purely laminar region exists, a change in its thickness could be reflected directly as a change in the profile constant. A stability criterion might be found for such a case, which reflects the effect of heat transfer, similar to the criterion suggested by Van Driest for the location of transition of the laminar turbulent interface[50].

Although a reasonable correlation of the data on the basis of the temperature ratio is shown in figure 39, the following correlating parameter was also considered:

$$\Delta^+ = \frac{1}{2} \frac{T_e - T_w}{T_e - T_\delta} u_\delta^+ \qquad (51)$$

Equation (51) is derived from the Crocco temperature-velocity relation by hypothesizing that the change in sublayer thickness is related to the thickness of the region between the wall and the maximum in the static temperature. As was pointed out when the temperature profiles were discussed, the maximum static temperature occurs very near the surface and in a region where the nondimensional distance y^+ is approximately equal to u^+. Thus, equation (44) can be differentiated and set equal to zero to find the $u^+ = y^+$ point corresponding to the maximum

temperature. The result is given by equation (51). The variation of C as a function of Δ^+ is shown in figure 41. The correlation is slightly better than that obtained in figure 39.

The Effect of Mass Transfer on C

Two analyses may be cited which used a similar approach to that used here for describing the effect of mass transfer on the boundary layer. Both the work of Rubesin[14] and Dorrance and Dore[15] start with the same equations and derive a relation which essentially corresponds to equations (42) and (43). At the time of their analyses (1954), no velocity profile data were available for mass transfer into the compressible turbulent boundary layer. Dorrance and Dore overcame this difficulty by making various mathematical assumptions in deriving a skin friction relation. They then evaluated the constants k and C from the incompressible, zero mass transfer limiting case using the Karman-Schoenherr equation. From these and some additional assumptions, they arrived at a value of k = .393, and C was taken as either 4.13 or 6.53.

In effect, Rubesin's approach was to determine the constant, C, by defining a sublayer thickness, where $u^+_a = y^+_a$, as the inner edge of the fully turbulent part of the profile. He used an equation similar to (43) to describe the velocity between the sublayer and the free stream. A further assumption was needed to define the sublayer thickness, and it was assumed that incompressible data without heat or mass transfer could be used to

determine the point (u^+_a, y^+_a). Values for y^+_a of 13.1 and $k = .392$ were recommended which corresponds to a C of 6.5.

The present experimental data provide an opportunity to extend the experimental data on the constant C to include the effect of mass transfer. Figures 42 and 43 show the result of transforming the velocity coordinate according to equation (42) and using the experimental temperature profile and wall mass transfer rate. Both sets of profiles at two wall temperatures show the same trend. As the mass transfer rate is increased, the profiles are lowered, and, as a consequence, C also decreases. It is very interesting to note that a semi-log relationship fits the measured points very well in the fully turbulent part of the boundary layer from $y^+ = 30$ to 100. There is no difficulty in drawing a line of slope, 1/k, through the points and determining C. Figure 44 summarizes the results by showing the change in C with the dimensionless mass transfer rate, c_q. Both wall temperature conditions approximately exhibit the same decrease of C with increasing injection coefficient.

The only other experimental data on the turbulent velocity profiles with mass transfer are the measurements reported by Mickley and Davis[51] and Tewfik[52] for incompressible flat plate boundary layers. Mickley's measurements indicate the opposite trend from the present $M = 6.7$ data and shows a strong Reynolds number effect. Tewfik's data, on the other hand, shows a marked decrease in C for the high injection rate profile given

in reference 52. Obviously, more profile measurements are required to establish the variation of C with Mach number and possibly the effect of surface material.

Theoretical analyses of mass transfer consider the idealized case of perfectly uniform injection. In practice, uniform injection can only be approximated with semi-solid materials, and, therefore, it is not surprising that mass transfer has a destabilizing effect on the sublayer. Although the injection of air has been shown to reduce the stability of laminar boundary layers[53], such a phenomenon would not explain the large decrease in C. If just the stability of the laminar sublayer were involved, the decrease in C would be expected to asymptotically approach some value that would correspond to the fully turbulent conditions throughout the sublayer. It appears more likely that the destabilizing effect is due to local nonuniformity of the injection, and the effect is similar to that of roughness. Although the profile constant is given by Schlichting[33] in a somewhat different form, examination shows that C decreases with increasing roughness height in incompressible flow. For small roughness heights, the decrease in C is explained by an increased turbulence level in the region near the wall which is related to the vortices shed from the disturbance elements.

The present porous plate is composed of small spheres 40 microns and smaller in diameter compressed under high pressure until a flat, smooth surface was obtained. The flow passages

through the material results in the air being injected as tiny jets of probably unequal strength and almost random direction. From a macroscopic view point, the mass transfer is very uniform, but from a more microscopic view point, the jets may be expected to induce a higher level of turbulence in the sublayer and buffer layer.

Skin Friction Law

Empirically correlated velocity profiles, such as the "log-law," are also essentially skin friction laws because they contain the skin friction as a parameter. The conversion to a skin friction Reynolds number relation is obtained by inserting the velocity and temperature profile correlations into the integrated momentum equation. The skin friction law is, of course, only as accurate as the accuracy of the correlations. On the other hand, because it is an integral method, the result does not require an exact solution near the wall. Correlated velocity and temperature profiles developed in the preceeding analysis were programmed on a high speed digital computer, and the skin friction was computed from the integral momentum equation as a function of the momentum thickness Reynolds number. The general availability of computing machines eliminates the need for closed form solutions to the equations which normally involve some mathematical approximations. The equations which were programmed for the U. S. Naval Ordnance Laboratory IBM 7090 computer were:

Momentum thickness (definition)

$$\theta^+ = \frac{\rho_w}{\rho_\delta} \int_0^\delta \frac{\rho u}{\rho_\delta u_\delta} \left(1 - \frac{u}{u_\delta}\right) dy^+ \tag{52}$$

$$Re_\theta = \sqrt{\frac{\rho_\delta}{\rho_w}} \frac{\mu_w}{\mu_\delta} \sqrt{\frac{2}{c_f}}\, \theta^+ \tag{53}$$

Velocity profile ("log-law")

$$u^{++} = u^+_\delta \int_0^{u/u_\delta} \frac{\sqrt{\rho/\rho_w}\, d\frac{u}{u_\delta}}{\sqrt{1 + \frac{2c_q}{c_f}\frac{u}{u_\delta}}} = \frac{1}{k} \ln y^+ + C \tag{42}$$

Density profile (modified Crocco temperature-velocity equation)

$$\frac{\rho_w}{\rho} = \frac{T}{T_w} = 1 + \frac{T_e - T_w}{T_w} \frac{u}{u_\delta} - \frac{T_e - T_\delta}{T_w} \left(\frac{u}{u_\delta}\right)^2 \tag{44}$$

The parameters specified for each calculation were:

$$c_f,\ c_q,\ \frac{T_w}{T_\delta},\ \frac{T_e}{T_\delta},\ C,\ k = .4$$

$\frac{T_e}{T_\delta}$ was adjusted to account for mass transfer effects using figure 8. Heat transfer and mass transfer effects on the profile constant, C, were calculated using the following approximate expression, which is a reasonably good fit to the data shown in figures 41 and 44.

$$C = 5.5 + .275 \frac{T_e - T_w}{T_e - T_\delta} \sqrt{\frac{T_\delta}{T_w} \frac{2}{c_f}} - .59 \times 10^4 c_q \tag{54}$$

Although equation (42) can be integrated in a general way in terms of elliptical integrals, it is simpler to perform the operation by numerical machine methods. In the calculation, only the "log-law" was considered, and the sublayer, buffer layer, and wake region were neglected. Thus, the momentum thickness Reynolds number may be somewhat higher than would be the case if these regions were included. However, no mathematical approximation is required to obtain the momentum thickness.

The velocity ratio was considered the independent variable, and at fixed values of u/u_δ, calculations were made of the temperature ratio, y^+, and the value of the momentum thickness integral out to that u/u_δ point. Adequate accuracy was obtained using increments in u/u_δ of .04.

Two sets of calculations corresponding to two wall temperature ratios of 7 and 4 are shown in figures 45 and 46. For each wall temperature, the zero mass transfer and three mass transfer cases are shown. Relatively good agreement is obtained between the calculations and the experimental data. Lowering the wall temperature ratio from 7 to 4 corresponds to a change in wall temperature of about 180°C and results in a decrease in the skin friction coefficient of 11 percent. It is a relatively simple addition calculation to find a length Reynolds number which corresponds to the momentum thickness Reynolds number. The integral momentum equation can be put in the following form:

$$\int_0^{Re_\theta} \frac{d\,Re_\theta}{\frac{c_f}{2} + c_q} = Re_x \qquad (55)$$

However, the main problem is in interpreting the length, x, in terms of the physical length from the leading edge. An effective starting length for a fully turbulent boundary layer must be defined, and since the objective of showing the correspondence between the velocity profile correlation and skin friction law has been accomplished, further consideration of the skin friction coefficient length relation Reynolds number should await a better understanding of transition from laminar to turbulent boundary layers.

CONCLUSIONS

Skin friction, heat transfer, and boundary layer characteristics have been measured on a flat plate at a Mach number of 6.7, Reynolds numbers between 3×10^6 and 11×10^6, wall to free-stream temperature ratios between 4 and 8, and with various rates of air transpiration. The experimental boundary layer profiles are presented and analyzed from the viewpoint of mixing length theory. The main conclusions are as follows:

1. Skin friction and heat transfer rates have been found to decrease with air transpiration at Mach number 6.7 in about the same amount as has been found by other investigators at lower Mach numbers. An injection rate of one quarter of one percent of the free-stream mass flow caused the skin friction to be reduced to twenty-five percent of its zero injection value.

2. The total boundary layer thickness and the displacement thickness decreased when the wall temperature was lowered, but the momentum and energy thicknesses increased. Air injection into the boundary layer was accompanied by increases in all of these thicknesses, although the momentum and energy thicknesses increased more rapidly than the total boundary layer thickness.

3. Both skin friction and heat transfer rates were measured under essentially identical conditions, and thus it was possible

to experimentally verify Reynolds analogy. Stanton numbers were found to be approximately equal to one-half of the corresponding skin friction coefficients. This was found valid both without and with air transpiration into the boundary layer. Colburn's form of Reynolds analogy predicts that the Stanton number is equal to about 63 percent ($S_t = c_f/2Pr^{2/3}$, $Pr = .7$) of the skin friction coefficient which is somewhat higher than the percentage found in the present results but still within the scatter of the data.

4. Temperature and velocity profiles were also obtained under essentially identical conditions, and these profile measurements show that the modified Crocco equation adequately describes the relationship between total temperature and velocity within the turbulent boundary layer. This conclusion was found to apply to boundary layers without and with air transpiration. The modified Crocco equation can be written as follows:

$$\frac{T_t - T_w}{T_{t_\delta} - T_w} = \beta \frac{u}{u_\delta} + (1-\beta)\left(\frac{u}{u_\delta}\right)^2, \quad \beta = \frac{T_e - T_w}{T_{t_\delta} - T_w} \qquad (34)$$

Temperature profiles calculated from the above equation do not describe all the features of the measured temperature profile, and, therefore, it should only be considered as a good approximation.

5. Prandtl's mixing length analysis has been shown to acceptably describe the experimental velocity profile in the fully turbulent region of the boundary layer if the effects of heat and mass transfer on the laminar sublayer are taken into account. The mixing length theory was used to develop the following transformation for the local velocity.

$$u^{++} = \int_0^{u^+} \frac{\sqrt{\rho/\rho_w}\, du^+}{\sqrt{1 + 2\,\frac{c_q}{c_f}\,\frac{u^+}{u_\delta^+}}} \tag{42}$$

This transformed velocity is related to the distance from the wall by the same semi-logarithmic equation established for incompressible turbulent boundary layers.

$$u^{++} = \frac{1}{k} \ln y^+ + C \tag{43}$$

Unlike incompressible flow, however, the constant C is found from the present and other available data to be a function of heat and mass transfer, but based on the available data, the constant is independent of Mach number under adiabatic wall conditions and equal to its incompressible value of 5.5.

6. Heat transfer was found to increase or decrease C depending on whether the heat transfer is toward or away from the wall. Apparently, the change in C with heat transfer is associated with a change in the turbulence level in the laminar sublayer which is similar to the effect of heat transfer on laminar boundary layer stability. An increasing rate of heat

transfer into the wall is accompanied by an increasing laminar sublayer thickness. This fact suggested that the distance between the wall and the maximum in the static temperature profile might be a suitable length with which to correlate the change in C. The maximum in the temperature profile occurs very near the surface inside the laminar sublayer, and it is directly related to the heat transfer rate. The present and other published profile constant data were correlated rather well by the nondimensional distance to the temperature peak,

$$\Delta^+ = \frac{1}{2} \frac{T_e - T_w}{T_e - T_\delta} u_\delta^+ \qquad (51)$$

which was calculated for each case using the modified Crocco temperature velocity relation.

7. Air transpiration into the turbulent boundary layer decreases the profile constant for the conditions tested in a manner analogous to roughness. It should be noted, however, that a large part of the effect of mass transfer on the velocity profile is taken out by the transformation, and the change in the profile constant is an additional effect. Apparently, transpiration increases the turbulence level in the laminar sublayer and decreases the sublayer thickness. This may be related to the nonuniformity of the mass transfer process when viewed on the scale of the pores in the porous plate or the thickness of the sublayer. It was found that the effects of

heat and mass transfer on the velocity profile constant could be accounted for by the following approximate equation:

$$C = 5.5 + .275 \frac{T_e - T_w}{T_e - T_\delta} u_\delta^+ + .59 \times 10^4 c_q \qquad (54)$$

8. Skin friction coefficients were computed as a function of momentum thickness Reynolds number by numerical techniques using:

a. The definition of the momentum thickness
b. The transformed velocity profile ("log-law" neglecting the sublayer, buffer layer, and wake region)
c. The modified Crocco temperature-velocity relation
d. An empirical profile constant accounting for the effect of heat and mass transfer derived from the experimental data

Good agreement was obtained between the measurements this simple analysis.

In addition to the principal conclusions, the following points appeared to be significant particularly for those interested in turbulent boundary layer experimentation at hypersonic Mach numbers.

9. At hypersonic speeds, boundary layer flow field interaction is important in the calculation of the boundary layer characteristics especially when mass transfer is involved. The pressure rise in the boundary layer was found to be given approximately by

$$\frac{p_\delta}{p_\infty} = 1 + \gamma M_\infty \left(c_q + \frac{d\delta^*}{dx} \right) \tag{25}$$

where $c_q + \frac{d\delta^*}{dx}$ represents the angle through which the flow must turn to accommodate to the growing boundary layer.

10. The experiments described here were measured in a turbulent boundary layer behind natural transition. However, the approach to the fully turbulent condition was found to be very slow, and it was necessary to go to the highest possible Reynolds number per foot in the NOL Hypersonic Tunnel No. 4. The observed slow approach to fully developed turbulent conditions is believed to be related to the unsteady movement of transition which at a given time may be a relatively large distance up or downstream of the mean transition location. As a consequence, some measuring stations that were initially thought to be in the fully turbulent region exhibited fuller velocity profiles (i.e., lower exponents in the power law velocity correlation than expected for fully turbulent conditions). More research needs to be done to determine the

characteristics of this part of the transition region and on developing techniques for tripping the boundary layer at hypersonic speeds.

APPENDIX I

ACCURACY OF PITOT PROBE MEASUREMENTS

Recently the use of impact pressure probes has been criticized because of several possible sources of inaccuracies associated with the instrument. Evidence of a contradiction between skin friction measurements obtained by the skin friction balance technique and Pitot pressure surveys has been reported by Matting, et al[37], for hypersonic turbulent boundary layers. No satisfactory explanation for the discrepancy has yet been offered. Therefore, the several possible sources of inaccuracy are considered here with the objective of estimating under what conditions and to what extent the probe gives erroneous results.

Probe Geometry--First of all, a round Pitot tube was chosen because of the greater certainty in establishing the position of the probe with respect to the wall. An uncertainty exists when two-dimensional probes are used because, for equal entrance area, the width is much larger than the height, and, therefore, any slight, hard-to-detect angle between the probe width and the wall produces an upward shift in the geometric center.

Vibration--Some experiments were made to determine if any vibration was present in the extremely thin probes during the tests particularly when the probe was near the surface. This could have an important effect on the evaluation of wall distances especially for points nearest the wall. The tests consisted of measuring the electric current flowing between the

probe and the model wall when a 1.5 volt battery with a 10^2 ohm resistance in series was connected between the electrically insulated probe and the plate. The output was recorded on a sensitive oscilloscope. If vibrations were present, it was expected that as the probe approached the wall the signal obtained would jump intermittently from zero. The observed result was a progressively decreasing contact resistance as wall contact was being established. No significant vibration was discerned.

Additional tests with an unsupported wire of .127 mm diameter, about 20 mm in length showed that wall contact could be repeated within $\pm$ .025 mm. This indicates the forces tending to bend the probe in the vicinity of the wall were extremely small.

Wall Interference--In addition to the considerations regarding the physical location of the instrument and the accuracy of pressure transmission and recording, there are also certain aerodynamic effects that should be considered. Probably the most important of these is that of wall-probe interference. That is, the disturbance to the flow, caused by the probe, propagates into the subsonic flow near the wall and there the disturbance propagates for some distance upstream. Under some conditions, this upstream disturbance may in turn effect the flow in front of the probe. In such a case, the presence of the probe changes the flow it is intended to detect[54].

Preliminary surveys with various size Pitot probes (.89, .559, and .406 mm in diameter) were conducted with the surveys extending through the boundary layer directly over a static pressure orifice in the plate. As might be expected, all the probes caused the static pressure to rise as they approached the wall, and the largest probe produced a large disturbance which affected the static pressure at greater distances from the wall. The maximum increase in wall pressure was also larger than observed with the two smaller probes. The latter produced about the same maximum increase in surface pressure ($\Delta p_w/p_w \cong 25$ percent when the probe center was one diameter from the wall). Since the smallest probe had a prohibitively long response time for the low values of Pitot pressures occurring near the wall, the .559 mm probe was chosen for the main test.

To determine whether or not the disturbance propagating on the surface influenced the Pitot measurements, the following experiment was performed. A dummy probe, i.e., a length of tubing soldered closed, was located on the model surface in order to produce a disturbance. The Pitot probe regularly used for the boundary layer surveys made a survey directly over the dummy. Within the measuring accuracy, the profiles were the same with or without the dummy except when the two probes were in direct contact. It was concluded that, except for a region about one probe diameter from the wall, the measurements are unaffected by wall interference. This justifies the

procedure of discounting some of the measurements nearest the wall as has been done by several other investigators[35,55-57].

Turbulent Fluctuations--Another possible source of interpretation error involves the Pitot pressure fluctuations caused by the turbulent nature of the flow. The effect of the velocity fluctuations in increasing the measured time average Pitot pressure has been considered for incompressible flow by many authors[58-62]. With respect to supersonic flow, authors have either ignored the possible effect or corrected their measurements employing the incompressible velocity fluctuation correction. Only Nothwang[63] considered the effects of density and velocity fluctuations and then only to explain qualitatively the discrepancy between various measuring techniques.

The importance of the density or temperature fluctuations can be demonstrated by noting that the Pitot pressure is approximately linearly dependent on the square of the local Mach number. The square of the local Mach number can be written:

$$M^2 = u^2/\gamma R\left[T_t - u^2/2c_p\right] \qquad (58)$$

In a hypersonic turbulent boundary layer, the translational energy represented by $u^2/2c_p$ is a large part of the total energy, represented by T_t, even quite near the wall, and the fluctuations in the total temperature are in general small. This velocity fluctuation affects the Mach number squared and thereby the Pitot pressure in two ways. First, the pressure is affected

directly through the square of the velocity as in incompressible flow and second through the temperature fluctuations. In both cases the tendency is to increase the Pitot pressure.

An analytical estimate of the importance of turbulent fluctuations was derived in reference 64. This calculation showed that the error could be quite large. For the experimental situation considered in the present investigation, the error in the local velocity very near the surface could be as much as 8-12 percent. This computed error is based on the maximum percentage turbulent fluctuations as measured in incompressible flow. This maximum is encountered, in practice, only when the probe is in direct contact with the wall, and since the turbulent fluctuations decrease very rapidly away from the maximum, the above errors are an upper limit affecting only the points nearest the wall. Furthermore, Kistler[65] has measured decreasing turbulent fluctuations with increasing Mach number.

Averaging over Probe Inlet Area--An estimate has been made of the possible error incurred by averaging the pressure over the finite inlet area of the probe. The measured pressures are considered as corresponding to the locus of the geometric center of the probe. Deviation from this assumption are important only where the Pitot pressure variation is sufficiently nonlinear, as for instance near the surface of the plate, where the variation of Pitot pressure with distance is approximately quadratic. Estimates for the conditions and the probe employed showed that

the measured values are at most 1.4 percent higher than the pressure corresponding to the probe's geometric center.

Slip Flow--The conditions of the present tests are such that the probe is not subject to significant slip flow effects, because the density, even near the wall, is not sufficiently low. The local mean free path is about 1/30th of the inside diameter of the probe under the worst condition.

Conclusion--For the circular entrance probe used and under the conditions of the investigation, the major errors are introduced into the measurements only for the last few points before wall contact. These particular points are normally disregarded because of probe-wall interference. The interference disappears within one probe diameter from the wall. Turbulent velocity fluctuations also affect the data near the wall contact point. An estimate shows that the latter causes the measured values to exceed the correct values. However, turbulent fluctuations become rapidly less important with increasing distance from the surface.

REFERENCES

1. Knuth, E. L., Dershin, H., "Use of Reference States in Predicting Transport Rates in High-Speed Turbulent Flows with Mass Transfers," International Journal of Heat and Mass Transfer, Vol. 6, No. 12, December 1963

2. Spalding, D. B., Auslander, D. M., and Sundaram, T. R., "The Calculation of Heat and Mass Transfer Through the Turbulent Boundary Layer on a Flat Plate at High Mach Numbers, With and Without Chemical Reaction," Northern Research and Engineering Corporation, Boston, Massachusetts, 1963

3. Rott, N., "On the Transfer of Heat and Mass in the Turbulent Boundary Layer," Report No. GM-TR-211, the Ramo-Wooldridge Corporation, Inglewood, California, July 1957

4. Persh, J., "A Theoretical Investigation of the Effect of Injection of Air on Turbulent Boundary Layer Skin Friction and Heat Transfer Coefficients at Supersonic Speeds," NAVORD Report 4220, January 1957

5. Prandtl, L., "Uber die Ausgebildete Turbulenz," AMM, 5, 136 (1925)

6. von Karman, T., "Mechanische Ähnlichkeit und Turbulenz," Proceedings of the 3rd International Congress for Applied Mechanics, Vol. I, pp. 85-92, August 29, 1930

7. von Karman, T., "Mechanical Similitude and Turbulence," NACA, TM-611, March 1931

8. Van Driest, E. R., "Turbulent Boundary Layer in Compressible Fluids," Journal of the Aeronautical Sciences, Vol. 18, No. 3, March 1951, p. 145

9. Wilson, R. E., "Turbulent Boundary Layer Characteristics at Supersonic Speeds - Theory and Experiment," Journal of the Aeronautical Sciences, Vol. 17, No. 9, September 1950,

10. Harkness, J. L., "Skin Friction and Heat Transfer Studies at Supersonic Speeds for Turbulent Boundary Layers," Report No. DRL-436 CM-940, Defense Research Laboratory, The University of Texas, Austin, Texas, June 1959

11. Moore, D. R., "Velocity Similarity in the Compressible Turbulent Boundary Layer with Heat Transfer," Report No. DRL 480, CM 1014, Defense Research Laboratory, The University of Texas, Austin, Texas, April 1962

12. Prandtl, L., Schlichting, H., "Das Widerstandsgesetz rauher Platten," Westf, Reedereie Hafen, Jahrg. 15, Heft 1, January 1934, p. 1.

13. Fenter, F. W., "The Turbulent Boundary Layer on Uniformly Rough Surfaces at Supersonic Speeds," Report No. RE-E92-2, Chance Vought Research Center, Dallas, Texas, December 1959

14. Rubesin, M. W., "Analytical Estimation of the Effect of Transpiration Cooling on the Heat-Transfer and Skin

Friction Characteristics of a Compressible Turbulent Boundary Layer," NACA TN 3341, 1954

15. Dorrance, W. H., and Dore, F. J., "Effect of Mass Transfer on the Compressible Turbulent Boundary Layer Skin Friction and Heat Transfer," Journal Aero. Science, Vol. 21, No. 6, June 1954 pp. 404-410

16. Lapin, Y. V., "Friction and Heat Transfer in a Compressible Turbulent Boundary Layer on a Flat Plate with the Injection of Matter," Soviet Physics Technical Physics, Vol. 5, pp. 920-928, 1960

17. Dorrance, W. H., "Viscous Hypersonic Flow," McGraw-Hill Book Co., Inc., New York, 1962

18. Crocco, L., "Sulle Transmissione del Calore da una Lamina Piana a un Fluido Scorrenta ad alta Velocita Aerotechnica, 12, 181-197, 1932

19. Wegener, P., "Summary of Recent Experimental Investigations in the NOL Hypersonic Wind Tunnel," Journal Aero. Science, Vol. 18, No. 10, pp. 665, October 1951

20. Wegener, P. and Lobb, R. K., "An Experimental Study of Hypersonic Wind Tunnel Diffuser," Journal Aero. Science, Vol. 20, No. 2, p. 105, February 1953

21. Danberg, J. E., Jackson, A. P., Brown, F. W., "NOL Hypersonic Tunnel No. 4," NOLTR 62-47

22. Watson, T. W., and Powell, F. J., "Thermal Conductivity of Specimen of Porous Sintered 316 Stainless Steel," NBS Report 6842, 1960

23. Robison, H. E., and Watson, T. W., "Thermal Conductivity at Low Temperatures of Types 316 and 347 Stainless Steel," NBS Report 5748, 1958

24. Scheidegger, A. E., "The Physics of Flow Through Porous Media," 1st Ed., p. 71; The MacMillan Co., New York, 1957

25. Ames Research Staff, "Tables and Charts for Compressible Flow," NACA TR 1135, 1953

26. Hilsenrath, J., et al., "Tables of Thermal Properties of Gases," NBS Circular No. 564, Nov. 1955

27. Eber, G. R., "Shielded Thermocouples," Physical Measurements in Gas Dynamics and Combustion, Vol. IX, High-Speed Aerodynamics and Jet Propulsion, Princeton University Press, Princeton, N. J., 1954, pp. 186-197

28. Goldstein, D. L., and Scherrer, R., "Design and Calibration of a Total Temperature Probe for Use at Supersonic Speeds," NACA TN 1885, May 1949

29. Winkler, E. M., "Stagnation Temperature Probes for Use at High Supersonic Speeds and Elevated Temperature," NAVORD Report 3834, October 1954

30. Wood, R. D., "An Experimental Investigation of Hypersonic Stagnation Temperature Probes," GALCIT Hypersonic Research Project Memo. 50, July 1959

31. Wood, R. D., "A Heated Hypersonic Stagnation Temperature Probe," Journal Aero/Space Sciences, Vol. 27, No. 7, July 1960, p. 556

32. Leadon, E. R., and Bartle, B. M., "Experimental Evaluation of Heat Transfer with Transpiration Cooling in a Turbulent Boundary Layer at Mach 3.2," Journal Aero/Space Sciences, Vol. 27, No. 1, p. 78, 1960

33. Schlichting, H., "Boundary Layer Theory," McGraw-Hill Book Co., Inc., London, 1955

34. Shapiro, A. H., "The Dynamics and Thermodynamics of Compressible Fluid Flow," Vol. I, p. 592, Ronald Press Co., New York, 1947

35. Winkler, E. M., and Cha, M. H., "Experimental Investigations of the Effect of Heat Transfer on Hypersonic Turbulent Boundary Layer Skin Friction," NAVORD Report 6631, September 1959

36. Sommer, S. C., and Short, B. J., "Free-Flight Measurements of Turbulent Boundary Layer Skin Friction in the Presence of Severe Aerodynamic Heating at Mach Numbers from 2.8 to 7.0," NACA TN 3392

37. Matting, F. W., Chapman, D. R., Nyholm, J. R., and Thomas, A. G., "Turbulent Skin Friction at High Mach Numbers and Reynolds Numbers in Air and Helium," NASA TR R-82, 1960

38. Klebanoff, P. S., "Characteristics of Turbulence in a Boundary Layer with Zero Pressure Gradient," NACA Technical Report 1247, 1955

39. Coles, D., "Measurements in the Boundary Layer on a Smooth Flat Plate in Supersonic Flow," Part I, The Problem of the Turbulent Boundary Layer, Report No. 20-69 Jet Propulsion Laboratory, California Institute of Technology, June 1, 1953

40. Nikuradse, J., "Laws of Flow in Rough Pipes," NACA TM 1292, 1950, Translation "Strömungsgesetze in rauhen Rohren. Ver. Deut. Ing. Forschungsheft 361, 1933

41. Ross, D., "A Study of Incompressible Turbulent Boundary Layers," PhD Thesis, The Pennsylvania State College, June 1953

42. Clauser, F. H., "Turbulent Boundary Layers in Adve se Pressure Gradient," Journal Aero. Sciences, Vol. 21, No. 2, February 1954, pp. 91-108

43. Smith, D. W., and Walker, J. H., "Skin Friction Measurements in Incompressible Flow," NASA TR R-26, 1959

44. Reynolds, W. C., Kays, W. M., and Kline, S. J., "Heat Transfer in the Turbulent Incompressible Boundary Layer I - Constant Wall Temperature," NASA Memo 12-1-58W, 1958

45. Coles, D., "Measurements in the Boundary Layer on a Smooth Flat Plate in Supersonic Flow III, Measurements in a Flat Plate Boundary Layer at the Jet Propulsion Laboratory," Report No. 20-71, Jet Propulsion Laboratory, California Institute of Technology, June 1, 1953

46. Monaghan, R. J., and Cooke, J. R., "Measurement of Heat Transfer and Skin Friction at Supersonic Speeds. Part III. Measurements of Overall Heat Transfer and of the Associated Boundary Layers on a Flat Plate at M = 2.43," RAE Technical Note No. AERO 2129, December 1951

47. Lobb, R. K., Winkler, E. M., and Persh, J., "NOL Hypersonic Tunnel No. 4, Results VII: Experimental Investigations of Turbulent Boundary Layers in Hypersonic Flow," NAVORD Report No. 3880 , U. S. Naval Ordnance Laboratory, Maryland, March 1955

48. Michel, R., "Resultats sur la Couche Limite Turbulente aux Grandes Vitesses," Memo Technique No. 22, 1961, Office National D'Etudes et de Recherches Aeronautiques, Chatillon - Sous - Bagneux, Seine, France

49. Dryden, H. L., "Transition from Laminar to Turbulent Flow," Turbulent Flows and Heat Transfer, Vol. V, High Speed Aerodynamics and Jet Propulsion, Princeton University Press, Princeton, New Jersey, 1959, p. 63

50. Van Driest, E. R., and Blumer, C. B., "Boundary Layer Transition: Free-Stream Turbulence and Pressure Gradient Effects," AIAA Journal, Vol. I, No. 6, June 1963, p. 1303, also see Van Driest, E. R., "On the Aerodynamic Heating of Blunt Bodies," Z. Angew. Math. Phys. IXb, 223-248, March 1958

51. Mickley, H. S., and Davis, R. S., "Momentum Transfer for Flow Over a Flat Plate with Blowing," NACA TN 4017, 1957

52. Tewfik, D. E., "Some Characteristics of the Turbulent Boundary Layer with Air Injection," AIAA Journal, Vol. I, No. 6, June 1963, p. 1306

53. Powers, J. O., and Heiche, G., "The Stability of Selected Boundary Layer Profiles," NOLTR 62-143, U. S. Naval Ordnance Laboratory, White Oak, Maryland, March 1963

54. Morkovin, M. V., and Bradfield, W. S., "Probe Interference in Measurements in Supersonic Laminar Boundary Layers," Journal Aero. Sciences, Vol. 21, No. 11, p. 785, November 1954

55. Wilson, R. E., and Young, E. C., "Aerodynamic Interference of Pitot Tubes in a Turbulent Boundary Layer at Supersonic Speed," D. R. L., U. T., Report DRL 228 (CM-1351), December 1949

56. Coles, D., "Measurements in the Boundary Layer on a Smooth Flat Plate in Supersonic Flow. II. Instrumentation and Experimental Techniques at the Jet Propulsion Lab.," JPL Report 20-70, June 1953

57. Hill, F. K., "Turbulent Boundary Layer Measurements at Mach Numbers from 8 to 10," Physics of Fluids, Vol. 2, No. 6, pp. 668-680, November - December 1959

58. Dutton, R. A., "The Accuracy of the Measurement of Turbulent Skin Friction by Means of Surface Pitot Tubes and Distribution of Skin Friction on a Flat Plate," ARC Technical Report 18,658, September 1956

59. Goldstein, S., "A Note on the Measurement of Total Head and Static Pressure in a Turbulent Stream," Proc. Roy. Soc. Series A., Vol. 155, No. 886, p. 570, July 1936

60. MacMillan, F. A., "Experiments on Pitot Tubes in Shear Flow," ARC 18,235, February 1956

61. Preston, J. H., "The Determination of Turbulent Skin Friction by Means of Pitot Tubes," J. Royal Aero. Soc., Vol. 58, No. 518, pp. 109-121, February 1954

62. Young, A. D., and Maas, J. N., "The Behaviour of a Pitot Tube in a Transverse Total Pressure Gradient," ARC Report and Memo. No. 1770, September 1937

63. Nothwang, G. J., "An Evaluation of Four Experimental Methods for Measuring Mean Properties of a Supersonic Turbulent Boundary Layer," NACA Report 1320, 1957

64. Danberg, J. E., "The Effect of Velocity and Temperature Fluctuations on Pitot Probe Measurements in Compressible Flow," NOLTR 61-28, U. S. Naval Ordnance Laboratory, White Oak, Maryland, 1961

65. Kistler, A. L., "Fluctuation Measurements in Supersonic Turbulent Boundary Layers," BRL Report No. 1052, August 1958

POROUS FLAT PLATE

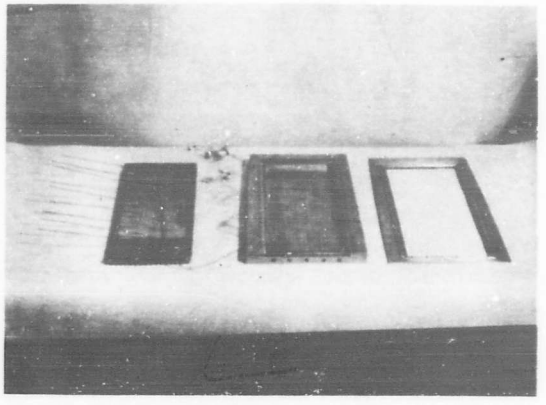

FIG. 1 POROUS INSERT, PLENUM AND INSERT HOLDER, AND SURFACE PLATE, IN THAT ORDER.

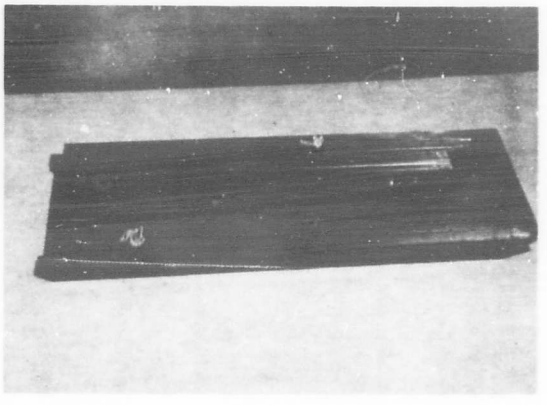

FIG. 2 PLENUM AND INSERT HOLDER SHOWING COOLING FLUID INLET HOLES AND INJECTED AIR INLET SLOT.

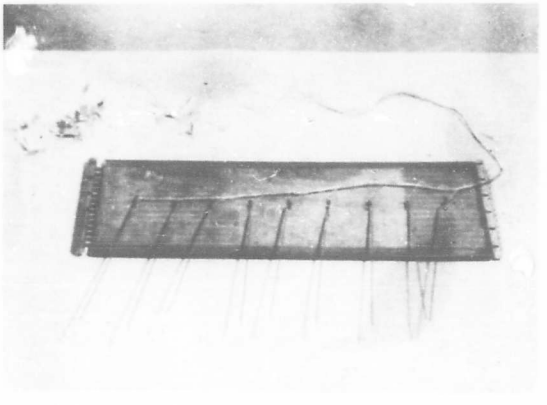

FIG. 3 UNDER SIDE OF POROUS INSERT, SHOWING STATIC PRESSURE TAPS AND THERMOCOUPLE STATIONS, THE COOLING TUBES PROTRUDE FROM EACH END.

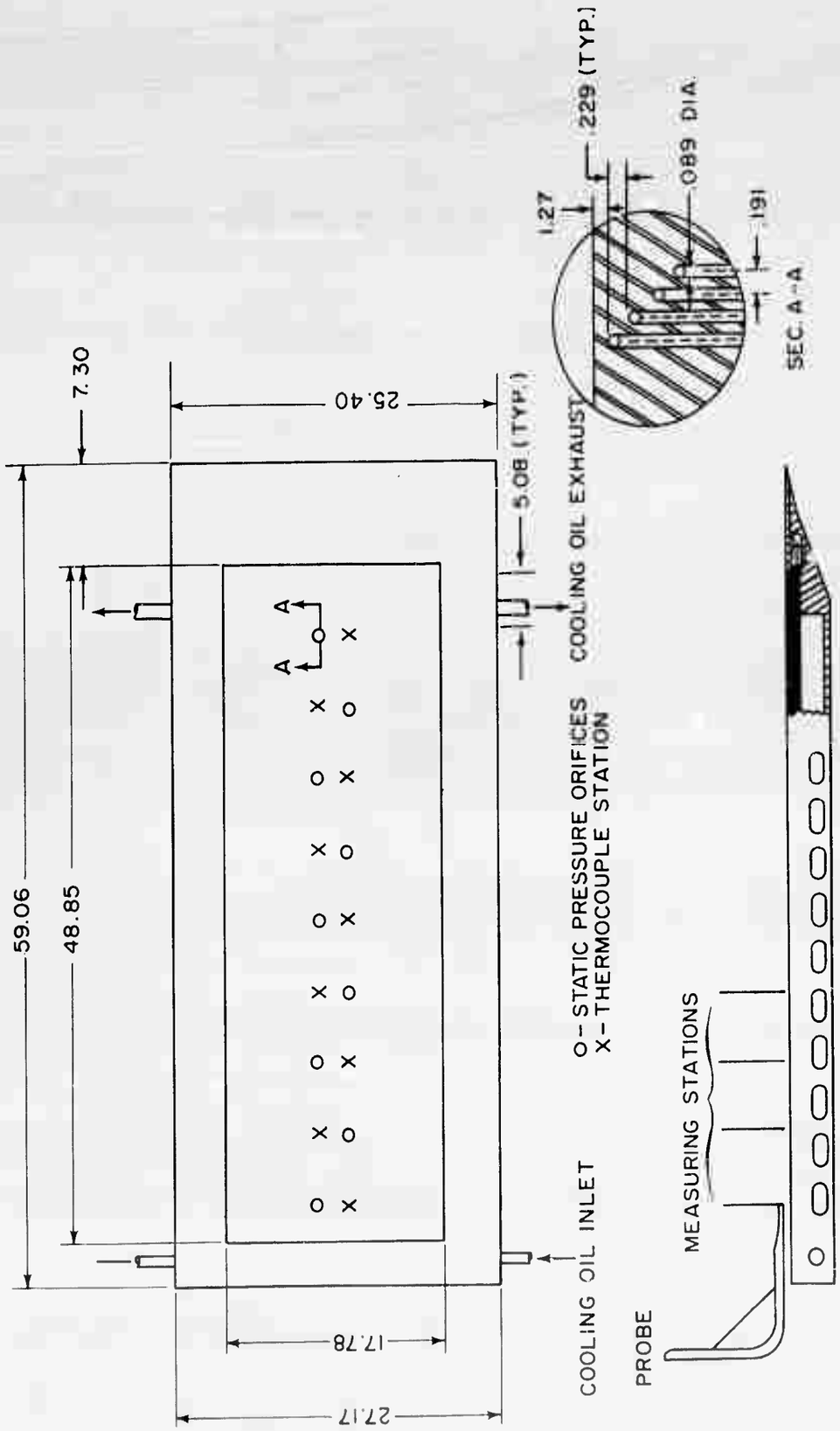

FIG. 4 SKETCH OF MODEL (ALL DIMENSIONS IN cm)

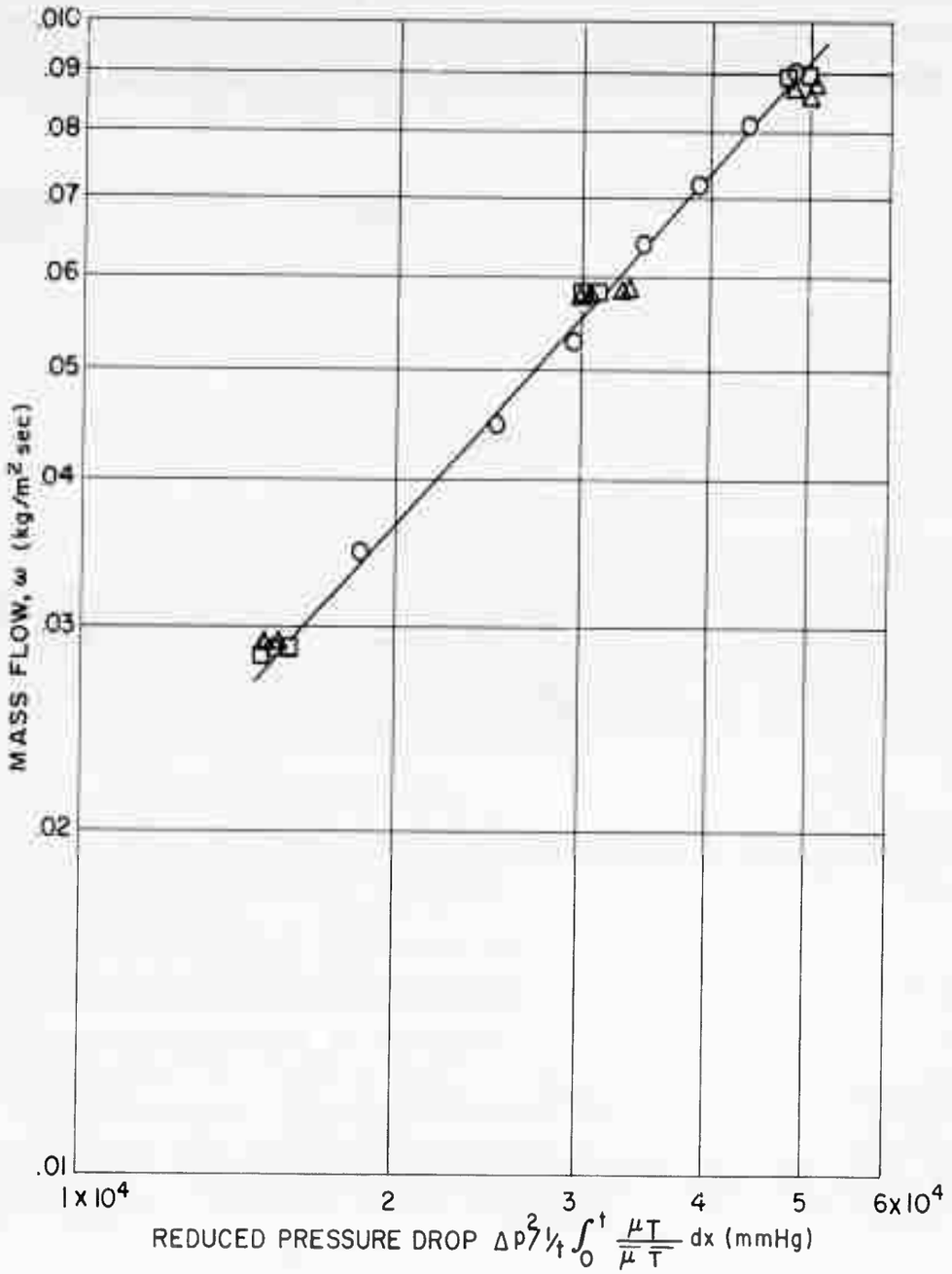

FIG. 5 POROUS FLAT PLATE AVERAGE MASS FLOW VS PRESSURE DROP. AVERAGE TEMPERATURE = 20° C.

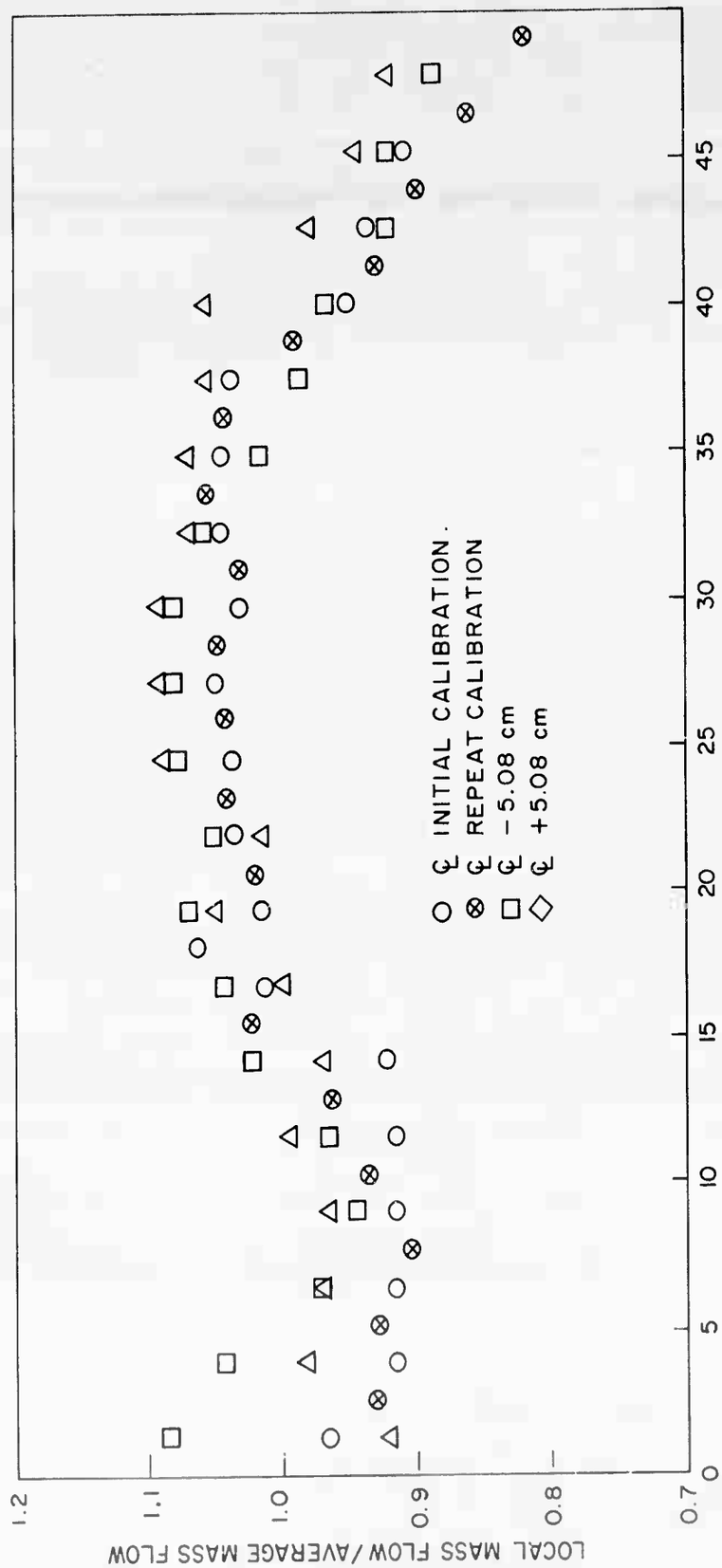

FIG. 6 LOCAL MASS FLOW ON THE POROUS PLATE CENTERLINE AND ±5.08 cm EITHER SIDE OF THE CENTERLINE

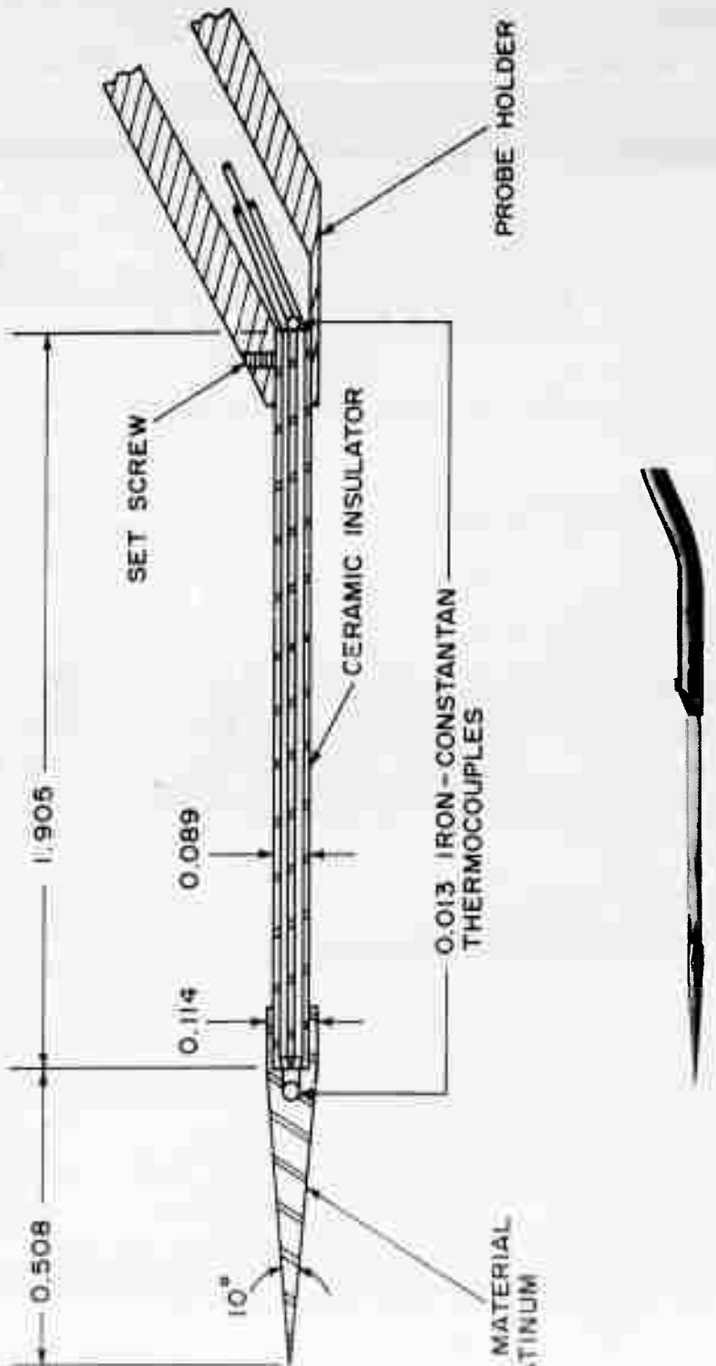

FIG. 7 EQUILIBRIUM TEMPERATURE PROBE (ALL DIMENSIONS IN cm)

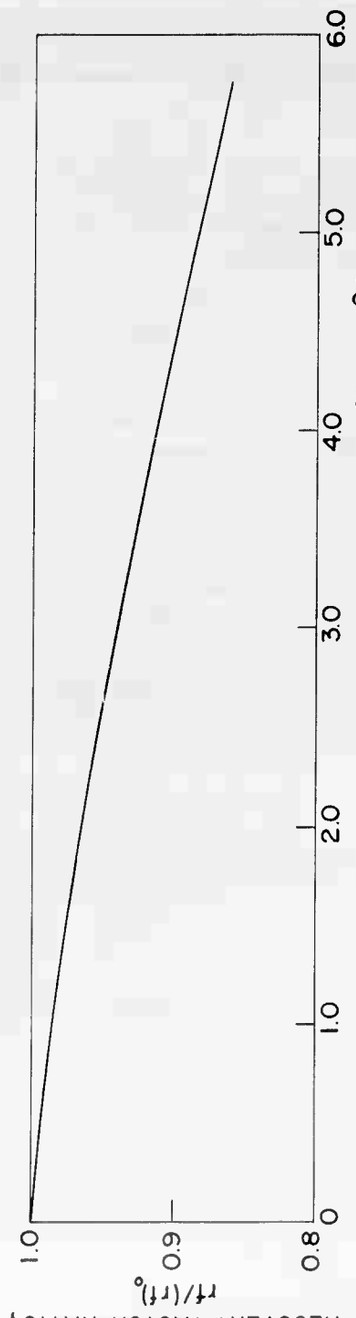

FIG. 8 RATIO OF RECOVERY FACTOR WITH MASS TRANSFER TO RECOVERY FACTOR WITHOUT MASS TRANSFER (REF. 32)

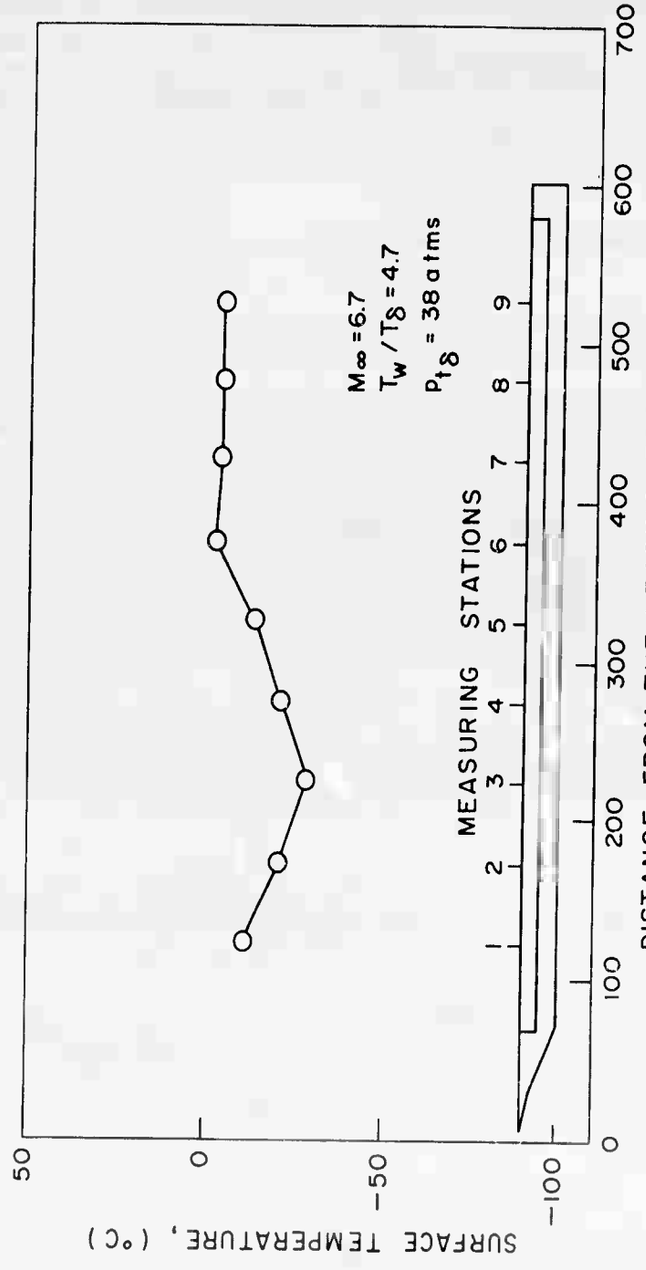

FIG. 9 SURFACE TEMPERATURE DISTRIBUTION

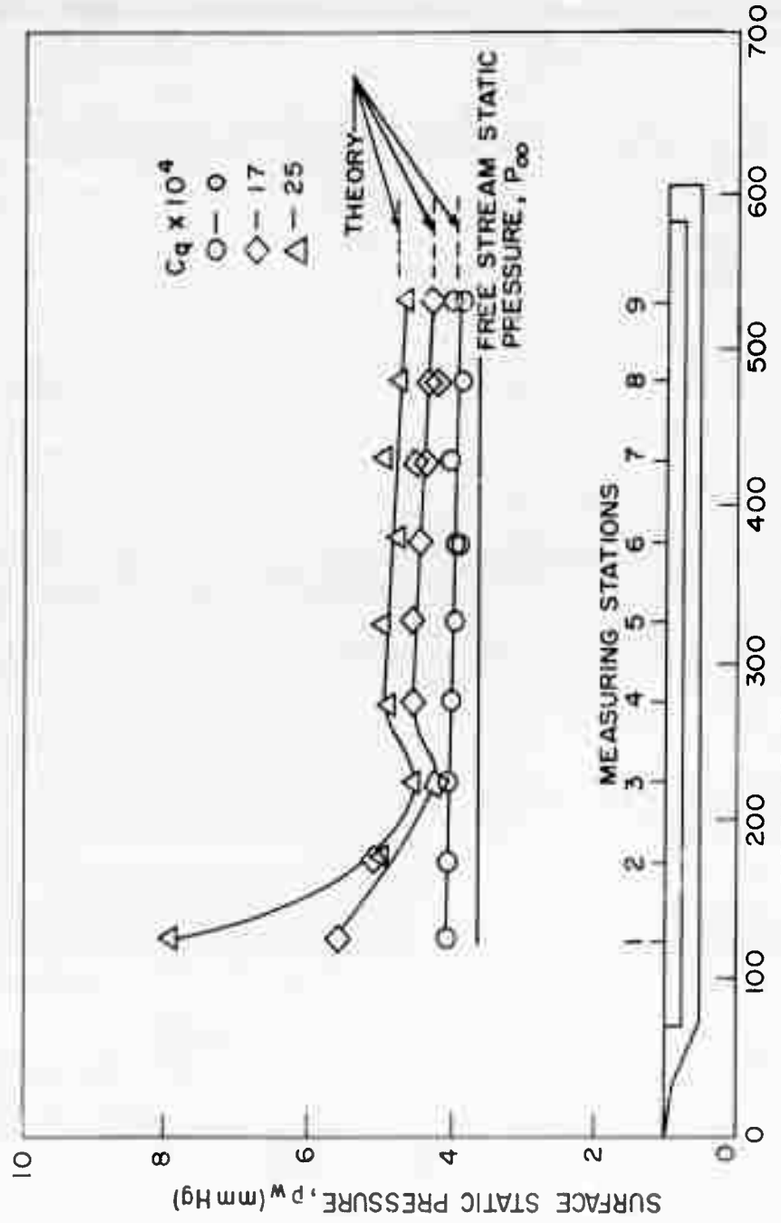

FIG. 10 SURFACE STATIC PRESSURE DISTRIBUTION

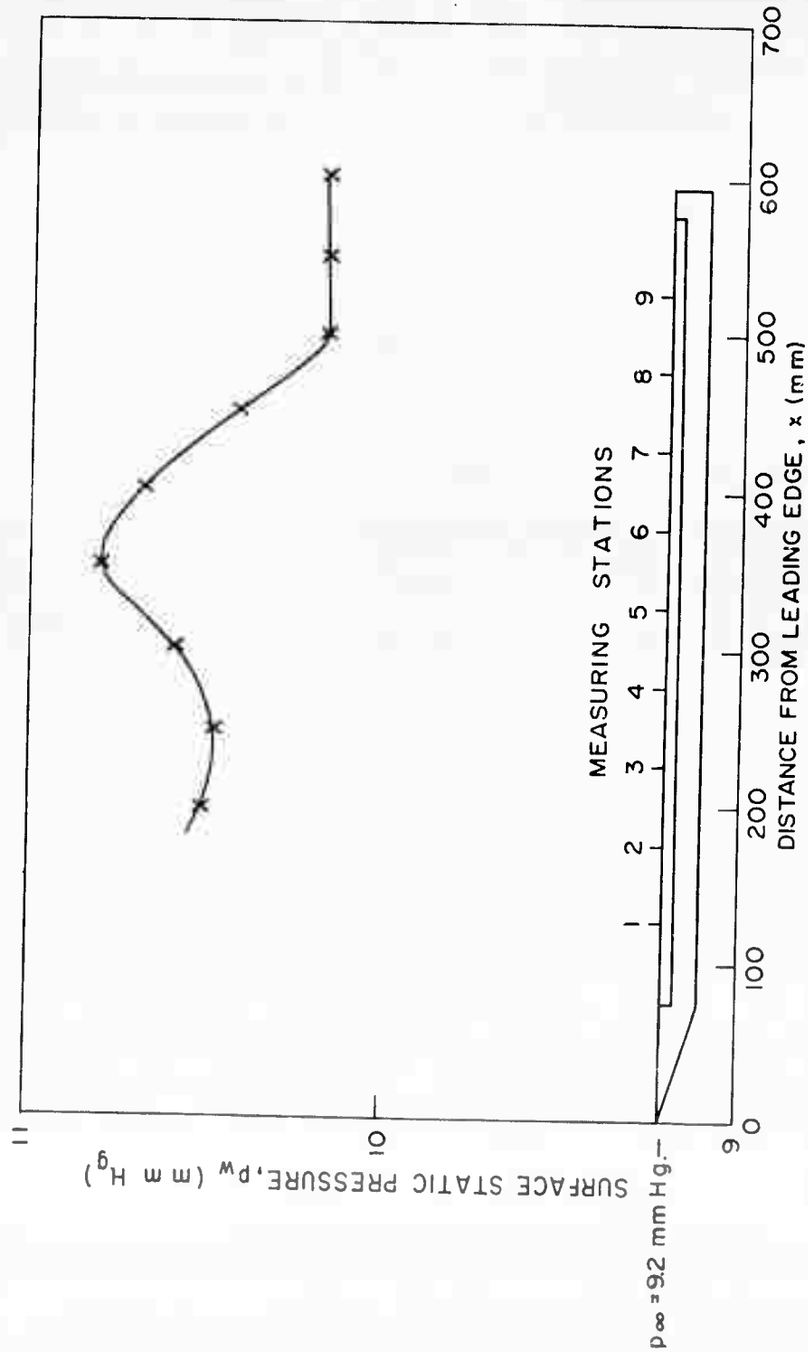

FIG. 11 SURFACE STATIC PRESSURE DISTRIBUTION, $M_\infty = 6.7$, $T_w/T_\delta = 4.7$, $p\,t_\delta = 38$ atms

1.5
1.3
1.1
1.3
1.1
1.3
1.1
1.3
AIR INJECTION
Cq = 17 x 10⁻⁴
LEADING EDGE
SHOCK WAVE
START OF
POROUS MATERIAL
SHOCK WAVE
INDUCED BY THE
AIR INJECTION
LEADING EDGE
ZERO INJECTION
STA 1
STA 2
STA 3
1.5
1.3
1.1
1.3
1.1
1.3
1.1
1.3

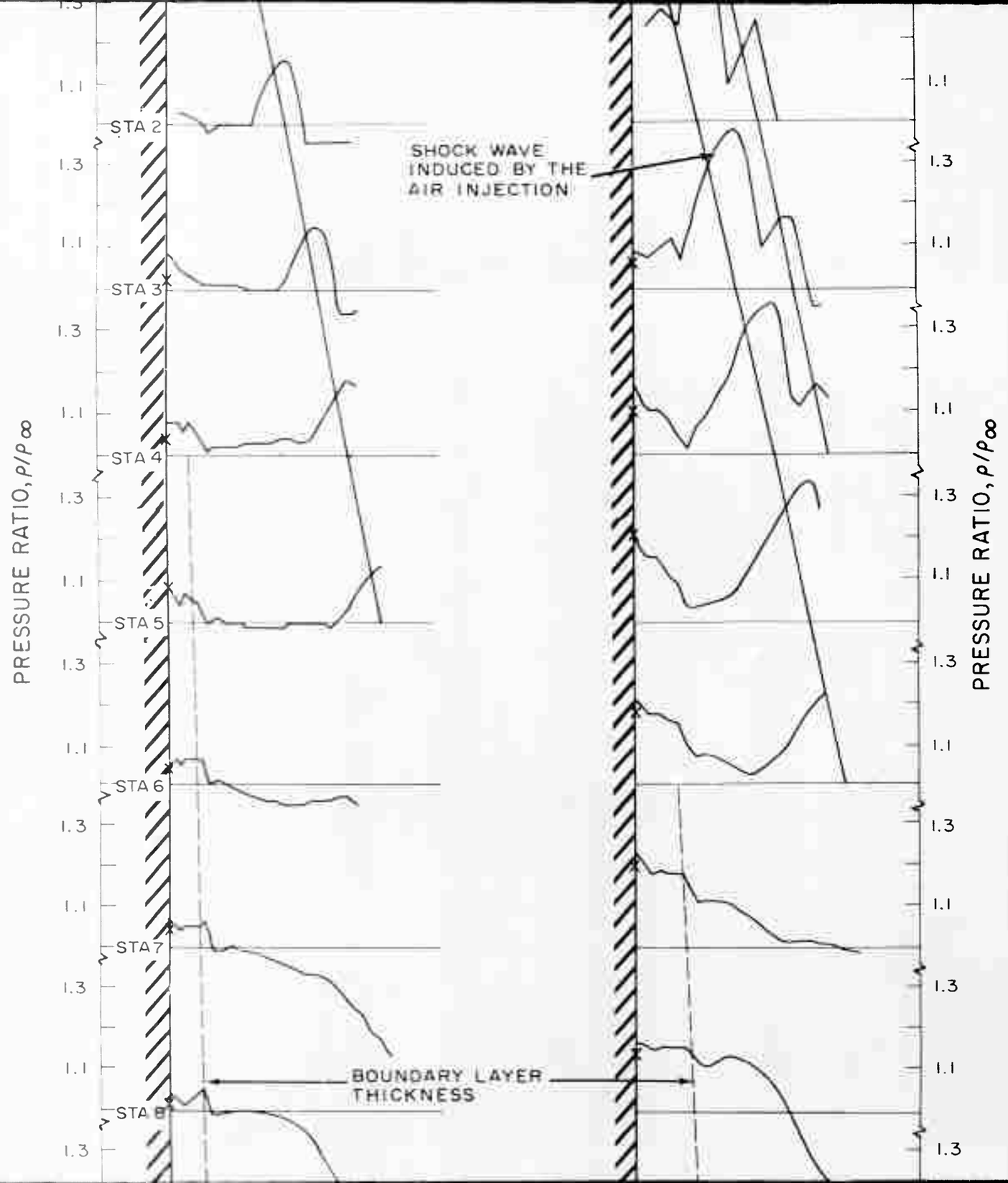
PRESSURE RATIO, ρ/ρ_∞
1.3
1.1
STA 2
STA 3
STA 4
STA 5
STA 6
STA 7
STA 8
SHOCK WAVE INDUCED BY THE AIR INJECTION
BOUNDARY LAYER THICKNESS
PRESSURE RATIO, ρ/ρ_∞

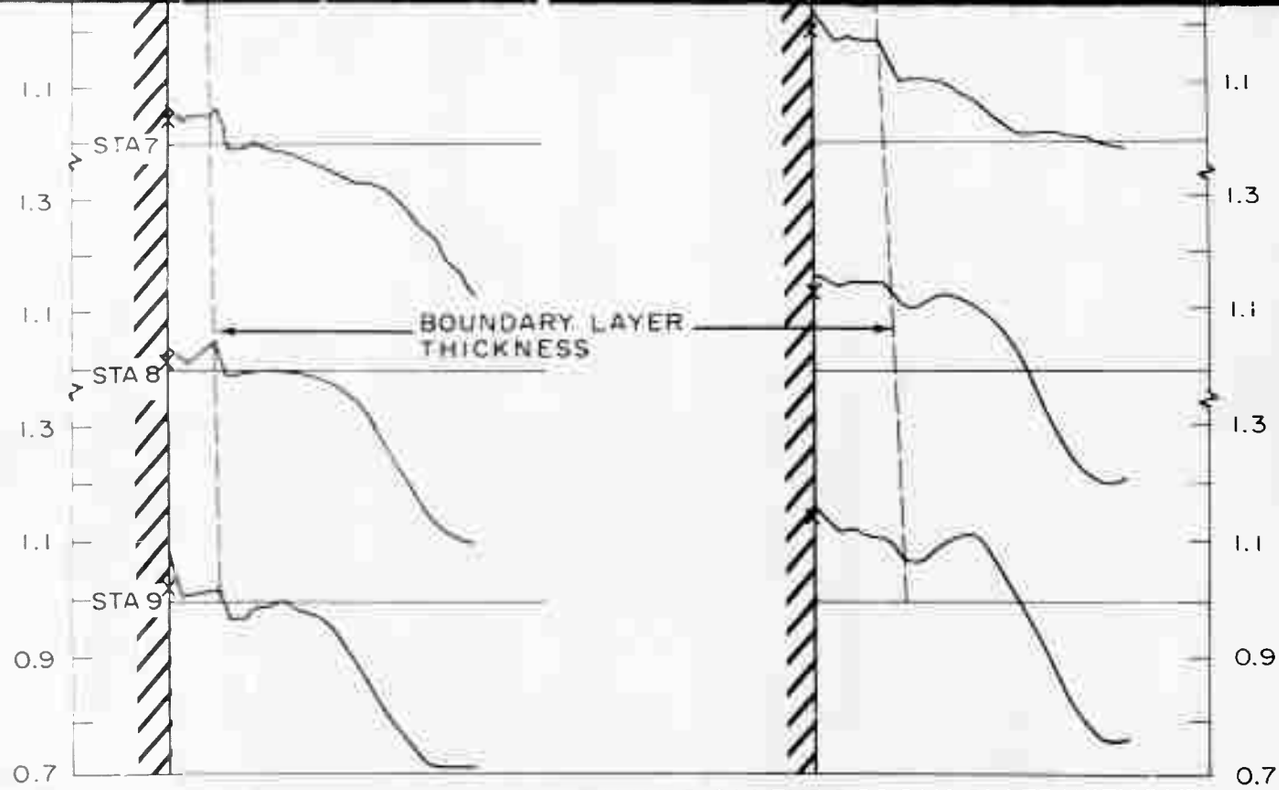

NOTE: 1. X INDICATES THE SURFACE PRESSURE ON THE POROUS PLATE WITHOUT PROBE INTERFERENCE. THE STATIC PRESSURE DISTRIBUTION MEASUREMENTS ARE INTERPOLATED TO THE SURFACE PRESSURE AS MEASURED WITH THE PROBE IN CONTACT WITH THE WALL.

2. THE STATIC PRESSURE PROBE WAS 3" FROM CONICAL TIP TO ORIFACE AND EXTENDED 1 1/2" DOWN STREAM FROM THE ORIFACE. BECAUSE OF THIS THE SHOCK WAVES INFLUENCED THE INDICATED PRESSURE AS LONG AS THE SHOCK WAVE INTERSECTED THIS REGION OF THE PROBE.

3. THE LOW STATIC PRESSURE OUTSIDE THE BOUNDARY LAYER AT STATIONS 7, 8, AND 9 ARE CAUSED BY AN EXPANSION WAVE ORIGINATING FROM THE NOZZLE EXIT.

4. ALL STATIC PRESSURES ARE NORMALIZED TO THE FREE STREAM STATIC PRESSURE CORRESPONDING TO A MACH NUMBER OF 6.7.

5. ALL DIMENSIONS FULL SCALE.

FIG. 12 STATIC PRESSURE DISTRIBUTIONS NORMAL TO THE POROUS FLAT PLATE

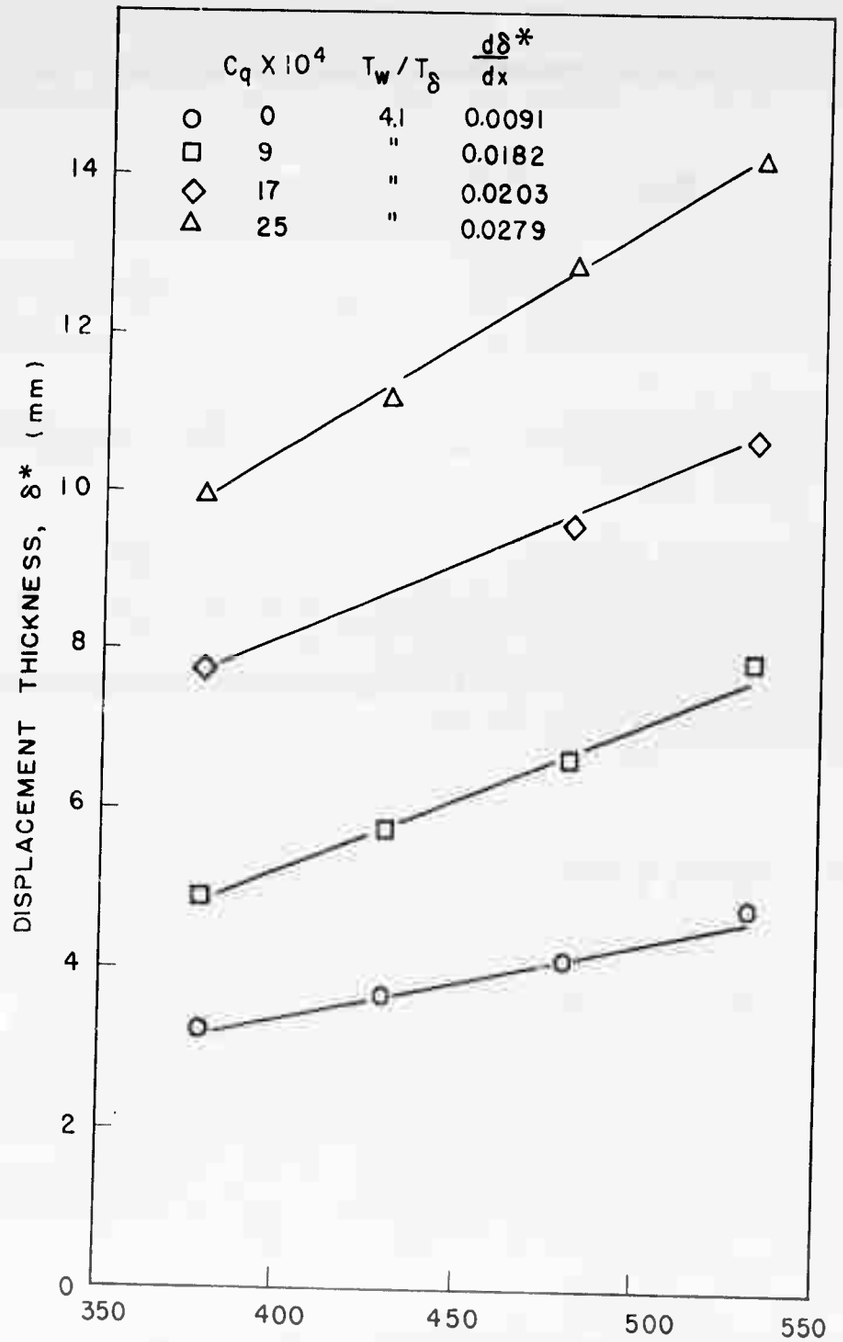

FIG. 13 DISPLACEMENT THICKNESS DISTRIBUTION

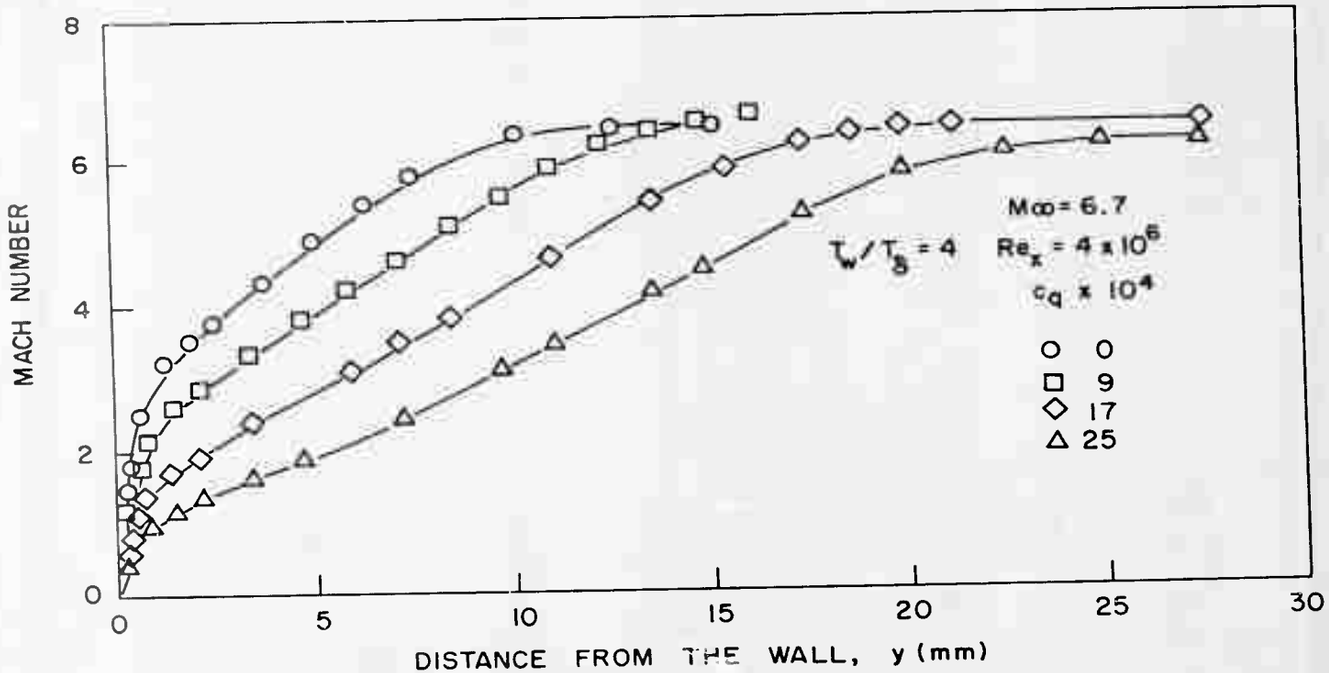

FIG. 14 EFFECT OF MASS TRANSFER ON COMPRESSIBLE TURBULENT BOUNDARY LAYER MACH NUMBER PROFILES.

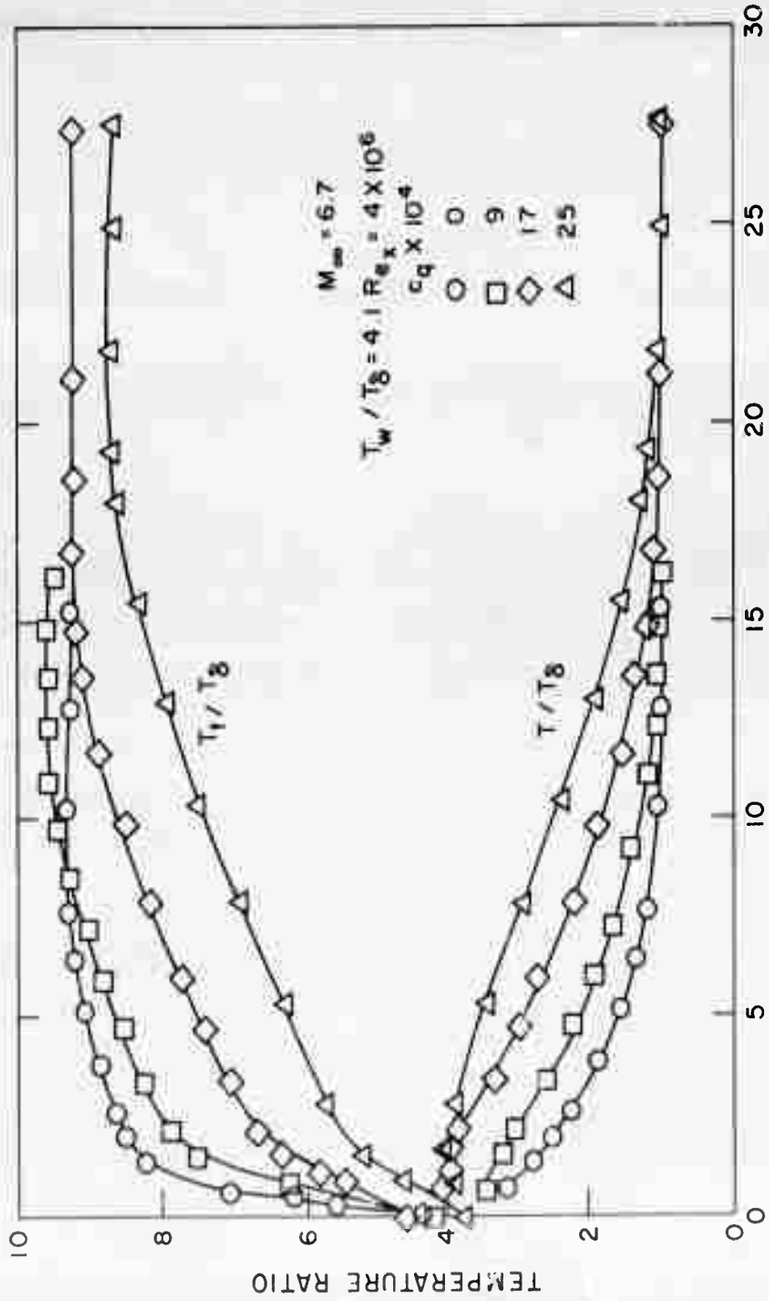

FIG. 15 EFFECT OF MASS TRANSFER ON COMPRESSIBLE TURBULENT BOUNDARY LAYER TOTAL AND STATIC TEMPERATURE PROFILES

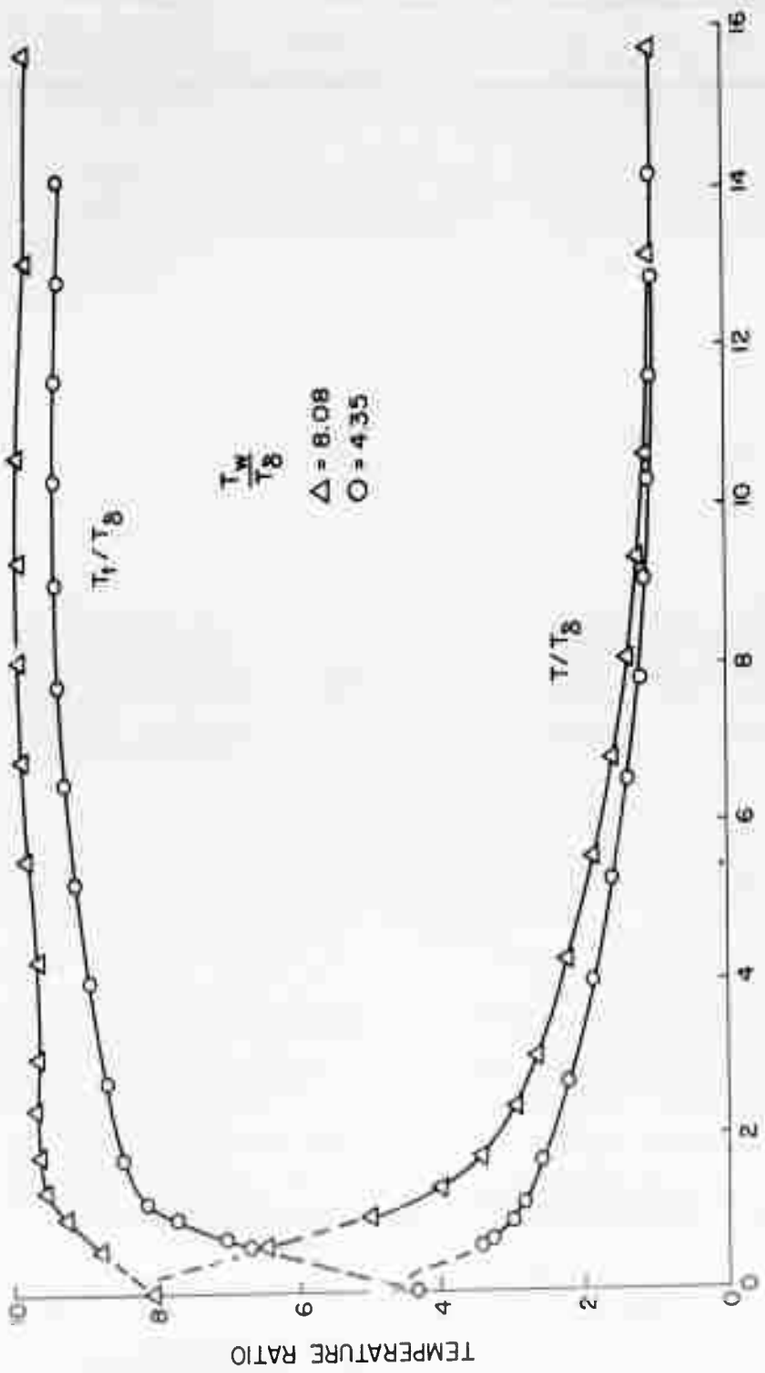

FIG. 16 EFFECT OF HEAT TRANSFER ON BOUNDARY LAYER TEMPERATURE PROFILES
$M_\infty = 6.7$, $Re_x = 4 \times 10^6$, $c_q = 0$

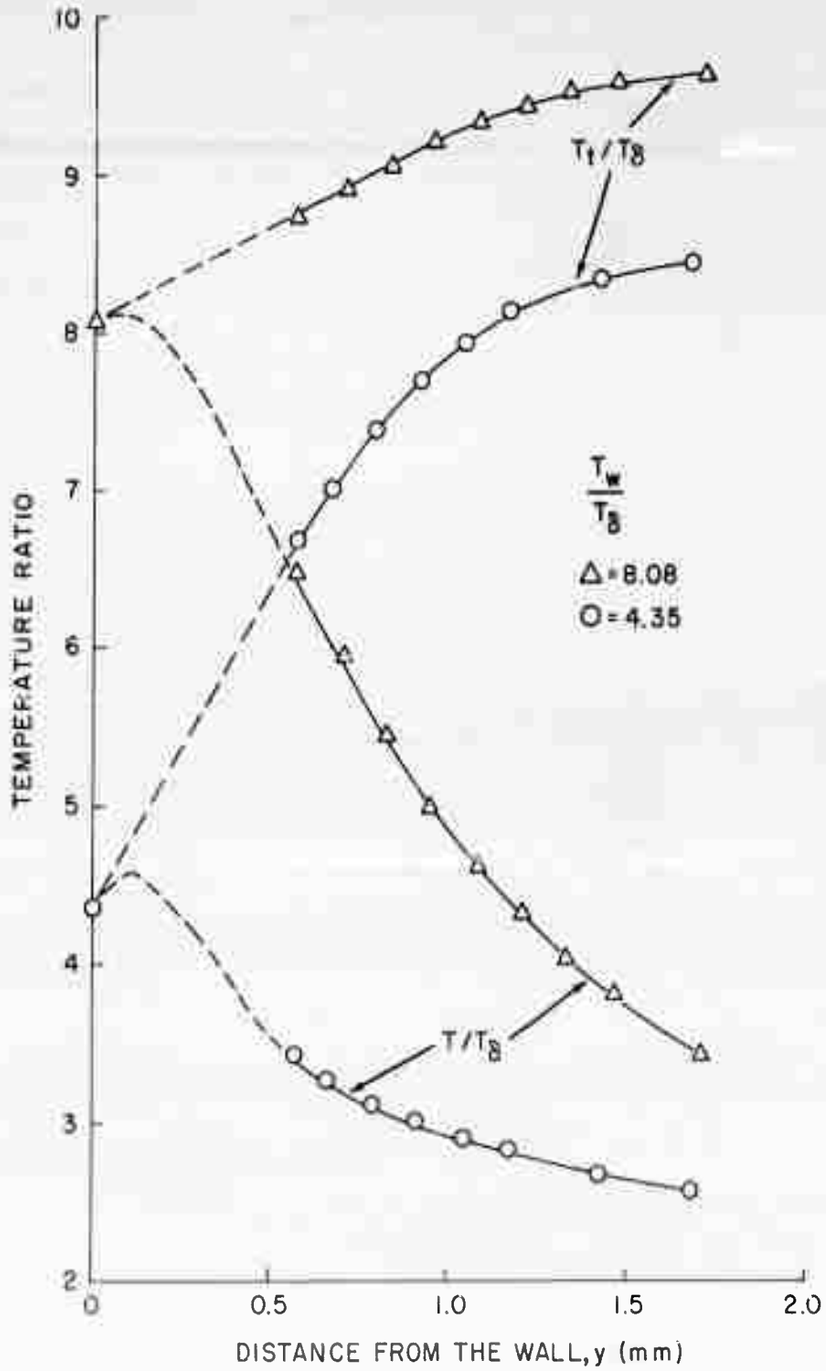

FIG. 17 BOUNDARY LAYER TEMPERATURE PROFILE NEAR THE WALL
$M_\infty = 6.7$, $Re_x\ 4 \times 10^6$, $c_q = 0$

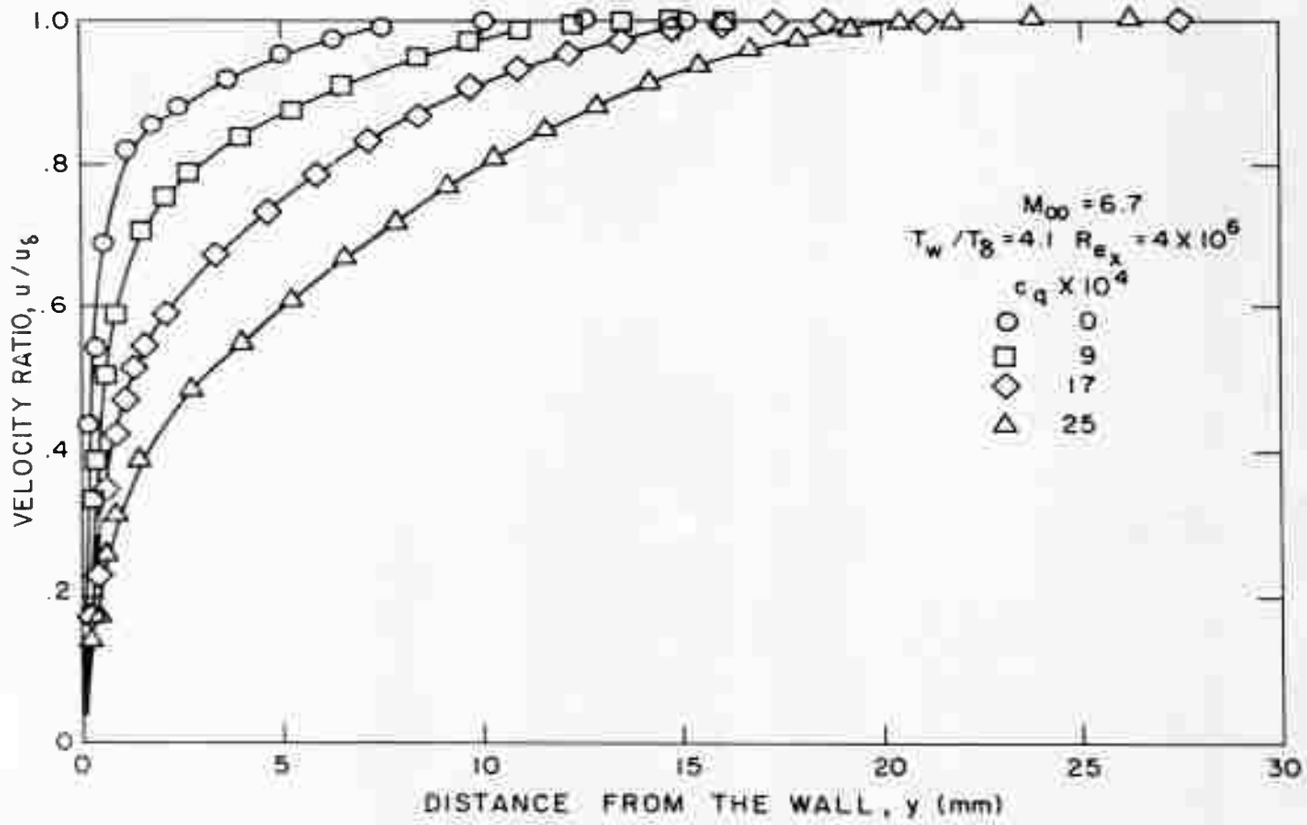

FIG. 18 EFFECT OF MASS TRANSFER ON COMPRESSIBLE TURBULENT BOUNDARY LAYER VELOCITY PROFILES

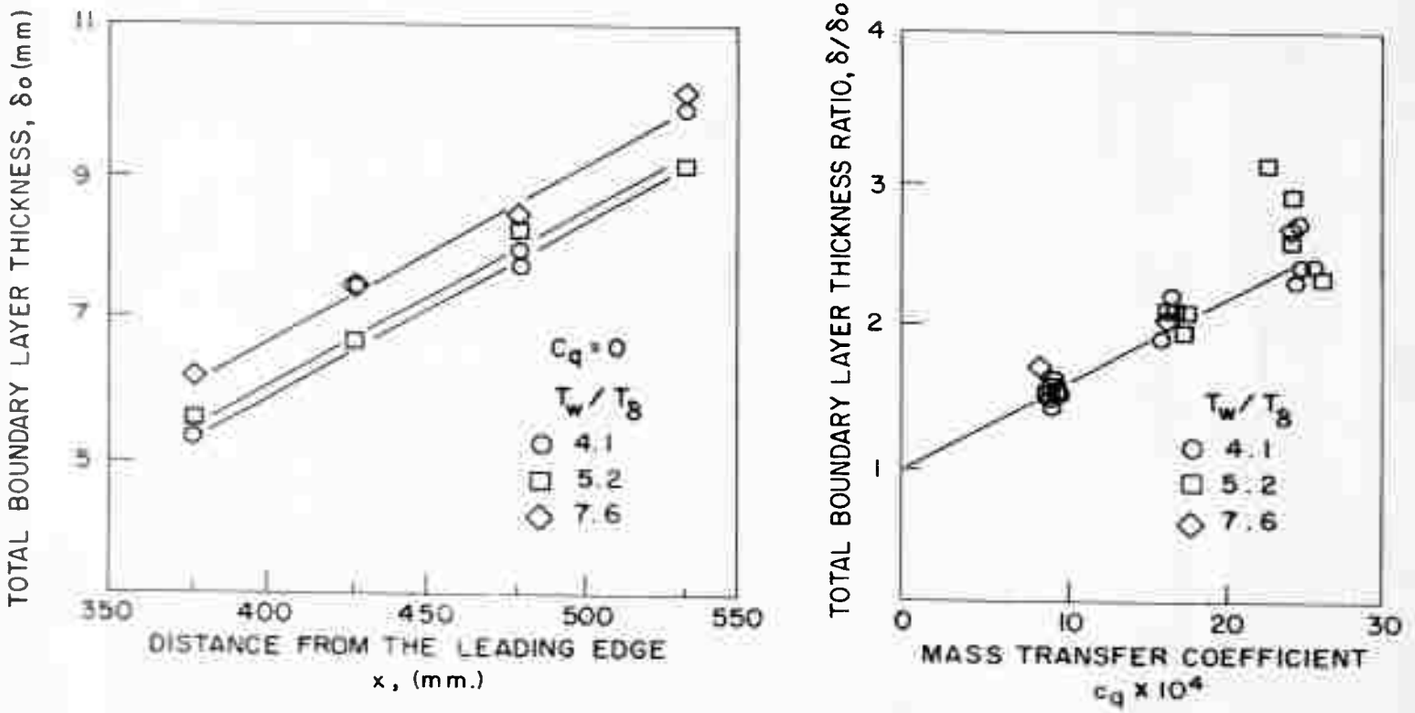

FIG. 19 EFFECT OF HEAT AND MASS TRANSFER ON TOTAL BOUNDARY LAYER THICKNESS

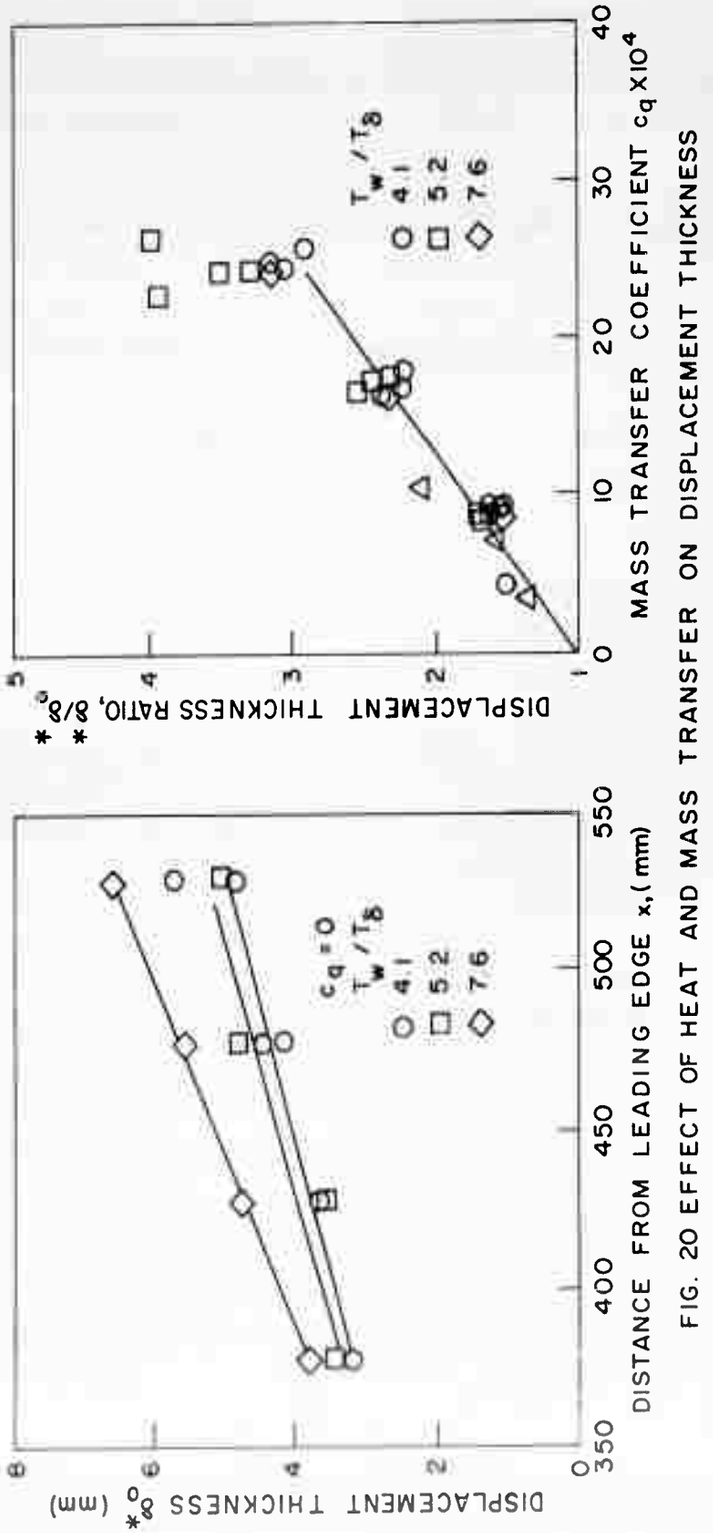

FIG. 20 EFFECT OF HEAT AND MASS TRANSFER ON DISPLACEMENT THICKNESS

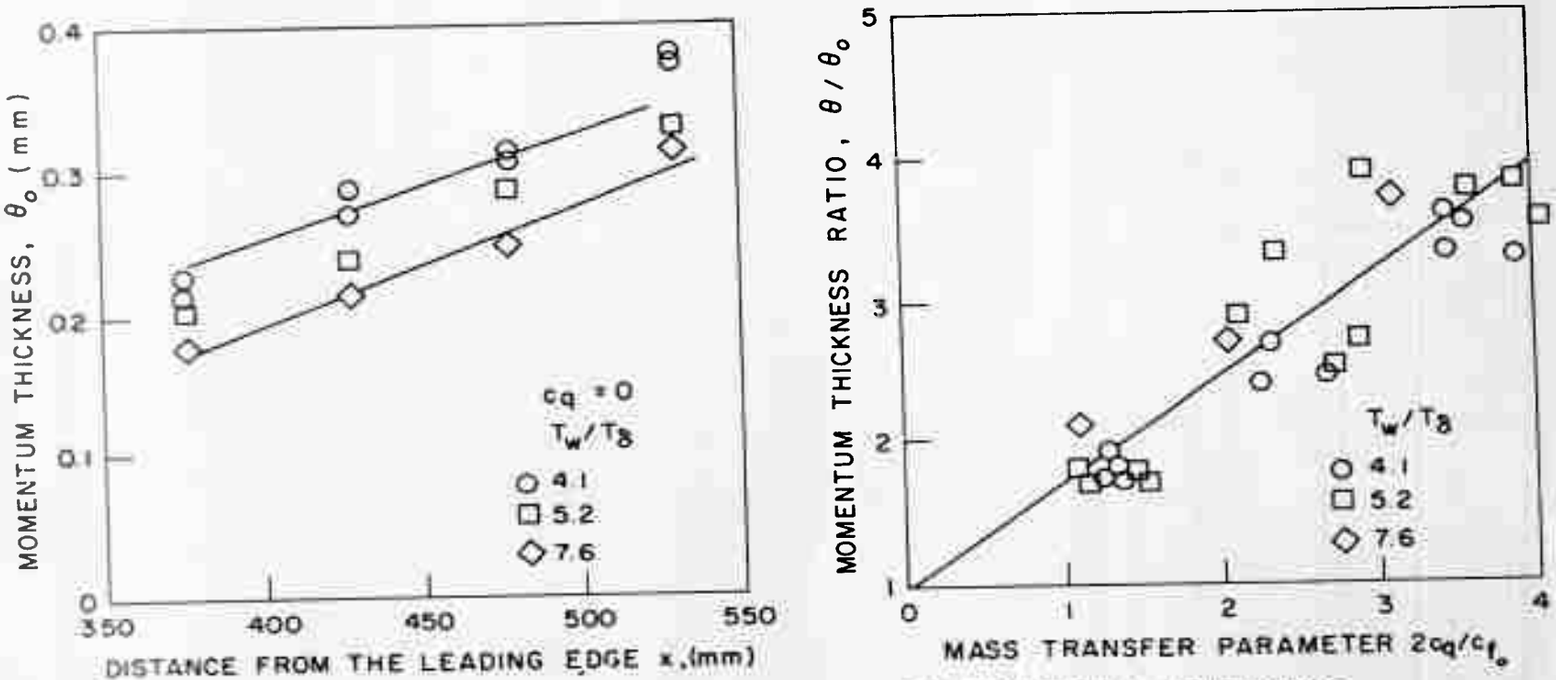

FIG. 21 EFFECT OF HEAT AND MASS TRANSFER ON MOMENTUM THICKNESS

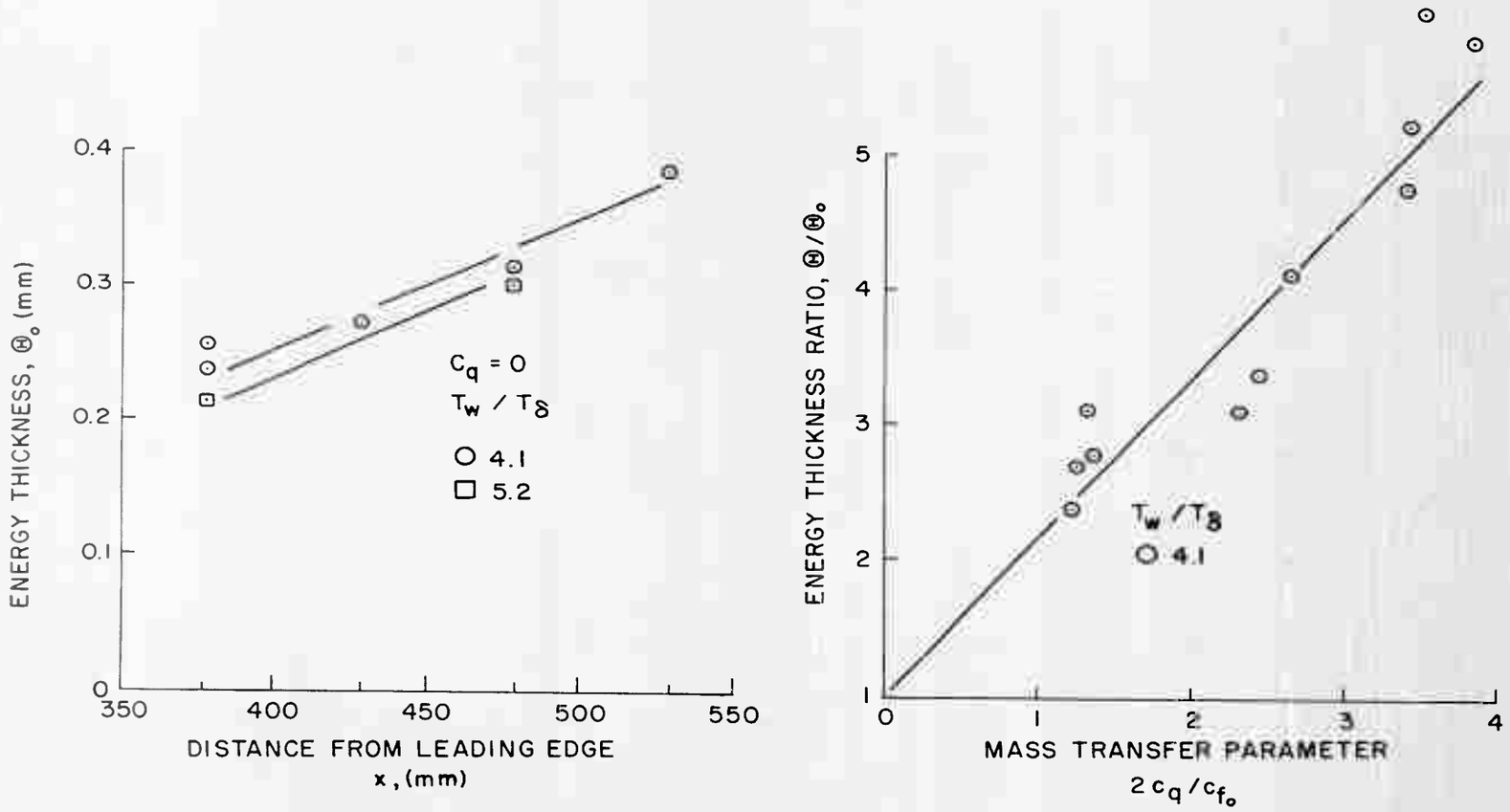

NOLTR 64-99

FIG. 22 EFFECT OF HEAT AND MASS TRANSFER ON ENERGY THICKNESS

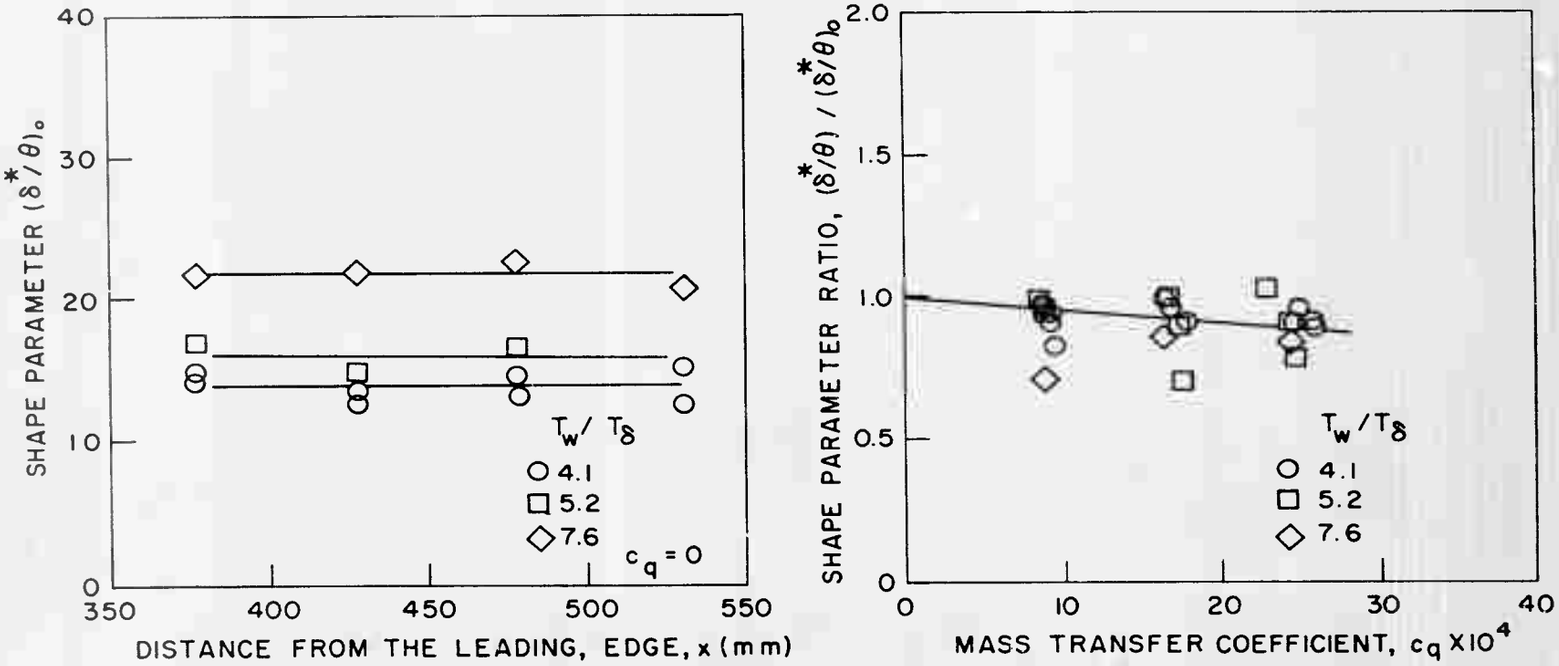

FIG. 23 EFFECT OF HEAT AND MASS TRANSFER ON SHAPE PARAMETER

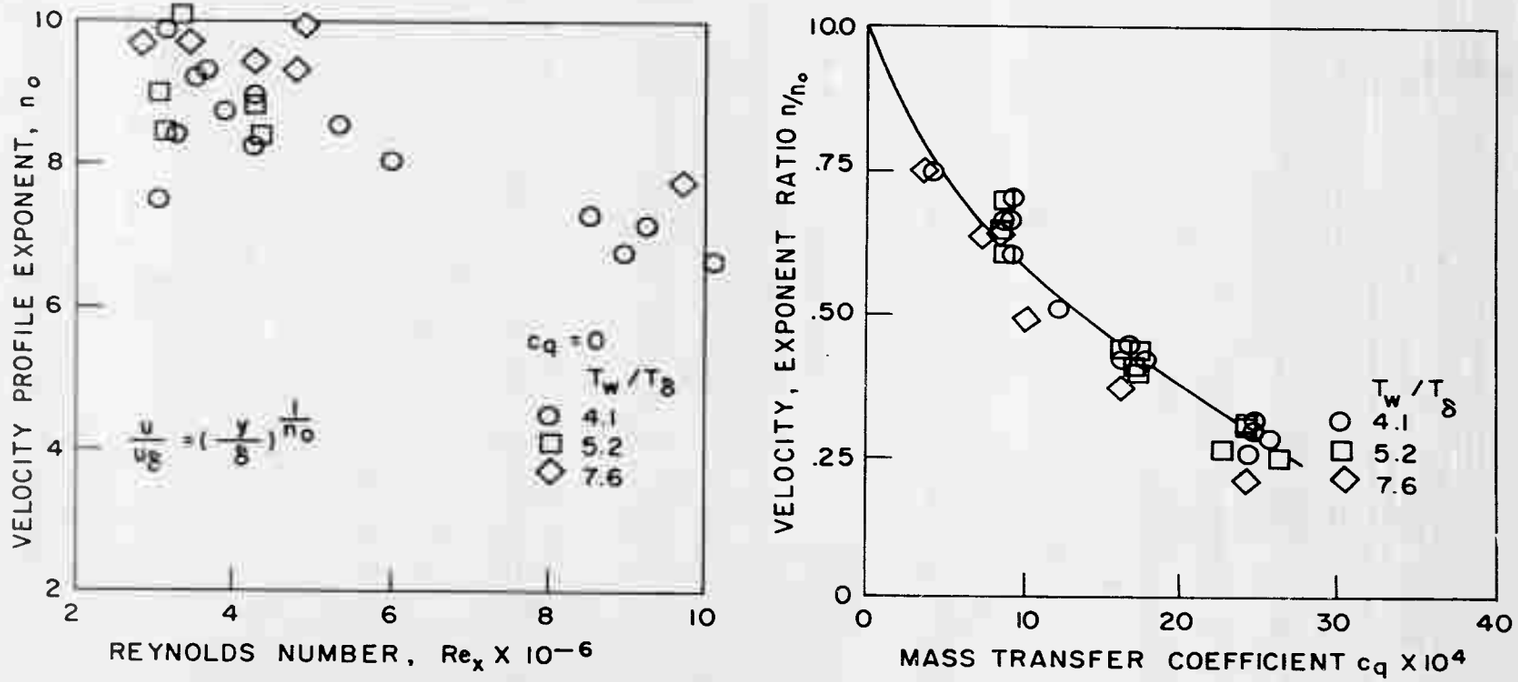

FIG. 24 EFFECT OF HEAT AND MASS TRANSFER ON VELOCITY PROFILE EXPONENT, n

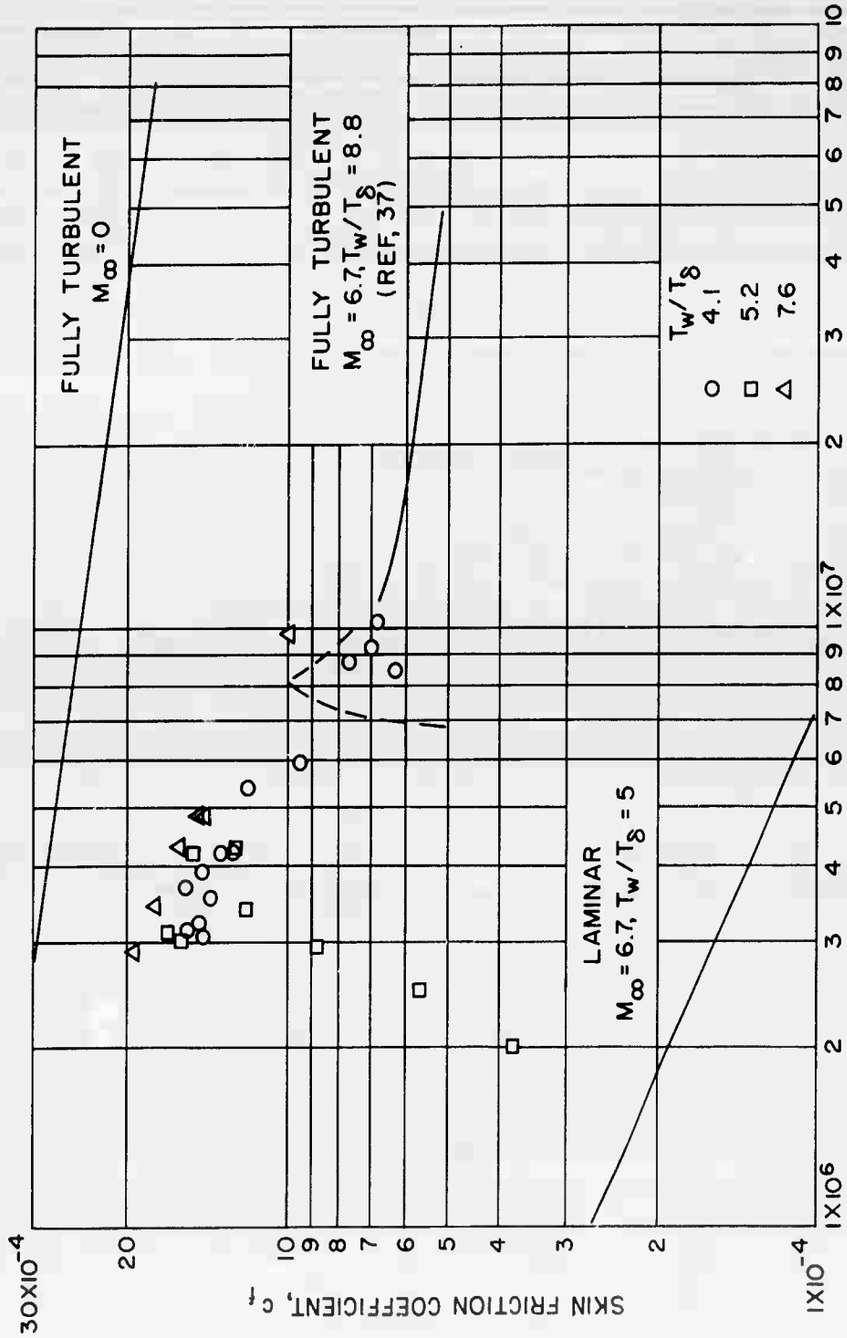

FIG. 25 VARIATION OF SKIN FRICTION WITH LENGTH REYNOLDS NUMBER

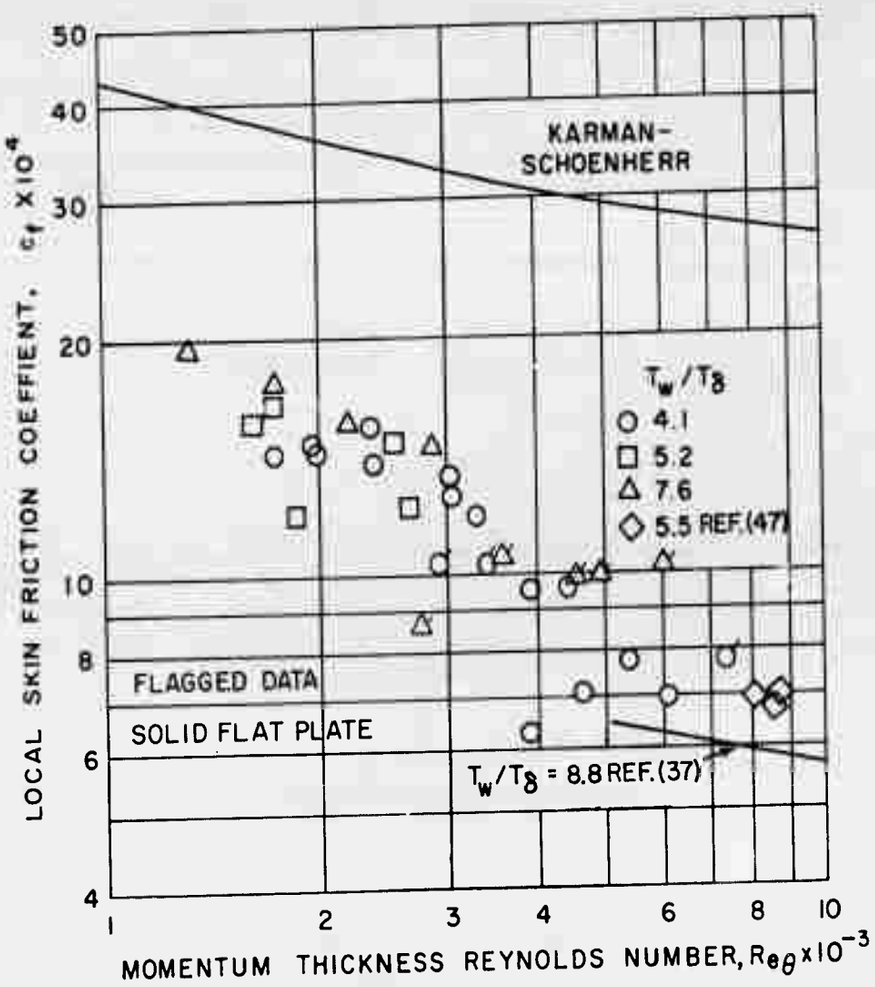

FIG. 26 VARIATION OF SKIN FRICTION COEFFICIENT WITH MOMENTUM THICKNESS REYNOLDS NUMBER

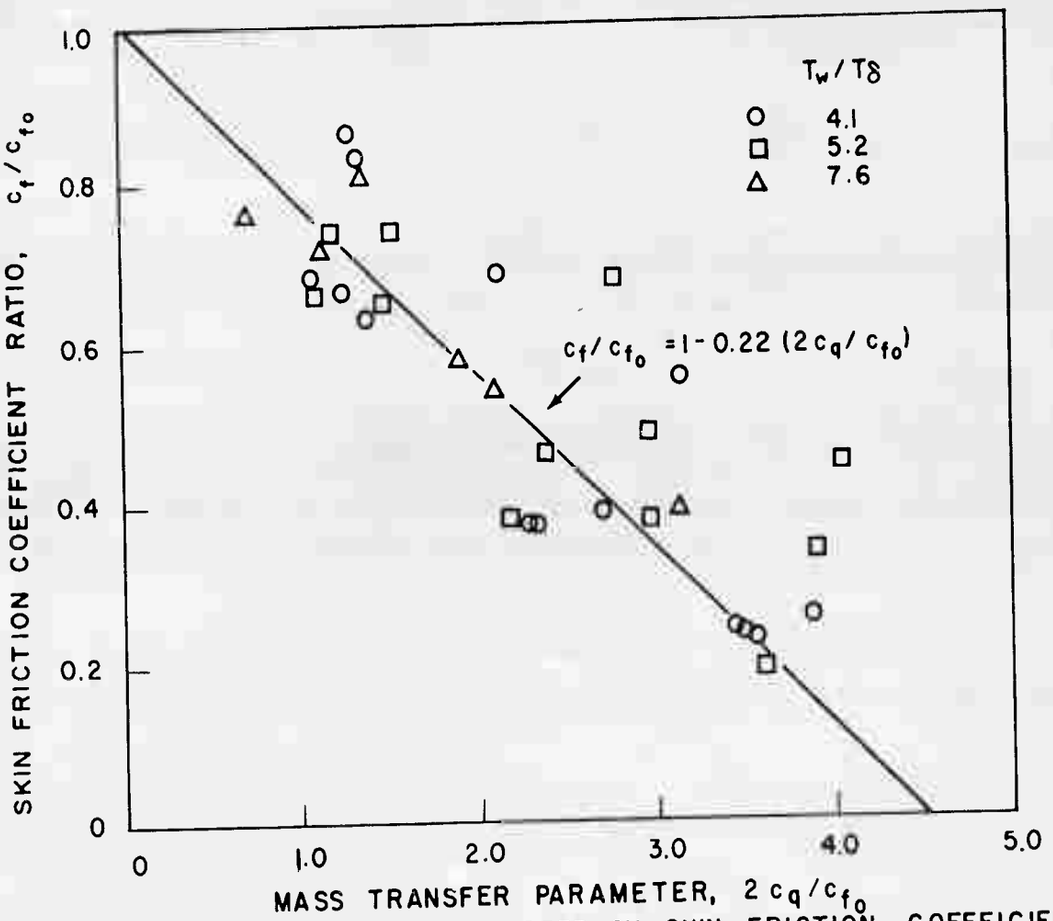

FIG 27 EFFECT OF MASS TRANSFER ON SKIN FRICTION COEFFICIENT

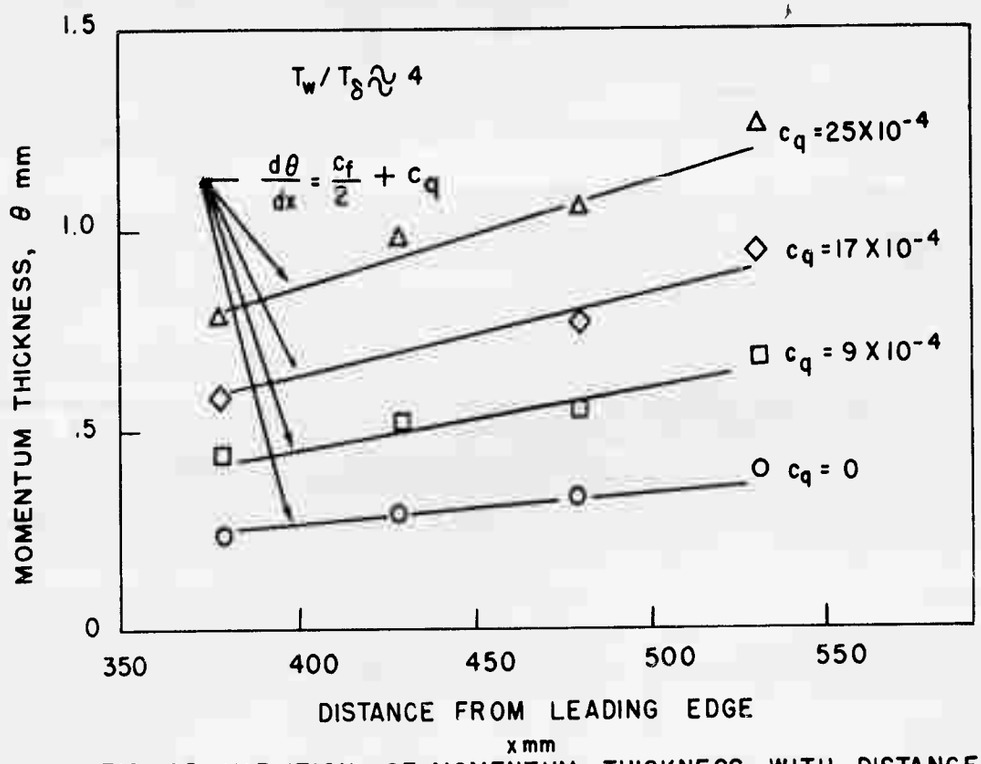

FIG. 28 VARIATION OF MOMENTUM THICKNESS WITH DISTANCE FROM THE LEADING EDGE FOR FOUR RATES OF MASS TRANSFER.

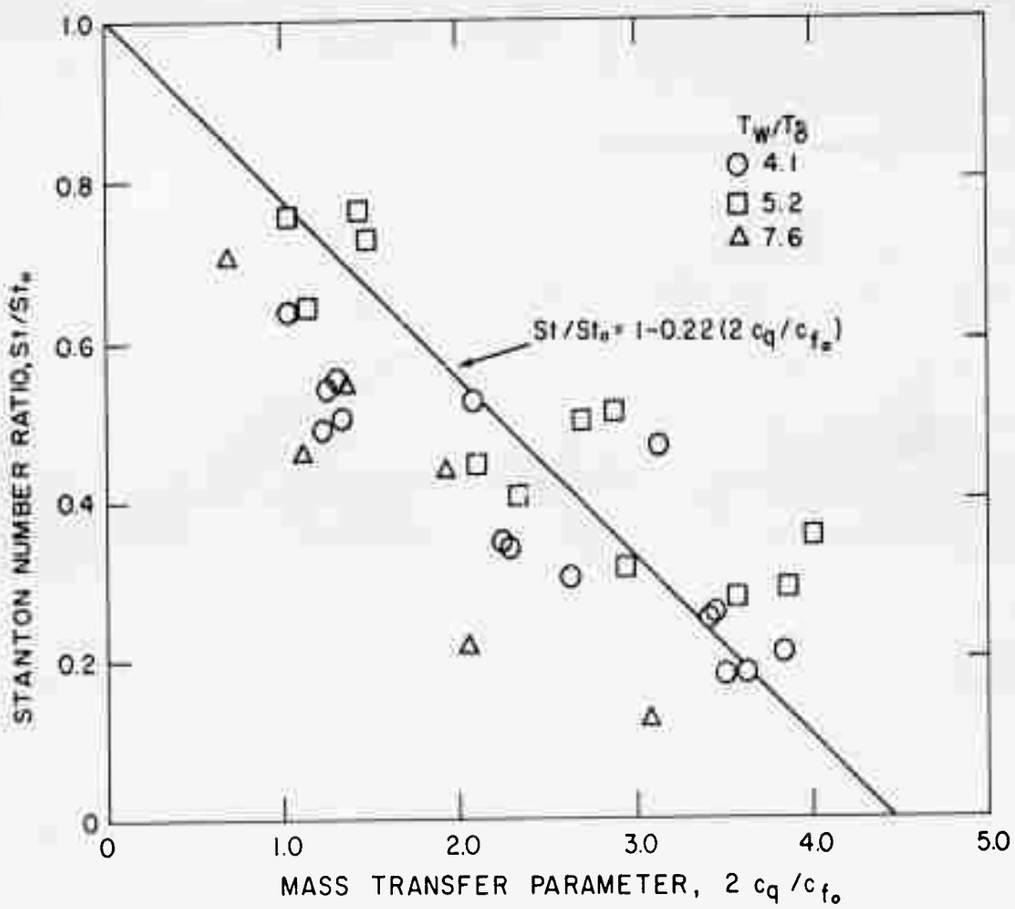

FIG. 29 EFFECT OF MASS TRANSFER ON STANTON NUMBER

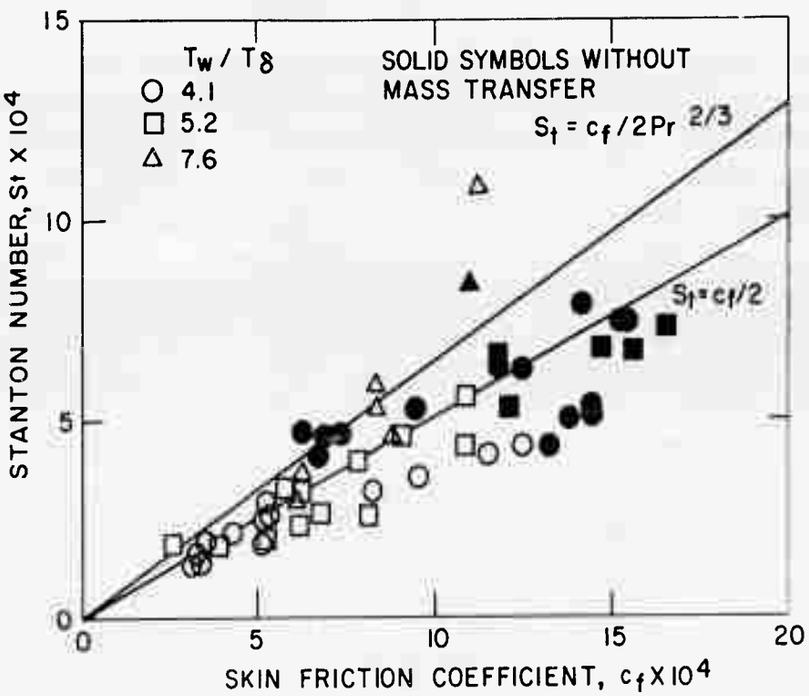

FIG. 30 REYNOLDS ANALOGY WITH AND WITHOUT MASS TRANSFER

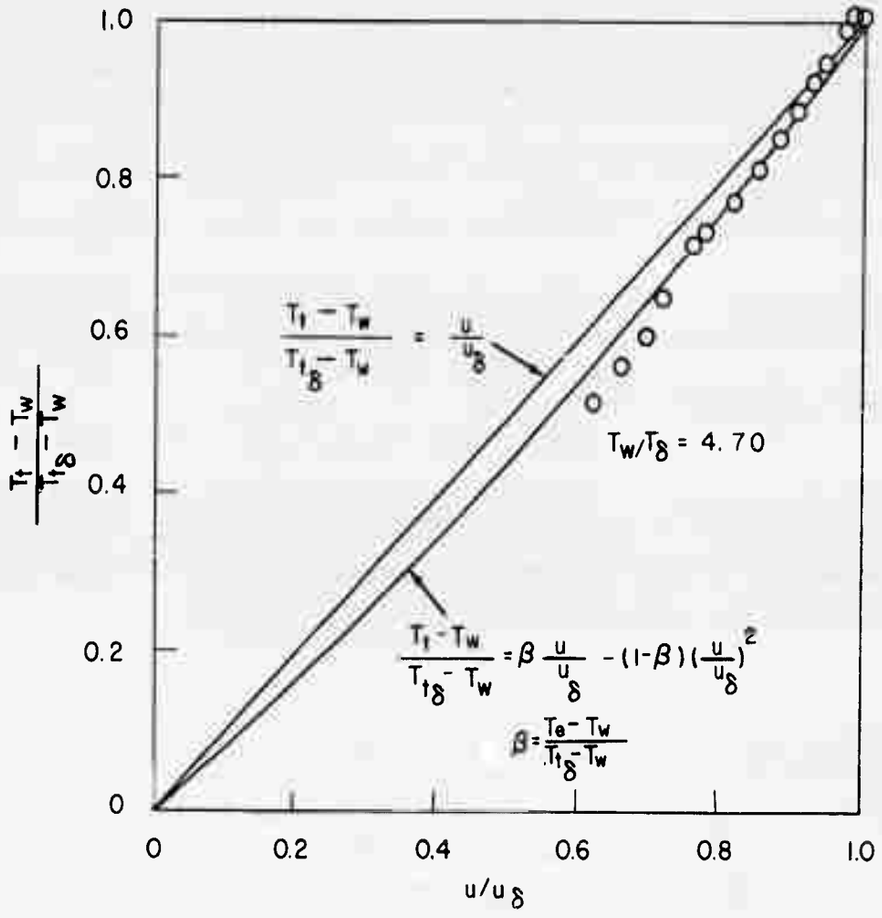

FIG. 31 COMPARISON OF EXPERIMENTAL AND THEORETICAL TEMPERATURE - VELOCITY DISTRIBUTIONS

$M_\delta = 6.37$, $Re_x = 10.1 \times 10^6$

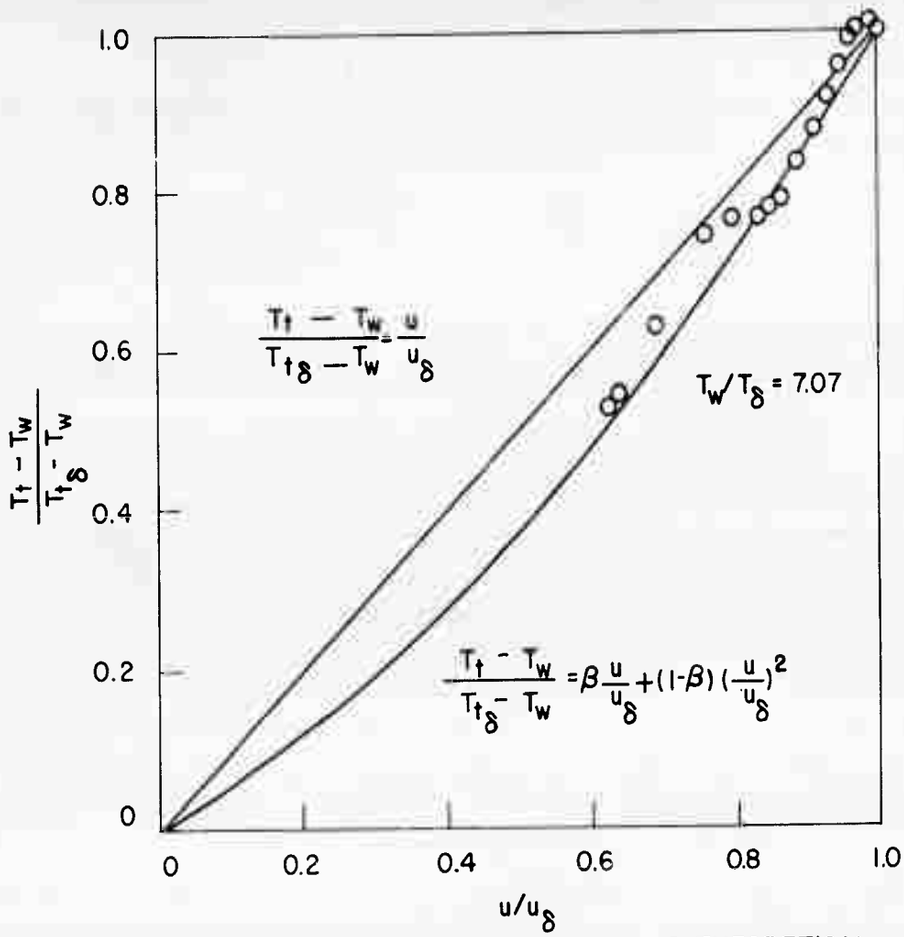

FIG. 32 COMPARISON OF EXPERIMENTAL AND THEORETICAL TEMPERATURE-VELOCITY DISTRIBUTIONS

$M_\delta = 6.34 \quad Re_x = 9.7 \times 10^6$

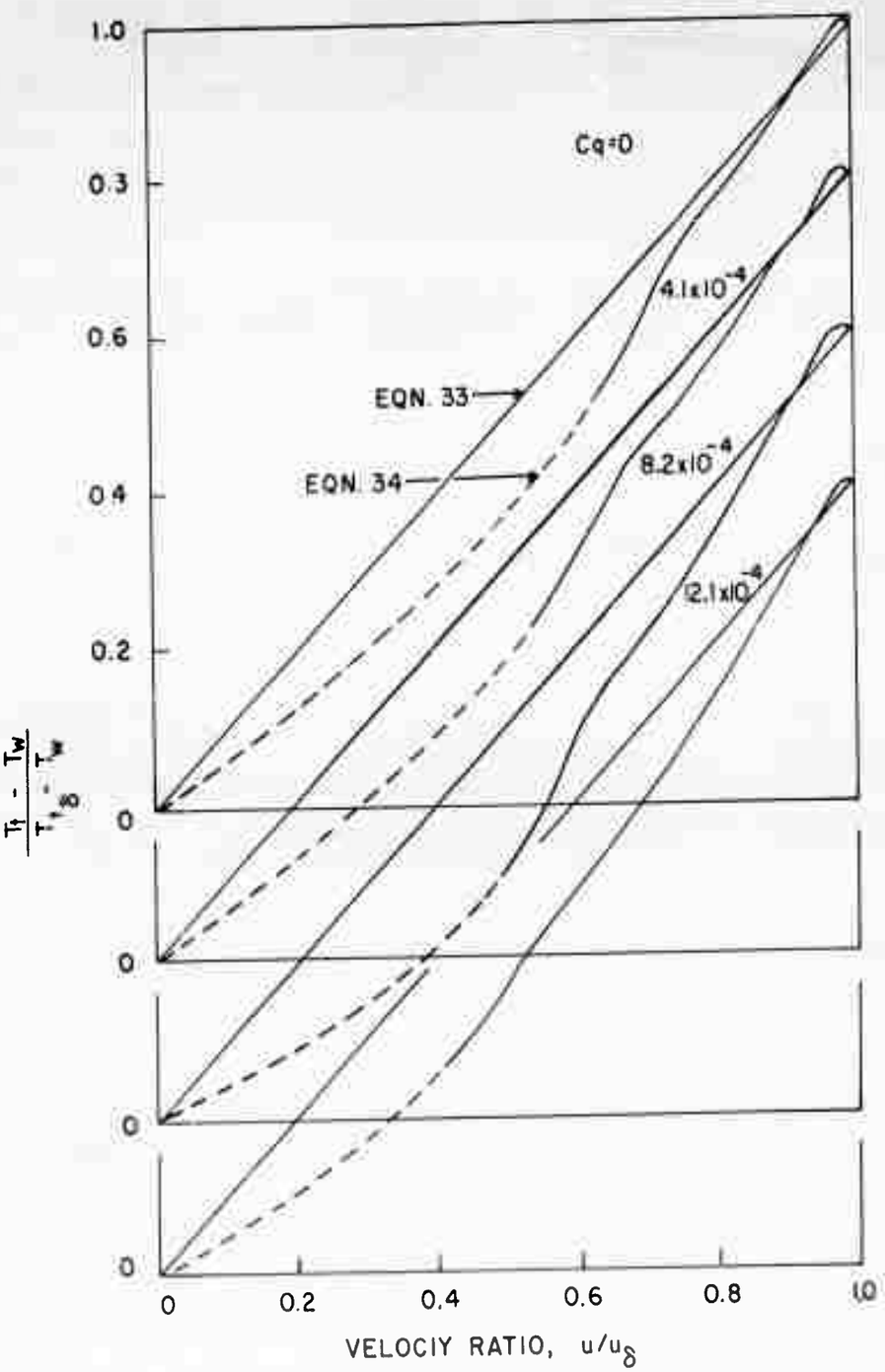

FIG. 33 EFFECT OF MASS TRANSFER ON THE TEMPERATURE- VELOCITY RELATION

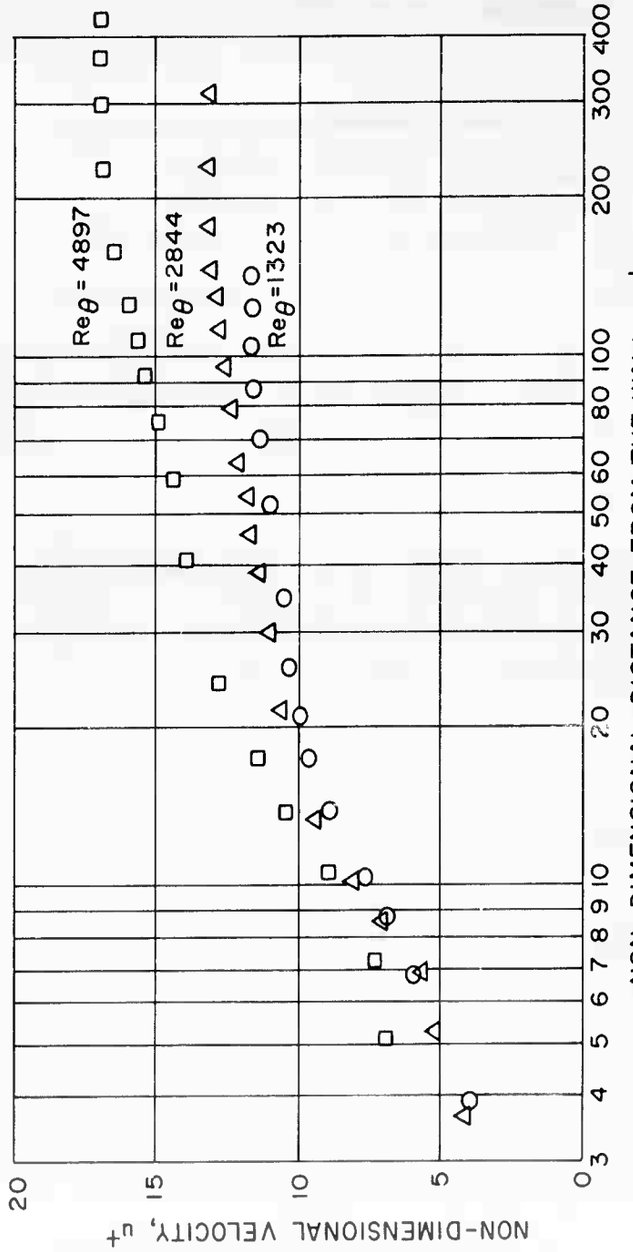

FIG.34 EFFECT OF REYNOLDS NUMBER ON NON-DIMENSIONAL VELOCITY PROFILE ($T_w/T_\delta \cong 4$)

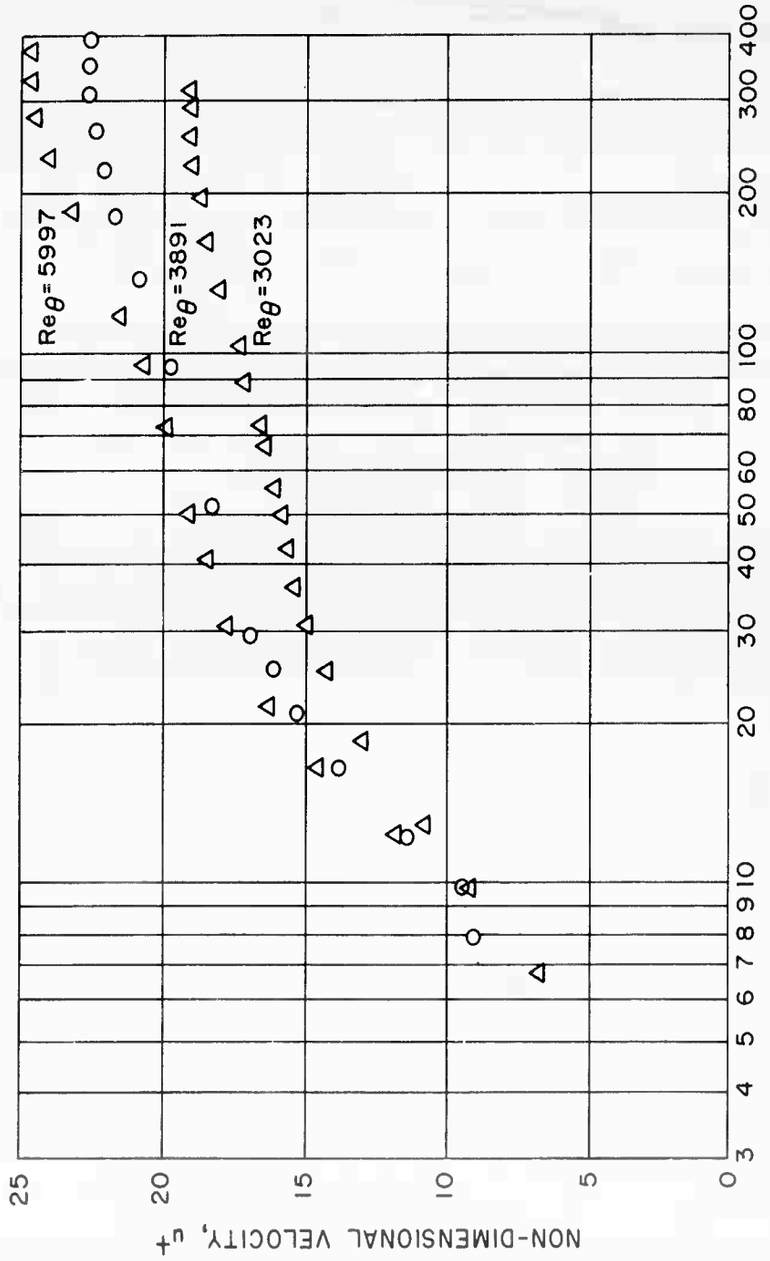

FIG. 35 EFFECT OF REYNOLDS NUMBER ON NON-DIMENSIONAL VELOCITY PROFILE ($T_w/T_\delta \cong 7$)

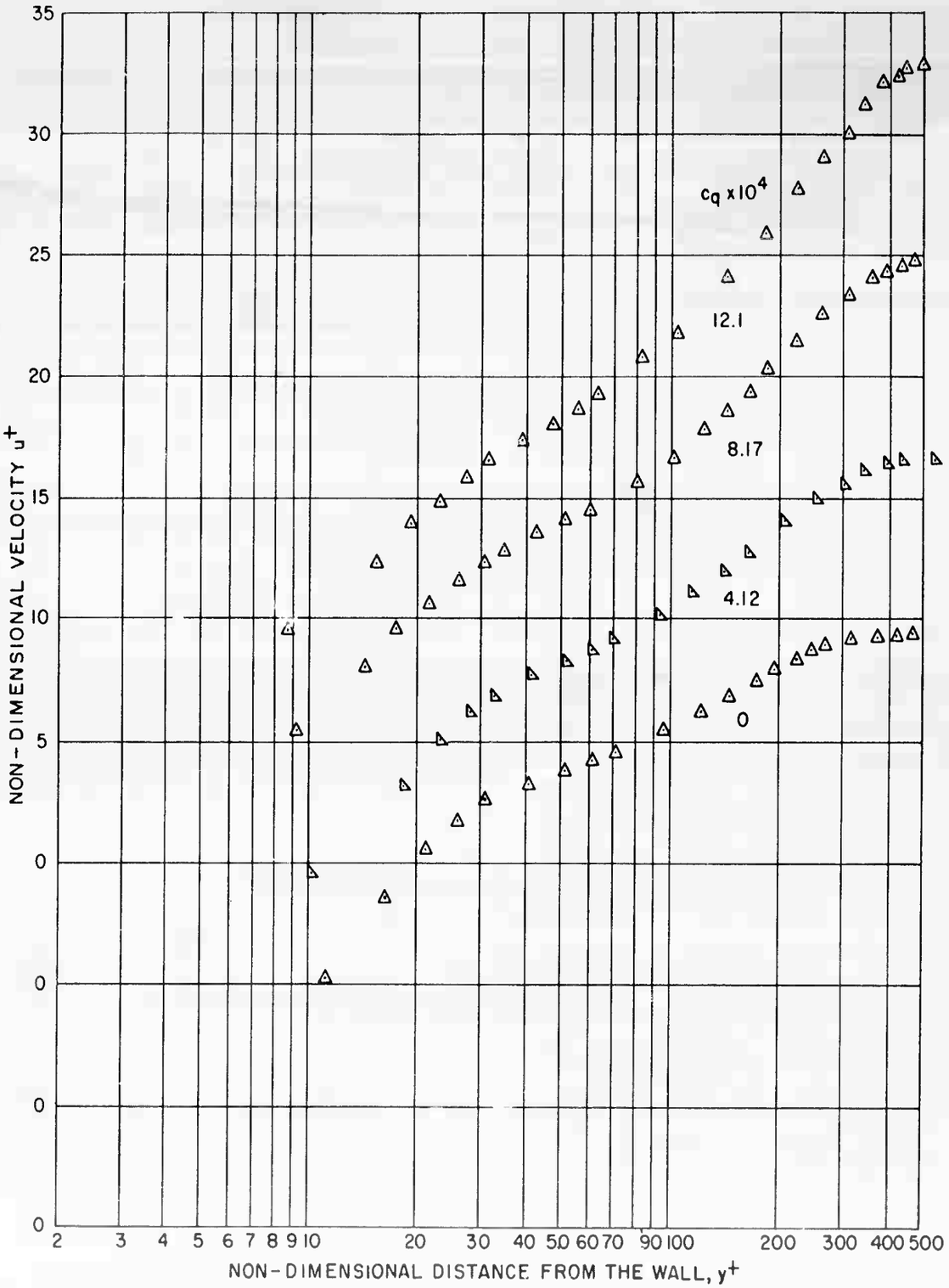

FIG. 36 EFFECT OF MASS TRANSFER ON NON-DIMENSIONAL VELOCITY PROFILE ($T_w / T_\delta = 4$)

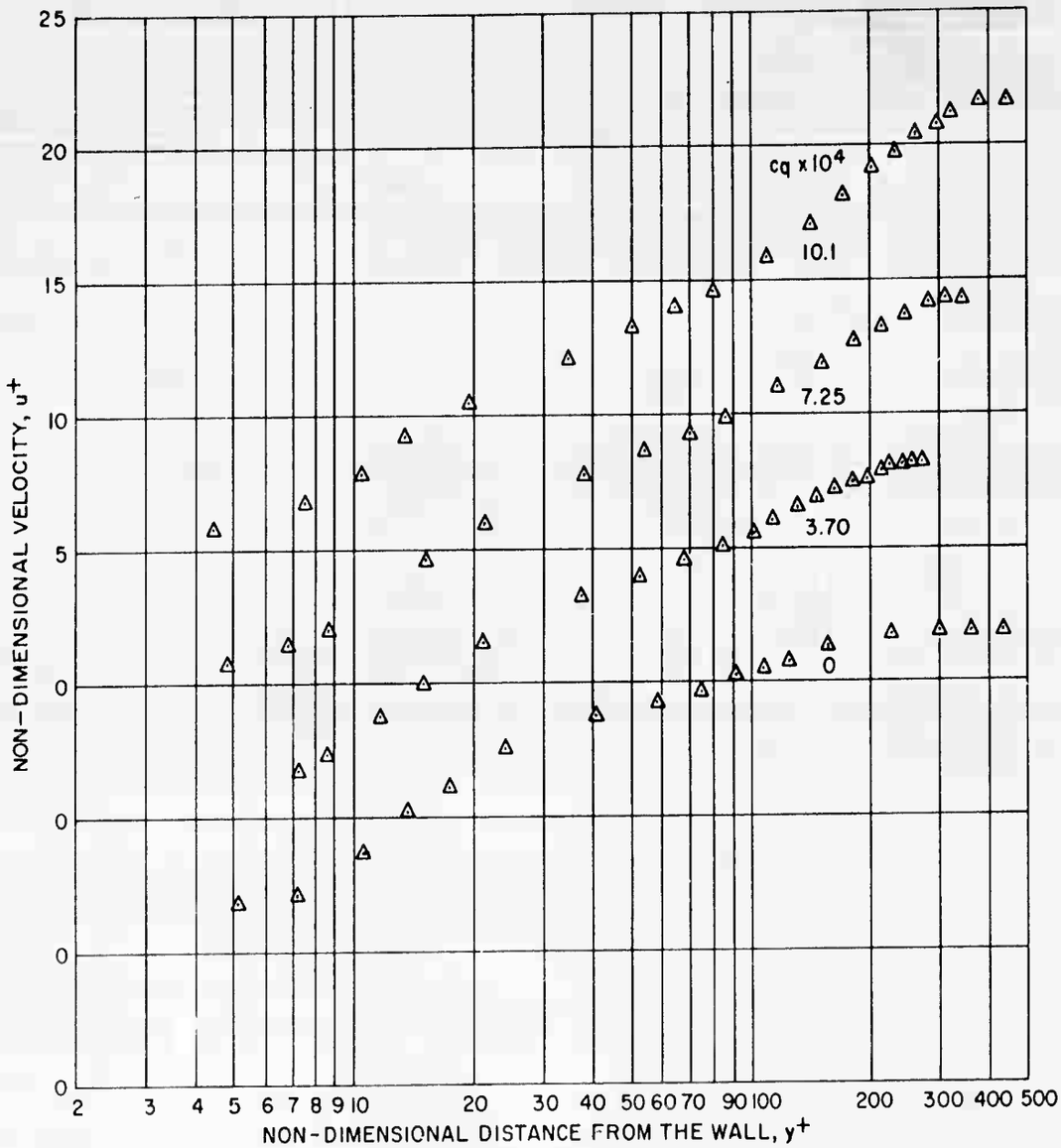

FIG. 37 EFFECT OF MASS TRANSFER ON NON-DIMENSIONAL VELOCITY PROFILE ($T_w/T_\delta = 7$)

M	REF.
◇ 2.43	MONAGHAN & COOKE
⌂ 2-4.5	COLES
⬯ 1.8-3	MICHEL
◺ 3,4.2	MATTING ET. AL,
□ 5	LOBB ET AL
⬡ 0	SMITH & WALKER
⌂ 0	REYNOLDS ET AL
▨ 0	SUMMARIES BY COLES ROSS CLAUSER

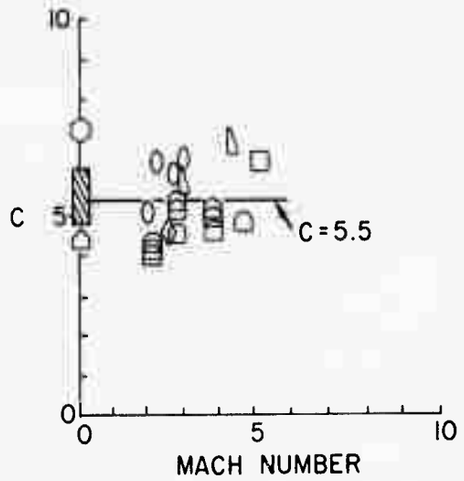

FIG. 38 EFFECT OF MACH NUMBER ON VELOCITY PROFILE CONSTANT
$T_W = T_e$, $c_q = 0$

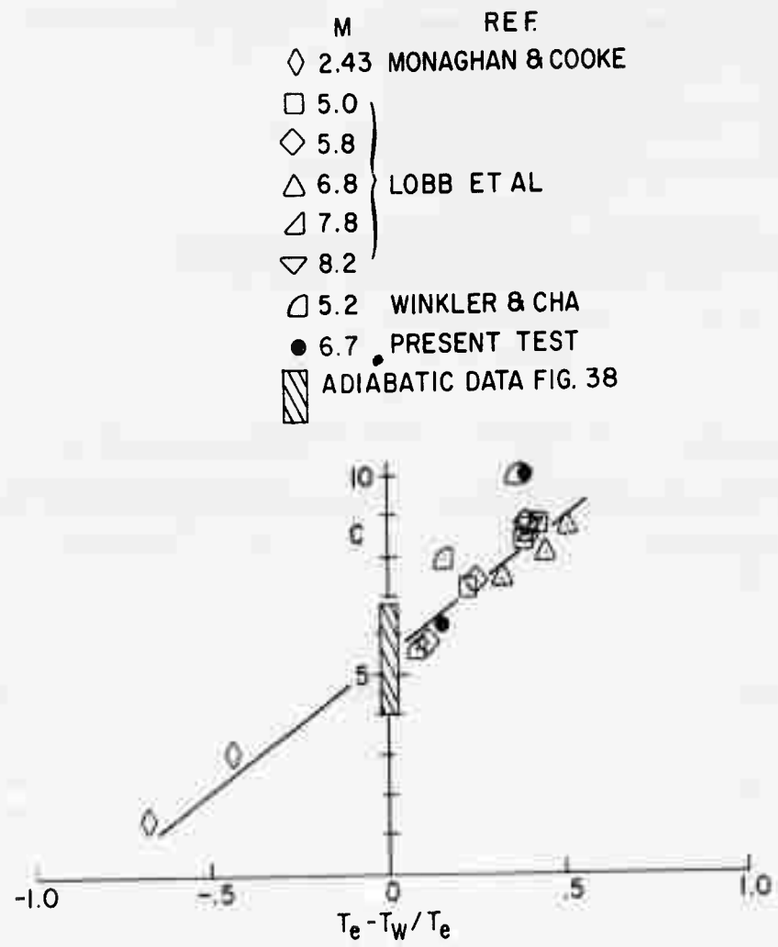

FIG. 39 EFFECT OF HEAT TRANSFER ON VELOCITY PROFILE CONSTANT ($c_q = 0$)

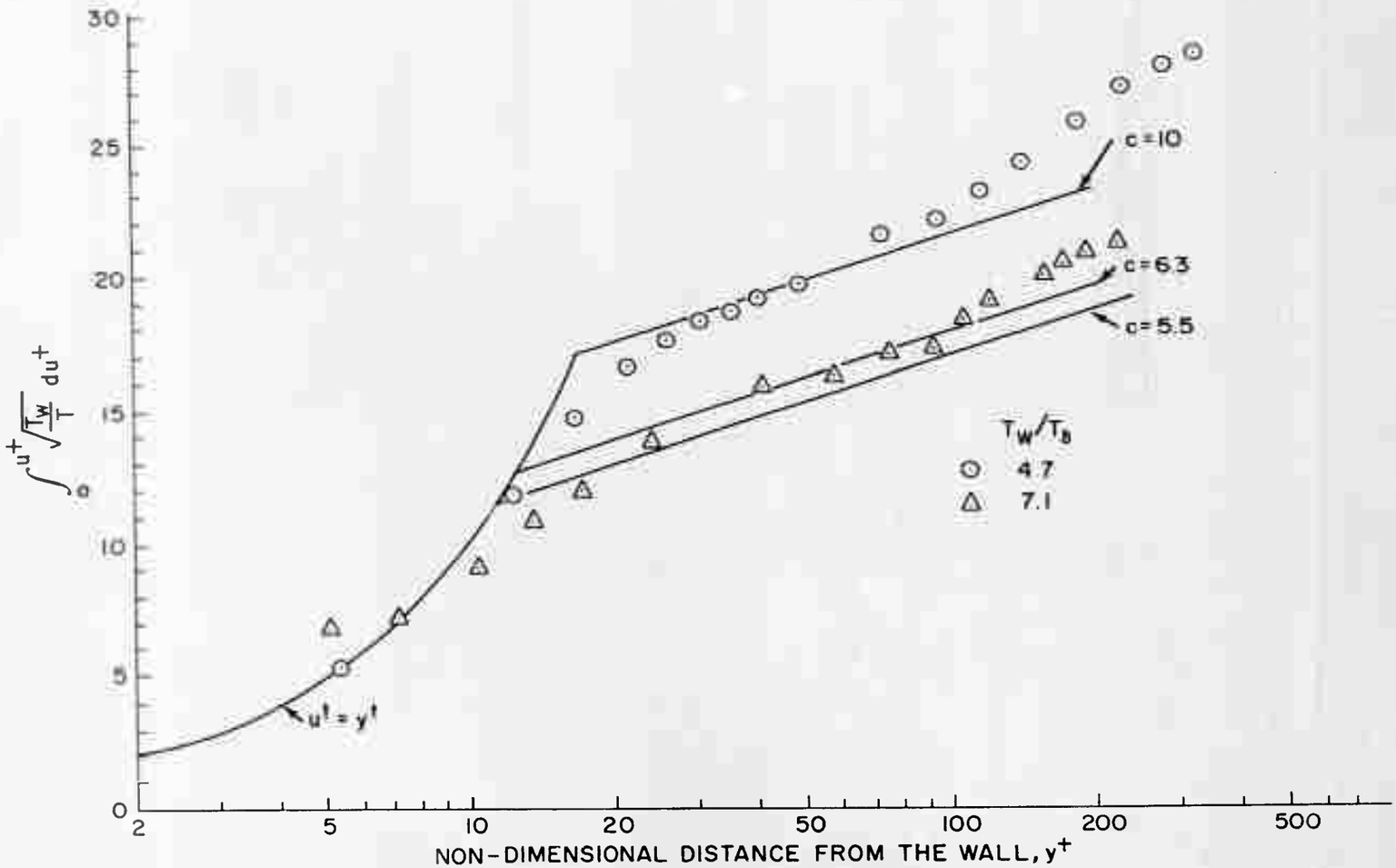

FIG. 40 EFFECT OF HEAT TRANSFER ON TRANSFORMED VELOCITY PROFILE

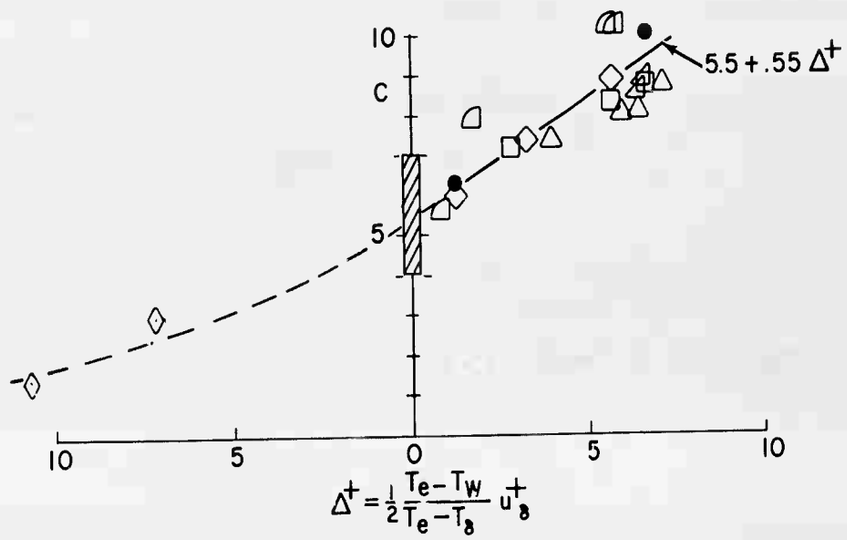

FIG. 41 EFFECT OF HEAT TRANSFER ON VELOCITY PROFILE CONSTANT ($c_q = 0$)

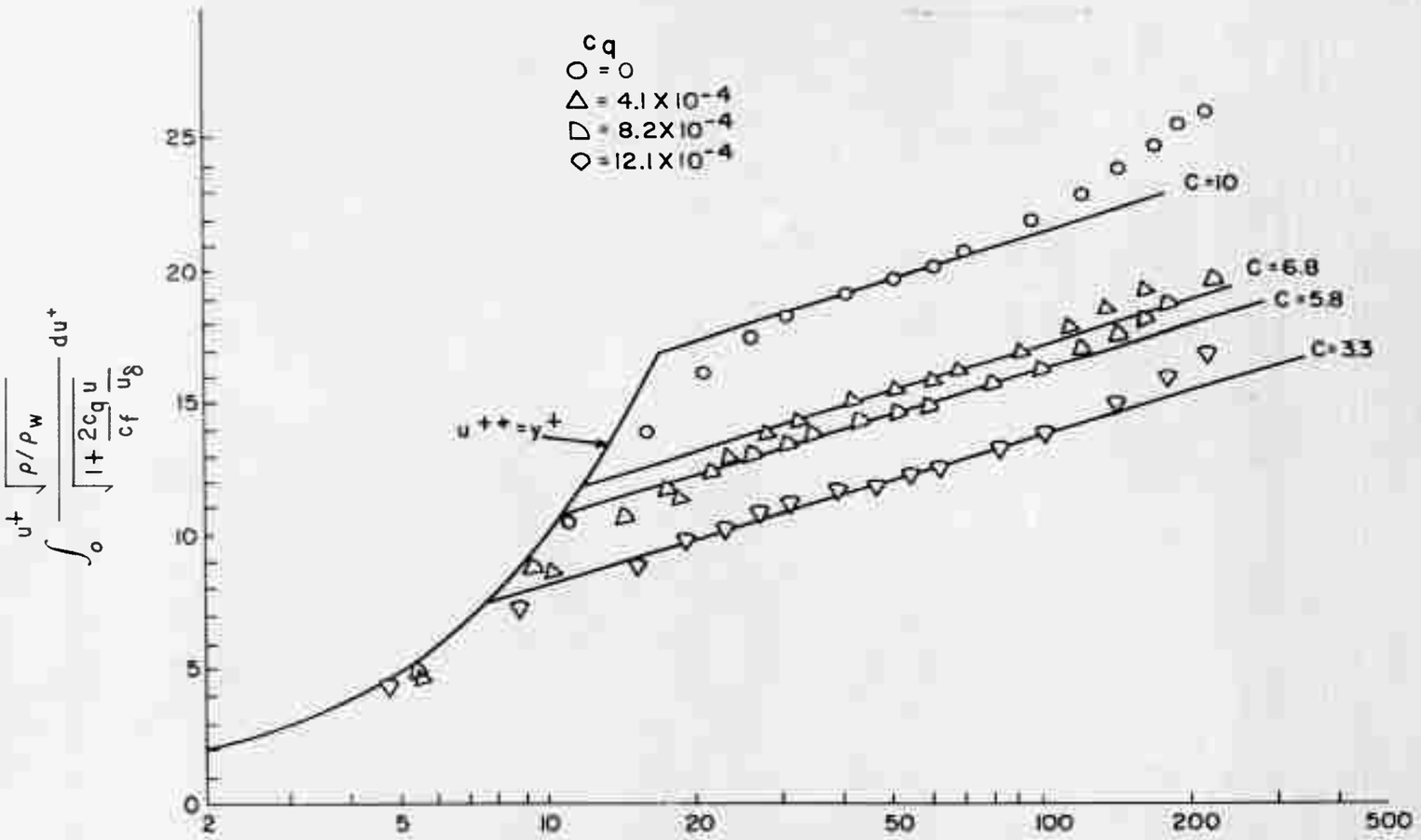

FIG 42 EFFECT OF MASS TRANSFER ON THE TRANSFORMED VELOCITY PROFILE ($T_w/T_\delta \cong 4$)

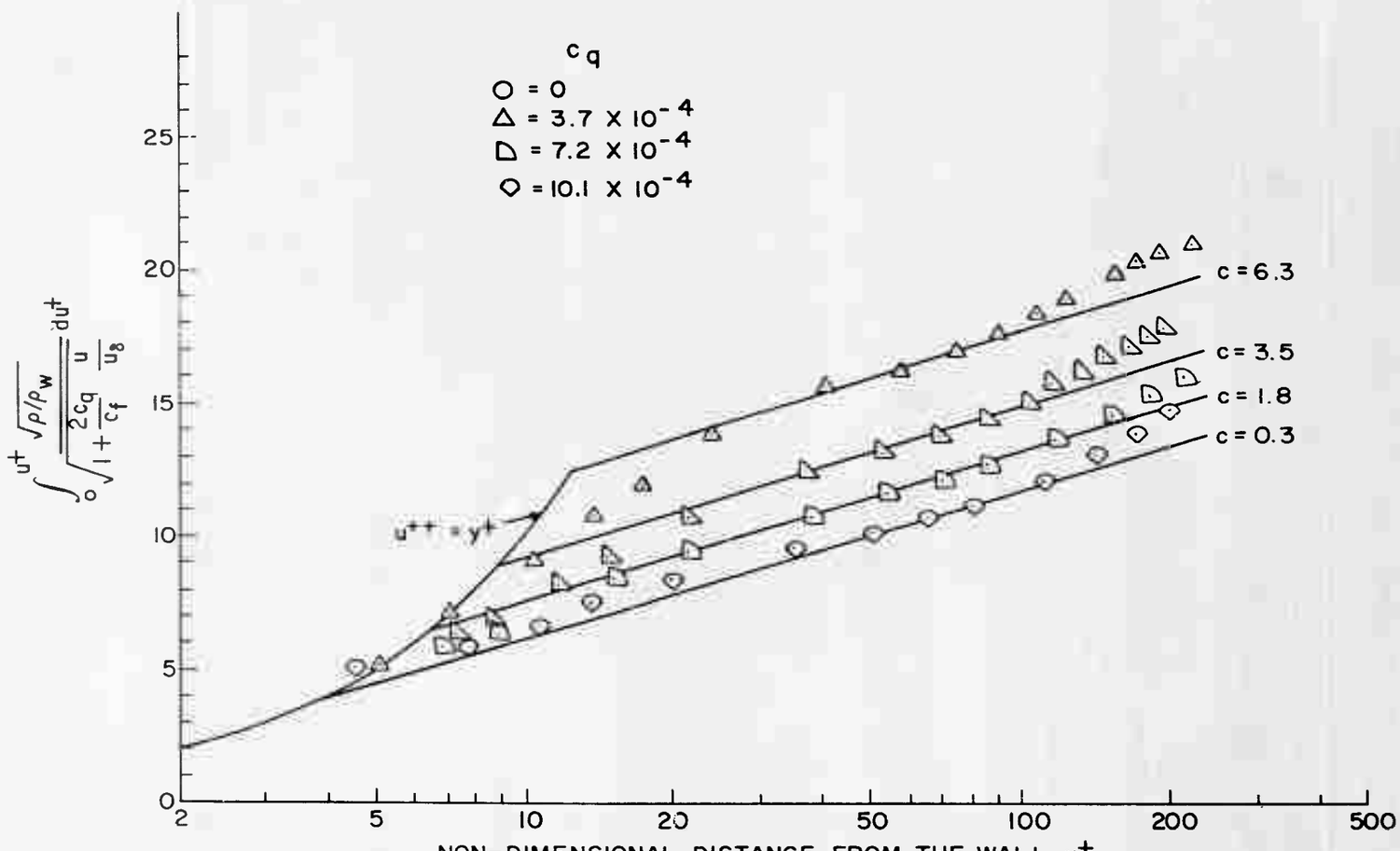

FIG. 43 EFFECT OF MASS TRANSFER ON TRANSFORMED VELOCITY PROFILE ($T_w / T_s \cong 7$)

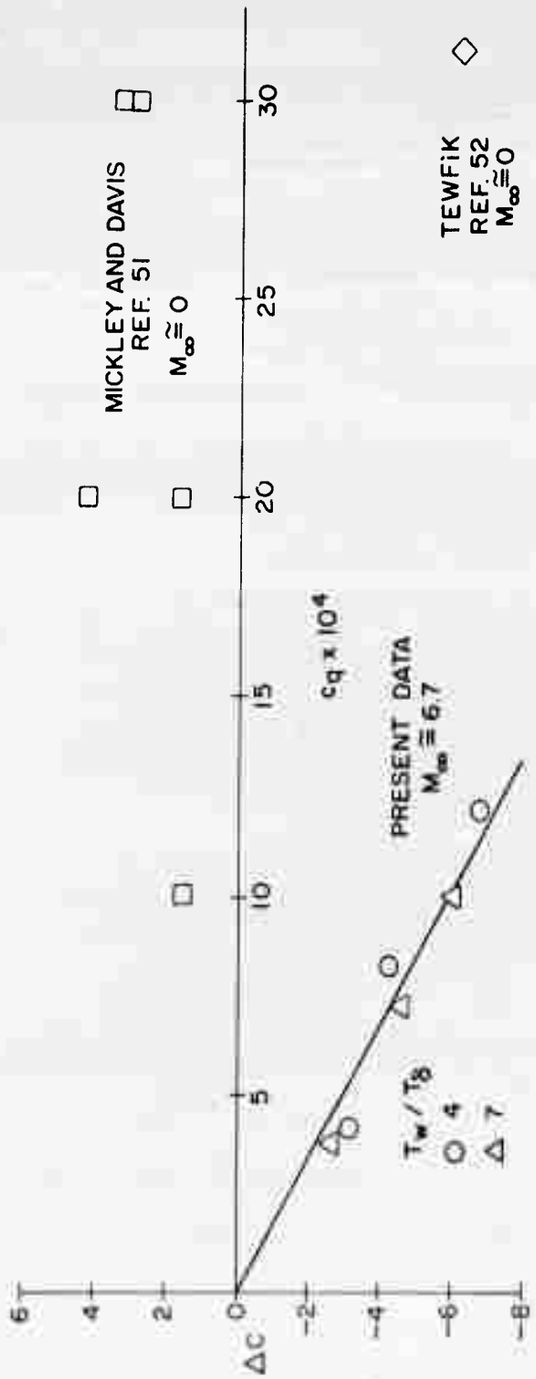

FIG. 44 EFFECT OF MASS TRANSFER ON THE PROFILE CONSTANT

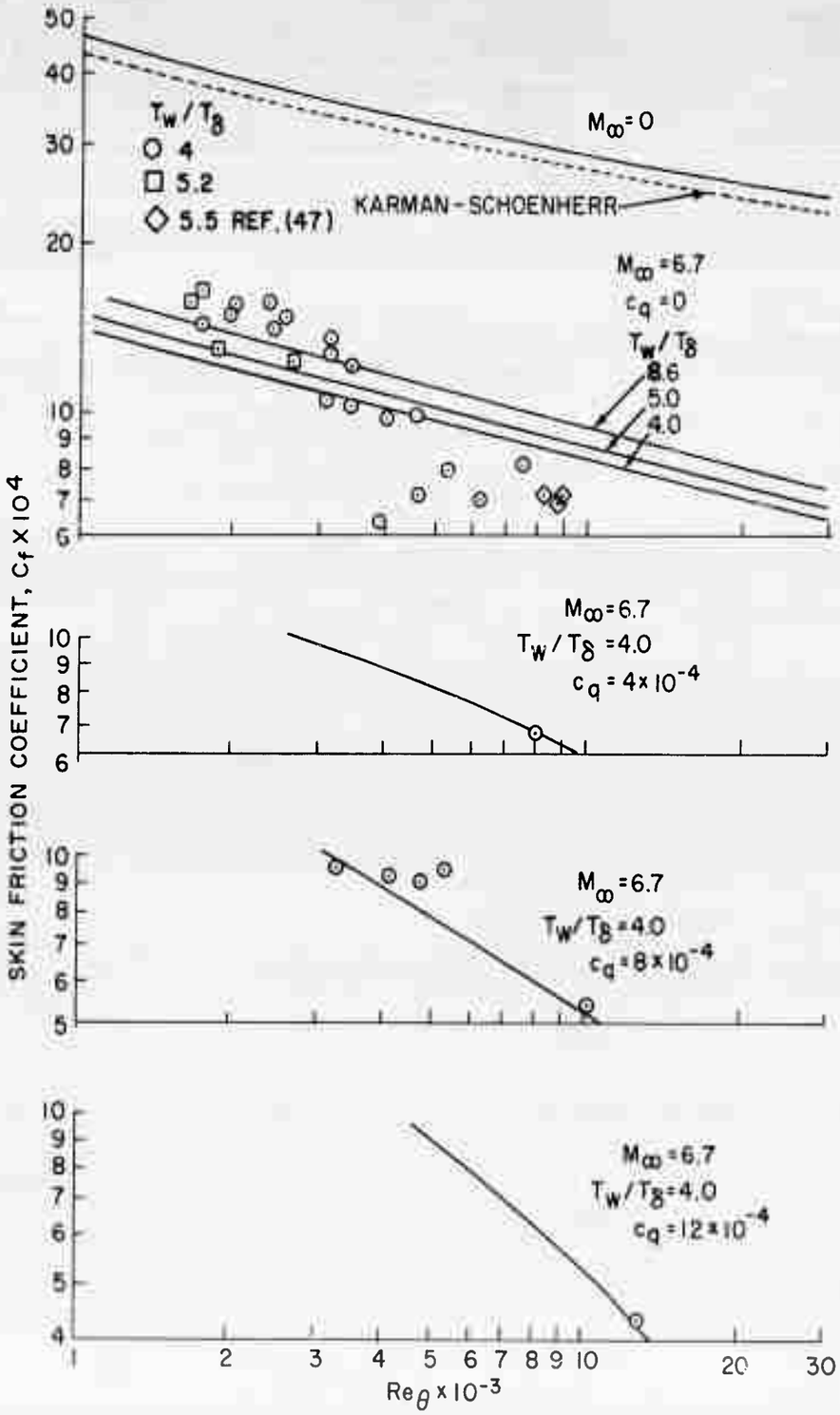

FIG. 45 COMPARISON BETWEEN ANALYSIS AND MEASUREMENT OF SKIN FRICTION COEFFICIENT VERSUS MOMENTUM THICKNESS REYNOLDS NUMBER
($T_w/T_\delta \cong 4$)

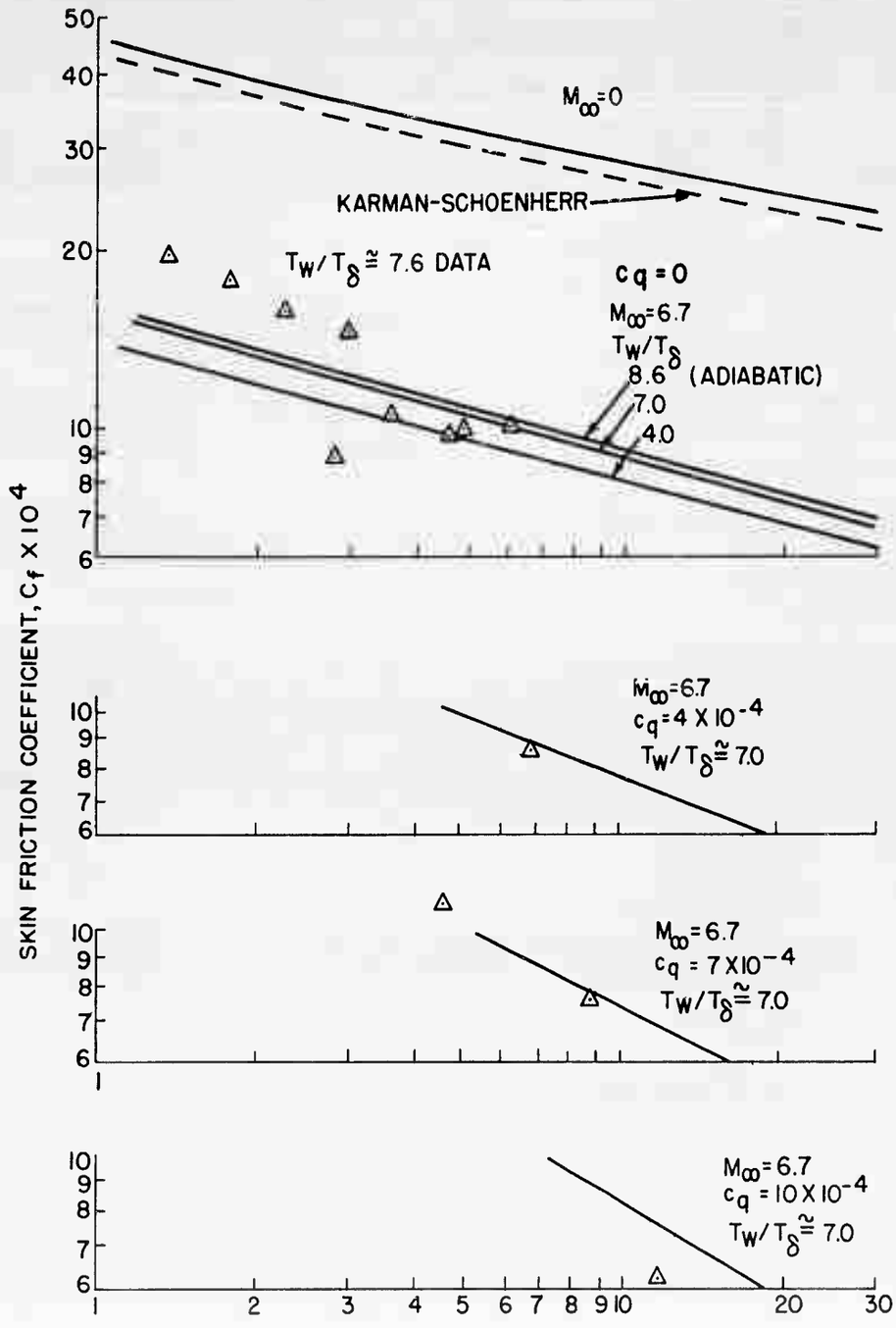

FIG. 46 COMPARISON BETWEEN ANALYSIS AND MEASUREMENT SKIN FRICTION COEFFICIENT VERSUS MOMENTUM THICKNESS REYNOLDS NUMBER ($T_w/T_\delta \cong 7$)

TABLE III SUMMARY OF SKIN FRICTION AND HEAT TRANSFER DATA, T_w/T_δ = 4.1

T_w/T_δ=4.1

X mm	M_δ	P_o atm	$Re_x x10^{-6}$	Re_θ	T_w/T_δ	$C_q x10^4$	$C_f x10^4$	C_f/C_{fo}	$2C_q/C_{fo}$	$St x10^4$	$\frac{St}{St_o}$
					C_q=0	T_w/T_δ=4.48					
377.8	6.60	15.18	3.255	1947	4.475	0	14.58	1.000	0	4.97	1.000
428.6	6.55	15.15	3.533	2374	4.480	0	13.85	1.000	0	4.97	1.000
479.4	6.54	15.15	3.880	2527	4.479	0	14.46	1.000	0	5.27	1.000
530.2	6.49	15.20	4.220	3037	4.490	0	13.36	1.000	0	4.29	1.000
					C_q= $9.09x10^{-4}$	T_w/T_δ= 4.17					
377.8	6.38	15.15	2.925	3206	4.102	9.23	12.53	.859	1.266	4.23	.537
428.6	6.49	15.22	3.446	4028	4.132	9.07	11.45	.827	1.310	4.09	.551
479.4	6.60	15.15	4.160	4698	4.263	8.85	9.60	.664	1.223	3.60	.482
530.2	6.48	15.22	4.261	5288	4.167	9.21	8.39	.628	1.379	3.17	.501
					C_q= $17.0x10^{-4}$	T_w/T_δ= 3.94					
377.8	6.39	15.17	3.249	4919	4.102	16.86	5.36	.368	2.312	2.65	.337
479.4	6.42	15.12	3.950	6081	3.991	16.24	5.37	.371	2.246	2.57	.344
530.2	6.37	15.18	4.264	7511	3.808	17.81	5.17	.387	2.670	1.90	.300
					C_q= $25.0x10^{-4}$	T_w/T_δ= 3.73					
377.8	6.28	15.15	3.185	6517	3.864	24.91	3.50	.240	3.416	1.96	.249
428.6	6.20	15.15	3.619	8156	3.640	24.52	3.07	.222	3.540	1.32	.178
479.4	6.22	15.15	3.945	8450	3.759	24.90	3.36	.232	3.440	1.68	.225
530.2	6.22	15.22	4.298	10166	3.662	25.80	3.40	.254	3.860	1.29	.204
					C_q= 0	T_w/T_δ=4.31 (Repeat Run)					
377.8	6.52	15.15	3.057	1716	4.418	0	14.29	1.000	0	7.87	1.000
428.6	6.32	15.15	3.163	1993	4.171	0	15.30	1.000	0	7.42	1.000
479.4	6.44	15.18	3.679	2347	4.346	0	15.47	1.000	0	7.46	1.000
530.2	6.45	15.15	4.260	3023	4.297	0	12.54	1.000	0	6.33	1.000
					C_q= 0	T_w/T_δ=4.12					
479.2	6.68	20.05	5.356	3296	4.381	0	11.86	1.000	0	6.16	1.000
479.4	6.41	24.95	5.997	3891	4.116	0	9.46	1.000	0	5.30	1.000

TABLE IV SUMMARY OF BOUNDARY LAYER PARAMETERS, T_w/T_δ = 4.1

T_w/T_δ=4.1

X mm	$Re_x \times 10^{-6}$	T_w/T_δ	$C_q \times 10^4$	θ mm	δ^* mm	δ mm	Θ mm	Re_θ	$\frac{\delta^*}{\theta}$
			C_q = 0		T_w/T_δ = 4.48				
377.8	3.255	4.475	0	.226	3.18	5.4	.238	1947	14.07
428.6	3.533	4.480	0	.288	3.66	7.45	.460	2374	12.71
479.4	3.880	4.479	0	.312	4.10	8.0	.464	2527	13.12
530.2	4.220	4.490	0	.382	4.84	9.2	.644	3037	12.67
			$C_q = 9.09 \times 10^{-4}$		T_w/T_δ = 4.17				
377.8	2.925	4.102	9.23	.414	4.82	8.8	.686	3206	11.64
428.6	3.446	4.132	9.07	.501	5.72	10.8	.848	4028	11.42
479.4	4.160	4.263	8.85	.541	6.81	12.0	.753	4698	12.59
530.2	4.231	4.167	9.21	.658	7.86	14.1	1.070	5288	11.94
			$C_q = 17.0 \times 10^{-4}$		T_w/T_δ = 3.94				
377.8	3.249	4.102	16.86	.572	7.68	12.1	.792	4919	13.43
479.4	3.950	3.991	16.24	.738	9.62	15.5	1.070	6081	13.04
530.2	4.264	3.808	17.81	.934	10.70	18.0	1.580	7511	11.46
			$C_q = 25.0 \times 10^{-4}$		T_w/T_δ = 3.73				
377.8	3.185	3.864	24.91	.773	9.96	14.8	1.216	6517	12.88
428.6	3.619	3.640	24.52	.966	11.20	17.3	1.640	8156	11.59
479.4	3.945	3.759	24.90	1.027	12.90	19.7	1.650	8450	12.56
530.2	4.298	3.662	25.80	1.250	14.20	22.7	2.250	10166	11.36
			C_q = 0		T_w/T_δ = 4.31				
377.8	3.057	4.418	0	.212	3.14	5.3	.256	1716	14.81
428.6	3.163	4.171	0	.270	3.64	6.7	.272	1993	13.48
479.4	3.679	4.346	0	.306	4.42	8.1	.316	2349	14.44
530.2	4.260	4.297	0	.376	5.68	10.0	.384	3023	15.11
			C_q = 0		T_w/T_δ = 4.12				
479.4		4.381	0	.295	4.34	7.9	.352	3296	14.71
479.4		4.116	0	.311	4.30	7.9	NC	3891	13.83

TABLE V SUMMARY OF SKIN FRICTION AND HEAT TRANSFER DATA, T_w/T_δ = 5.2

T_w/T_δ=5.2

X mm	M_δ	P_o atm	Re_xx10-6	Re_θ	T_w/T_δ	C_qx10^4	C_fx10^4	C_f/C_{fo}	$2C_q/C_{fo}$	Stx10^4	$\frac{St}{St_o}$
					C_q=0		T_w/T_δ=5.44				
377.8	6.46	15.22	3.028	1619	5.45	0	15.6			6.77	
428.6	6.46	15.25	3.323	1853	5.116	0	11.85	1.000	0	6.42	1.000
479.4	6.62	15.08	4.210	2520	5.722	0	14.74	1.000	0	6.69	1.000
530.2	6.45	15.12	4.285	2667	5.427	0	12.10	1.000	0	5.18	1.000
					$C_q=8.77\text{x}10^{-4}$		T_w/T_δ=5.45				
377.8	6.45	15.01	3.468	2994	5.210	8.944	10.91	.656	1.076	5.45	.754
428.6	6.50	15.15	3.552	3448	5.502	8.932	9.11	.738	1.508	4.66	.726
479.4	6.64	15.08	4.438	4554	5.741	8.432	10.83	.735	1.144	4.26	.637
530.2	6.55	15.05	4.701	5281	5.348	8.756	7.82	.646	1.439	3.97	.765
					$C_q=17.2\text{x}10^{-4}$		T_w/T_δ=5.07				
377.8	6.21	15.22	2.894	4519	4.752	17.57	6.22	.374	2.114	3.19	.441
428.6	6.30	15.15	3.495	5365	4.954	17.14	5.76	.486	2.892	3.28	.511
479.4	6.39	15.20	3.885	6223	5.119	17.45	6.75	.458	2.368	2.68	.401
530.2	6.62	15.05	5.050	8048	5.468	16.46	8.14	.673	2.721	2.58	.498
					$C_q=24.6\text{x}10^{-4}$		T_w/T_δ=4.85				
377.8	6.27	15.08	3.264	6826	4.800	24.42	6.26	.377	2.938	2.26	.312
428.6	6.33	15.12	4.045	8651	4.872	22.96	3.98	.336	3.875	1.85	.288
479.4	6.27	15.15	3.940	8969	4.838	26.47	2.58	.184	3.592	1.98	.276
530.2	6.37	15.12	4.773	10640	4.887	24.44	5.34	.441	4.040	1.88	--
					C_q=0		T_w/T_δ=5.58				
377.8	6.53	15.05	3.141	1713	5.582	0	16.62	1.000	0	7.23	1.000

TABLE VI SUMMARY OF BOUNDARY LAYER PARAMETERS, T_w/T_δ = 5.2

T_w/T_δ=5.2

X mm	$Re_x x10^{-6}$	T_w/T_δ	$C_q x10^{-4}$	θ mm	δ^* mm	δ mm	Θ mm	Re_θ	$\frac{\delta^*}{\theta}$
			C_q = 0		T_w/T_δ = 5.44				
377.8	3.028	5.45	0	.202	3.22	5.65	NC	1619	
428.6	3.323	5.116	0	.239	3.54	6.70	NC	1853	14.81
479.4	4.210	5.722	0	.287	4.77	8.30	.300	2520	16.62
530.2	4.285	5.427	0	.330	5.02	9.15	NC	2667	15.21
			$C_q = 8.77x10^{-4}$		T_w/T_δ = 5.45				
377.8	3.468	5.210	8.944	.370	5.25	9.00	.328	2994	14.19
428.6	3.552	5.502	8.932	.416	5.94	10.70	NC	3448	14.29
479.4	4.438	5.741	8.482	.492	8.04	12.70	.604	4554	16.34
530.2	4.701	5.348	8.756	.596	8.58	14.20	1.016	5281	14.33
			$C_q = 17.2x10^{-4}$		T_w/T_δ = 5.07				
377.8	2.894	4.752	17.570	.590	7.42	12.00	.880	4519	12.58
428.6	3.495	4.954	17.140	.658	8.65	14.20	NC	5365	13.14
479.4	3.885	5.119	17.450	.964	11.06	16.50	1.285	6223	11.47
530.2	5.050	5.468	16.460	.845	12.74	19.4	1.620	8048	15.08
			$C_q = 24.6x10^{-4}$		T_w/T_δ = 4.85				
377.8	3.264	4.800	24.420	.790	11.24	16.50	1.28	6826	14.23
428.6	4.045	4.872	22.960	.917	14.00	21.00	1.39	8651	15.28
479.4	3.940	4.838	26.470	1.090	14.26	19.70	1.86	8969	13.07
530.2	4.773	4.887	24.440	1.182	16.56	24.00	2.14	10640	14.01
			C_q = 0		T_w/T_δ = 5.58				
377.8	3.141	5.582	0	.206	3.47	5.90	.214	1713	16.85

TABLE VII SUMMARY OF SKIN FRICTION AND HEAT TRANSFER DATA, T_w/T_δ = 7.6

T_w/T_δ = 7.6

X mm	M	P_o atm	$Re_x x10^{-6}$	Re_θ	T_w/T_δ	$C_q x10^4$	$C_f x10^4$	C_f/C_{fo}	$2C_q/C_{fo}$	$St x10^4$	$\frac{St}{St_o}$
					C_q = 0		T_w/T_δ = 7.87				
377.8	6.31	15.12	2.840	1323	7.614	0	19.54	1.000	0	28.3	1.000
428.6	6.45	15.05	3.429	1720	7.780	0	17.70	1.000	0	29.4	1.000
479.4	6.61	15.12	4.252	2200	8.080	0	15.74	1.000	0	23.3	1.000
530.2	6.62	15.08	4.803	2844	8.018	0	14.50	1.000	0	20.6	1.000
					$C_q = 8.68x10^{-4}$		T_w/T_δ = 7.65				
377.8 428.6 479.4 530.2	6.51	15.08	4.099	4541	7.650	8.68	11.20	.712	1.103	10.71	.460
					$C_q = 16.2x10^{-4}$		T_w/T_δ = 7.65				
377.8 428.6 479.4 530.2	6.57	15.08	4.514	6365	7.649	16.17	8.41	.534	2.055.	5.18	.222
					$C_q = 24.4x10^{-4}$		T_w/T_δ = 7.26				
377.8 428.6 479.4 530.2	6.49	15.01	4.632	8928	7.259	24.42	6.06	.385	3.103	2.82	.121
					C_q = 0		T_w/T_δ = 7.81				
479.4	6.43	20.01	4.897	2860	7.805	0	14.56	1.000	0	23.08	1.000

TABLE VIII SUMMARY OF BOUNDARY LAYER PARAMETERS, T_w/T_δ = 7.6

T_w/T_δ=7.6

X mm	$Re_x x10^{-6}$	T_w/T_δ	$C_q x10^4$	θ mm	δ^* mm	δ mm	Θ mm	Re_θ	$\frac{\delta^*}{\theta}$
			C_q=0		T_w/T_δ=7.87				
377.8	2.840	7.614	0	.176	3.78	6.2		1323	21.48
428.6	3.429	7.780	0	.215	4.72	7.5		1720	21.95
479.4	4.252	8.080	0	.248	5.56	8.5		2200	22.42
530.2	4.803	8.018	0	.314	6.57	10.2		2844	20.92
			C_q=8.68x10^{-4}		T_w/T_δ=7.65				
377.8 428.6 479.4 530.2	4.099	7.650	8.68	.531	8.45	15.0		4541	15.91
			C_q-16.2x10^{-4}		T_w/T_δ=7.65				
377.8 428.6 479.4 530.2	4.514	7.649	16.17	.676	12.90	17.5		6365	19.08
			C_q=24.4x10^{-4}		T_w/T_δ=7.26				
377.8 428.6 479.4 530.2	4.632	7.259	24.42	.924	17.42	23.0		8928	18.85
			C_q=0		T_w/T_δ=7.81				
479.4	4.897	7.805	0	.280	5.24	8.7		2860	18.71

TABLE IX SUMMARY OF SKIN FRICTION AND HEAT TRANSFER DATA, $T_w/T_\delta = 7.6$

$T_w/T_\delta = 7.6$

x mm	M_δ	p_o atm	$Re_x \times 10^{-6}$	Re_θ	T_w/T_δ	$c_q \times 10^4$	$c_f \times 10^4$	c_f/c_{fo}	$2c_q/c_{fo}$	$St \times 10^4$	$\frac{St}{St_o}$
530.2	6.34	38.07	9.70	4897	7.06	0	9.92	1.000	0	8.3	1.000
530.2	6.46	38.07	10.76	6824	7.19	3.70	8.35	.841	.746	5.83	.702
530.2	6.47	38.07	10.84	8753	7.01	7.25	7.6	.767	1.464	4.49	.541
530.2	6.52	38.07	11.03	11737	6.87	10.13	6.25	.630	2.040	3.64	.439

TABLE X SUMMARY OF BOUNDARY LAYER PARAMETERS, T_w/T_δ = 7.6

T_w/T_δ=7.6

x mm	$Re_x x10^{-6}$	T_w/T_δ	$c_q x10^4$	θ mm	δ^* mm	δ mm		Re_θ	$\frac{\delta^*}{\theta}$
530.2	9.70	7.06	0	.255	4.66	8.0	.150	4897	17.6
530.2	10.76	7.19	3.70	.336	6.26	9.5	.640	6824	16.91
532.0	10.84	7.01	7.25	.428	7.80	11.0	1.36	8753	18.22
530.2	11.03	6.87	10.13	.564	9.80	14.2	2.74	11737	17.38

TABLE XI SUMMARY OF SKIN FRICTION AND HEAT TRANSFER DATA, T_w/T_δ = 4.1

T_w/T_δ=4.1

X mm	M_δ	P_o atm	$Re_x x10^{-6}$	Re_θ	T_w/T_δ	$C_q x10^4$	$C_f x10^4$	C_f/C_{fo}	$2C_q/C_{fo}$	$\delta x10^4$	$\frac{St}{St_o}$
					C_q=0		T_w/T_δ=4.70				
377.8											
428.6	6.50	38.07	8.529	3841	4.665	0	6.26	1.000	0	4.61	1.000
479.4	6.49	38.07	9.260	4557	4.735	0	6.97	1.000	0	4.47	1.000
530.2	6.37	38.01	10.13	5997	4.700	0	6.81	1.000	0	4.00	1.000
					C_q-0		T_w/T_δ=4.32				
530.2	6.34	35.01	8.98	5218	4.32	0	7.73	1.000	0	4.64	1.000
					C_q=4.12x10^{-4}		T_w/T_δ=4.41				
530.2	6.50	35.01	9.57	7816	4.41	4.12	6.41	.83	1.066	2.95	.636
					C_q=8.17x10^{-4}		T_w/T_δ=4.37				
530.2	6.45	35.01	9.41	10011	4.37	8.17	5.30	.686	2.114	2.44	.526
					C_q=12.1x10^{-4}		T_w/T_δ=4.35				
530.2	6.47	35.01	9.89	12775	4.35	12.1	4.23	.547	3.123	2.14	.461

TABLE XII SUMMARY OF BOUNDARY LAYER PARAMETERS, T_w/T_δ = 4.1

T_w/T_δ=4.1

x mm	$Re_x \times 10^{-6}$	T_w/T_δ	$C_q \times 10^{-4}$	θ mm	δ^* mm	δ mm	θ mm	Re_θ	$\frac{\delta^*}{\theta}$
			C_q=0	T_w/T_δ=4.32					
377.8									
428.6	8.529	4.665	0	.193	2.78	5.20	.248	3841	14.40
479.4	9.26	4.735	0	.236	3.51	5.85	.284	4557	14.88
530.2	10.13	4.700	0	.313	4.70	7.70	.408	5997	15.01
			C_q=0	$T_w T_\delta$=4.32					
530.2	8.98	4.32	0	.308	4.63	7.8		5218	15.02
			$C_q=4.12\times10^{-4}$	T_w/T_δ=4.41					
530.2	9.57	4.41	4.12	.433	6.52	10.7		7816	15.06
			$C_q=8.17\times10^{-4}$	T_w/T_δ=4.37					
530.2	9.41	4.37	8.17	.564	7.64			10011	13.55
			$C_q=12.1\times10^{-4}$	T_w/T_δ=4.35					
530.2	9.89	4.35	12.1	.685	9.22	14.8		12775	13.46

TABLE XIII SUMMARY OF SKIN FRICTION AND HEAT TRANSFER DATA, UNPUBLISHED NOL SOLID FLAT PLATE DATA

x mm	M_δ	P_o atm	$Re_x \times 10^{-6}$	Re_θ	T_w/T_δ	$C_q \times 10^4$	$C_f \times 10^4$	θ mm	δ^* mm	δ mm	$\frac{\delta^*}{\theta}$
					$T_w/T_\delta = 5.24$						
305	6.25	35.0	6.84	3000	5.26	0	10.2	.134	1.87	4.32	13.95
381	6.44	35.0	8.54	3317	5.35	0	10.1	.148	2.14	5.46	14.45
457	6.20	35.0	10.3	4418	5.23	0	9.58	.197	2.60	6.05	13.20
534	6.14	35.0	12.0	7250	5.12	0	7.80	.323	4.19	8.82	13.00
					$T_w/T_\delta = 7.22$						
305	6.28	35.0	6.84	2782	7.26	0	8.82	.124	2.15	4.19	17.35
381	6.12	35.0	8.54	3557	7.29	0	10.5	.158	2.51	5.28	15.90
457	6.13	35.0	10.3	4566	7.20	0	9.62	.203	3.18	6.93	15.67
534	6.16	35.0	12.0	5991	7.14	0	10.0	.267	4.14	8.64	15.50

AERODYNAMICS DEPARTMENT
EXTERNAL DISTRIBUTION LIST (A1)

	No. of Copies
Chief, Bureau of Naval Weapons Department of the Navy Washington, D. C. 20360 Attn: DLI-3 Attn: R-14 Attn: RRRE-4 Attn: RMGA-811 Attn: RMMO-42	2
Office of Naval Research T-3 Washington, D. C. Attn: Head, Structural Mechanics Branch Attn: Head, Fluid Dynamics Branch	
Director, David Taylor Model Basin Aerodynamics Laboratory Washington, D. C. Attn: Library	
Commander, U. S. Naval Ordnance Test Station China Lake, California Attn: Technical Library Attn: Code 406	
Director, Naval Research Laboratory Washington, D. C. Attn: Code 2027	
Commanding Officer Office of Naval Research Branch Office Box 39, Navy 100 Fleet Post Office New York, New York	
NASA High Speed Flight Station Box 273 Edwards Air Force Base, California	
NASA Ames Research Center Moffett Field, California Attn: Librarian	

AERODYNAMICS DEPARTMENT
EXTERNAL DISTRIBUTION LIST (A1)

No. of Copies

NASA
Langley Research Center
Langley Station, Hampton, Virginia
Attn: (Mrs.) Elizabeth R. Gilman, Librarian, Bldg. 1244
Attn: C. H. McLellan
Attn: Adolph Busemann
Attn: Comp. Res. Div.
Attn: Theoretical Aerodynamics Division

NASA
Lewis Research Center
21000 Brookpark Road
Cleveland 11, Ohio
Attn: Librarian
Attn: Chief, Propulsion Aerodynamics Division

NASA
600 Independence Ave., S. W.
Washington, D. C.
Attn: Chief, Division of Research Information
Attn: Dr. H. H. Kurzweg, Director of Research

Office of the Assistant Secretary of Defense (R&D)
Room 3E1065, The Pentagon
Washington 25, D. C.
Attn: Technical Library

Research and Development Board
Room 3D1041, The Pentagon
Washington 25, D. C.
Attn: Library

Defense Documentation Center 10
Cameron Station
Alexandria, Virginia 22314

Commander, Pacific Missile Range
Point Mugu, California
Attn: Technical Library

Commanding General
Aberdeen Proving Ground, Maryland
Attn: Technical Information Branch
Attn: Ballistic Research Laboratories

AERODYNAMICS DEPARTMENT
EXTERNAL DISTRIBUTION LIST (A1)

	No. of Copies
Commander, Naval Weapons Laboratory Dahlgren, Virginia Attn: Library	
Director, Special Projects Department of the Navy Washington 25, D. C. Attn: SP-2722	
Director of Intelligence Headquarters, USAF Washington 25, D. C. Attn: AFOIN-3B	
Headquarters - Aero. Systems Division Wright-Patterson Air Force Base Dayton, Ohio Attn: WWAD Attn: RRLA-Library	2
Commander Air Force Ballistic Systems Division Norton Air Force Base San Bernardino, California Attn: BSRVA	2
Chief, Defense Atomic Support Agency Washington 25, D. C. Attn: Document Library	
Headquarters, Arnold Engineering Development Center ARO, Inc. Arnold Air Force Station, Tennessee Attn: Technical Library Attn: AEOR Attn: AEOIM	
Commanding Officer, Harry Diamond Laboratories Washington 25, D. C. Attn: Library, Room 211, Bldg. 92	
Commanding General U. S. Army Missile Command Redstone Arsenal, Alabama Attn: AMSMI-RR (Mr. N. Shapiro) Attn: AMSMI-RB (Redstone Scientific Information Center)	

AERODYNAMICS DEPARTMENT
EXTERNAL DISTRIBUTION LIST (A1)

	No. of Copies
NASA George C. Marshall Space Flight Center Huntsville, Alabama Attn: Dr. E. Geissler Attn: Mr. T. Reed Attn: Mr. H. Paul Attn: Mr. W. Dahm Attn: Mr. H. A. Connel Attn: Mr. J. Kingsbury Attn: ARDAB-DA	
APL/JHU (NOw 7386) 8621 Georgia Avenue Silver Spring, Maryland Attn: Technical Reports Group Attn: Mr. D. Fox Attn: Dr. F. Hill Attn: Dr. L. L. Cronvich	2
Scientific & Technical Information Facility P. O. Box 5700 Bethesda, Maryland Attn: NASA Representative (S-AK/DL)	
Commander Air Force Flight Test Center Edwards Air Force Base Muroc, California Attn: FTOTL	
Air Force Office of Scientific Research Hollomon Air Force Base Alamogordo, New Mexico Attn: SRLTL	
U. S. Army Engineer Research & Development Laboratories Fort Belvoir, Virginia Attn: STINFO Branch	

AERODYNAMICS DEPARTMENT
EXTERNAL DISTRIBUTION LIST (A2)

No. of Copies

University of Minnesota
Minneapolis 14, Minnesota
Attn: Dr. E. R. G. Eckert
Attn: Heat Transfer Laboratory
Attn: Technical Library

Rensselaer Polytechnic Institute
Troy, New York
Attn: Dept. of Aeronautical Engineering

Dr. James P. Hartnett
Department of Mechanical Engineering
University of Delaware
Newark, Delaware

Princeton University
James Forrestal Research Center
Gas Dynamics Laboratory
Princeton, New Jersey
Attn: Prof. S. Bogdonoff
Attn: Dept. of Aeronautical Engineering Library

Defense Research Laboratory
The University of Texas
P. O. Box 8029
Austin 12, Texas
Attn: Assistant Director

Ohio State University
Columbus 10, Ohio
Attn: Security Officer
Attn: Aerodynamics Laboratory
Attn: Dr. J. Lee
Attn: Chairman, Dept. of Aero. Engineering

California Institute of Technology
Pasadena, California
Attn: Guggenheim Aero. Laboratory,
Aeronautics Library
Attn: Jet Propulsion Laboratory
Attn: Dr. H. Liepmann
Attn: Dr. L. Lees
Attn: Dr. D. Coles
Attn: Dr. A. Roshko
Attn: Dr. J. Laufer

Case Institute of Technology
Cleveland 6, Ohio
Attn: G. Kuerti

AERODYNAMICS DEPARTMENT
EXTERNAL DISTRIBUTION LIST (A2)

No. of Copies

North American Aviation, Inc.
Aerophysics Laboratory
Downey, California
Attn: Chief, Aerophysics Laboratory
Attn: Missile Division (Library)

Department of Mechanical Engineering
Yale University
400 Temple Street
New Haven, Connecticut
Attn: Dr. P. P. Wegener

MIT Lincoln Laboratory
Lexington, Massachusetts

RAND Corporation
1700 Main Street
Santa Monica, California
Attn: Library, USAF Project RAND
Attn: Technical Communications

Mr. J. Lukasiewicz, Chief
Gas Dynamics Facility
ARO, Incorporated
Tullahoma, Tennessee

Massachusetts Institute of Technology
Cambridge 39, Massachusetts
Attn: Prof. J. Kaye
Attn: Prof. M. Finston
Attn: Mr. J. Baron
Attn: Prof. A. H. Shapiro
Attn: Naval Supersonic Laboratory
Attn: Aero. Engineering Library
Attn: Prof. Ronald F. Probstein
Attn: Prof. C. C. Lin

Polytechnic Institute of Brooklyn
527 Atlantic Avenue
Freeport, New York
Attn: Dr. M. Bloom
Attn: Aerodynamics Laboratory

Brown University
Division of Engineering
Providence, Rhode Island
Attn: Librarian

AERODYNAMICS DEPARTMENT
EXTERNAL DISTRIBUTION LIST (A2)

No. of Copies

Air Ballistics Laboratory
Army Ballistic Missile Agency
Huntsville, Alabama

Applied Mechanics Reviews
Southwest Research Institute
8500 Culebra Road
San Antonio, Texas

BUWEPS Representative
Aerojet-General Corporation
6352 N. Irwindale Avenue
Azusa, California

The Boeing Company
Seattle, Washington
Attn: J. H. Russell, Aero-Space Division
Attn: Research Library

United Aircraft Corporation
400 Main Street
East Hartford 8, Connecticut
Attn: Chief Librarian
Attn: Mr. W. Kuhrt, Research Department
Attn: Mr. J. G. Lee 2

Hughes Aircraft Company
Florence Avenue at Teale Streets
Culver City, California
Attn: Mr. D. J. Johnson
R&D Technical Library

McDonnell Aircraft Corporation
P. O. Box 516
St. Louis 3, Missouri

Lockheed Missiles and Space Company
P. O. Box 504
Sunnyvale, California
Attn: Dr. L. H. Wilson
Attn: Mr. M. Tucker
Attn: Dr. R. Smelt

Martin Company
Baltimore, Maryland
Attn: Library
Attn: Chief Aerodynamicist
Attn: Dr. W. Morkovin, Aerophysics Division

AERODYNAMICS DEPARTMENT
EXTERNAL DISTRIBUTION LIST (A2)

	No. of Copies
CONVAIR A Division of General Dynamics Corporation Fort Worth, Texas Attn: Library Attn: Theoretical Aerodynamics Group	
Purdue University School of Aeronautical & Engineering Sciences LaFayette, Indiana Attn: R. L. Taggart, Library	
University of Maryland College Park, Maryland Attn: Director Attn: Dr. J. Burgers Attn: Librarian, Engr. & Physical Sciences Attn: Librarian, Institute for Fluid Dynamics and Applied Mathematics Attn: Prof. S. I. Pai	2
University of Michigan Ann Arbor, Michigan Attn: Dr. A. Kuethe Attn: Dr. A. Laporte Attn: Department of Aeronautical Engineering	
Stanford University Palo Alto, California Attn: Applied Mathematics & Statistics Lab. Attn: Prof. D. Bershader, Dept. of Aero. Engr.	
Cornell University Graduate School of Aeronautical Engineering Ithaca, New York Attn: Prof. W. R. Sears	
The Johns Hopkins University Charles and 34th Streets Baltimore, Maryland Attn: Dr. F. H. Clauser	
University of California Berkeley 4, California Attn: G. Maslach Attn: Dr. S. A. Schaaf Attn: Dr. Holt Attn: Institute of Engineering Research	

AERODYNAMICS DEPARTMENT
EXTERNAL DISTRIBUTION LIST (A2)

No. of Copies

Cornell Aeronautical Laboratory, Inc.
4455 Genesee Street
Buffalo 21, New York
Attn: Librarian
Attn: Dr. Franklin Moore
Attn: Dr. J. G. Hall
Attn: Mr. A. Hertzberg

University of Minnesota
Rosemount Research Laboratories
Rosemount, Minnesota
Attn: Technical Library

Director, Air University Library
Maxwell Air Force Base, Alabama

Douglas Aircraft Company, Inc.
Santa Monica Division
3000 Ocean Park Boulevard
Santa Monica, California
Attn: Chief Missiles Engineer
Attn: Aerodynamics Section

CONVAIR
A Division of General Dynamics Corporation
Daingerfield, Texas

CONVAIR
Scientific Research Laboratory
5001 Kearney Villa Road
San Diego, California
Attn: Asst. to the Director of Scientific Research
Attn: Dr. B. M. Leadon
Attn: Library

Republic Aviation Corporation
Farmingdale, New York
Attn: Technical Library

General Applied Science Laboratories, Inc.
Merrick and Stewart Avenues
Westbury, L. I., New York
Attn: Mr. Walter Daskin
Attn: Mr. R. W. Byrne

AERODYNAMICS DEPARTMENT
EXTERNAL DISTRIBUTION LIST (A2)

	No. of Copies
Arnold Research Organization, Inc. Tullahoma, Tennessee Attn: Technical Library Attn: Chief, Propulsion Wind Tunnel Attn: Dr. J. L. Potter	
General Electric Company Missile Space Division 3198 Chestnut Street Philadelphia, Pennsylvania Attn: Larry Chasen, Mgr. Library Attn: Mr. R. Kirby Attn: Dr. J. Farber Attn: Dr. G. Sutton Attn: Dr. J. D. Stewart Attn: Dr. S. M. Scala Attn: Dr. H. Lew Attn: Mr. J. Persh	2
Eastman Kodak Company Navy Ordnance Division 50 West Main Street Rochester 14, New York Attn: W. B. Forman	2
Library AVCO-Everett Research Laboratory 2385 Revere Beach Parkway Everett 49, Massachusetts	3
Chance-Vought Corp. Post Office Box 5907 Dallas, Texas Library 1-6310/3L-2884	
National Science Foundation 1951 Constitution Avenue, N. W. Washington 25, D. C. Attn: Engineering Sciences Division	
New York University University Heights New York 53, New York Attn: Department of Aeronautical Engineering	

AERODYNAMICS LABORATORY
EXTERNAL DISTRIBUTION LIST (A2)

No. of Copies

New York University
25 Waverly Place
New York, New York
Attn: Library, Institute of Math. Sciences

NORAIR
A Division of Northrop Corporation
Hawthorne, California
Attn: Library

Northrop Aircraft, Inc.
Hawthorne, California
Attn: Library

Gas Dynamics Laboratory
Technological Institute
Northwestern University
Evanston, Illinois
Attn: Library

Pennsylvania State University
University Park, Pennsylvania
Attn: Library, Dept. of Aero. Engineering

The Ramo-Wooldridge Corporation
8820 Bellanca Avenue
Los Angeles 45, California

Gifts and Exchanges
Fondren Library
Rice Institute
P. O. Box 1892
Houston, Texas

University of Southern California
Engineering Center
Los Angeles 7, California
Attn: Librarian

The Editor
Battelle Technical Review
Battelle Memorial Institute
505 King Avenue
Columbus, Ohio

Douglas Aircraft Company, Inc.
Long Beach, California
Attn: Library

AERODYNAMICS DEPARTMENT
EXTERNAL DISTRIBUTION LIST (A2)

No. of Copies

FluiDyne Engineering Corporation
5740 Wayzata Boulevard
Golden Valley
Minneapolis, Minnesota

Grumman Aircraft Engineering Corporation
Bethpage, Long Island, New York

Lockheed Missiles and Space Company
P. O. Box 551
Burbank, California
Attn: Library

Marquardt Aircraft Corporation
7801 Havenhurst
Van Nuys, California

Martin Company
Denver, Colorado

Martin Company
Orlando, Florida
Attn: J. Mayer

Mississippi State College
Engineering and Industrial Research Station
Aerophysics Department
P. O. Box 248
State College, Mississippi

Lockheed Missiles and Space Company
3251 Hanover Street
Palo Alto, California
Attn: Library

General Electric Company
Research Laboratory
Schenectady, New York
Attn: Dr. H. T. Nagamatsu
Attn: Library

Fluid Dynamics Laboratory
Mechanical Engineering Department
Stevens Institute of Technology
Hoboken, New Jersey
Attn: Dr. R. H. Page, Director

AERODYNAMICS DEPARTMENT
EXTERNAL DISTRIBUTION LIST (A2)

No. of Copies

Department of Mechanical Engineering
University of Arizona
Tucson, Arizona
Attn: Dr. E. K. Parks

Vitro Laboratories
200 Pleasant Valley Way
West Orange, New Jersey

Department of Aeronautical Engineering
University of Washington
Seattle, Washington
Attn: Prof. R. E. Street
Attn: Library

American Institute of Aeronautics & Astronautics
1290 Avenue of the Americas
New York, New York
Attn: Managing Editor
Attn: Library

Department of Aeronautics
United States Air Force Academy
Colorado

MHD Research, Inc.
Newport Beach, California
Attn: Technical Director

University of Alabama
College of Engineering
University, Alabama
Attn: Head, Dept. of Aeronautical Engineering

ARDE Associates
100 W. Century Road
Paramus, New Jersey
Attn: Mr. Edward Cooperman

Aeronautical Research Associates of Princeton
50 Washington Road
Princeton, New Jersey
Attn: Dr. C. duP. Donaldson, President

AERODYNAMICS DEPARTMENT
EXTERNAL DISTRIBUTION LIST (A2)

No. of Copies

Daniel Guggenheim School of Aeronautics
Georgia Institute of Technology
Atlanta, Georgia
Attn: Prof. A. L. Ducoffe

University of Cincinnati
Cincinnati, Ohio
Attn: Prof. R. P. Harrington, Head
Dept. of Aeronautical Engineering
Attn: Prof. Ting Yi Li, Aerospace Engineering Dept.

Virginia Polytechnic Institute
Dept. of Aerospace Engineering
Blacksburg, Virginia
Attn: Dr. R. T. Keefe
Attn: Dr. J. B. Eades, Jr.
Attn: Library

IBM Federal System Division
7220 Wisconsin Avenue
Bethesda, Maryland
Attn: Dr. I. Korobkin

Superintendent
U. S. Naval Postgraduate School
Monterey, California
Attn: Technical Reports Section Library

National Bureau of Standards
Washington 25, D. C.
Attn: Chief, Fluid Mechanics Section

North Carolina State College
Raleigh, North Carolina
Attn: Division of Engineering Research
Technical Library

Defense Research Corporation
P. O. Box No. 3587
Santa Barbara, California
Attn: Dr. J. A. Laurmann

Aerojet-General Corporation
6352 North Irwindale Avenue
Box 296
Azusa, California

AERODYNAMICS DEPARTMENT
EXTERNAL DISTRIBUTION LIST (A2)

No. of Copies

Apollo - DDCS
General Electric Company
A&E Building, Room 204
Daytona Beach, Florida
Attn: Dave Hovis

University of Minnesota
Institute of Technology
Minneapolis, Minnesota
Attn: Prof. J. D. Akerman

Guggenheim Laboratory
Stanford University
Stanford, California
Attn: Prof. D. Bershader, Department of Aero. Engineering

Space Technology Laboratory, Inc.
1 Space Park
Redondo Beach, California 90200
Attn: STL Tech. Lib. Doc. Acquisitions

University of Illinois
Department of Aeronautical and Astronautical Engineering
Urbana, Illinois
Attn: Prof. H. S. Stilwell

Armour Research Foundation
Illinois Institute of Technology
10 West 35th Street
Chicago, Illinois
Attn: Dr. L. N. Wilson

Institute of the Aeronautical Sciences
Pacific Aeronautical Library
7600 Beverly Boulevard
Los Angeles, California

University of California
Department of Mathematics
Los Angeles, California
Attn: Prof. A. Robinson

Louisiana State University
Department of Aeronautical Engineering
College of Engineering
Baton Rouge, Louisiana

AERODYNAMICS DEPARTMENT
EXTERNAL DISTRIBUTION LIST (A2)

No. of Copies

Mathematical Reviews
American Mathematical Society
80 Waterman Street
Providence, Rhode Island

Stanford University
Department of Aeronautical Engineering
Stanford, California
Attn: Library

University of California
Aeronautical Sciences Laboratory
Richmond Field Station
1301 South 46th Street
Richmond, California

University of Denver
Department of Aeronautical Engineering
Denver 10, Colorado

University of Chicago
Laboratories for Applied Sciences
Museum of Science and Industry
Chicago, Illinois
Attn: Librarian

University of Colorado
Department of Aeronautical Engineering
Boulder, Colorado

University of Illinois
Aeronautical Department
Champaign, Illinois

University of Kentucky
Department of Aeronautical Engineering
College of Engineering
Lexington, Kentucky

University of Toledo
Department of Aeronautical Engineering
Research Foundation
Toledo, Ohio

AERODYNAMICS DEPARTMENT
EXTERNAL DISTRIBUTION LIST (A2)

No. of Copies

Aerospace Corporation
P. O. Box 95085
Los Angeles, California
Attn: Advanced Propulsion & Fluid Mechanics Department
Attn: Gas Dynamics Department

Boeing Scientific Research Laboratory
P. O. Box 3981
Seattle, Washington
Attn: Dr. A. K. Sreekanth
Attn: G. J. Appenheimer

Vidya, Inc.
2626 Hanover
Palo Alto, California
Attn: Mr. J. R. Stalder
Attn: Library

General Electric Company
FPD Technical Information Center F-22
Cincinnati, Ohio

Northwestern University
Technological Institute
Evanston, Illinois
Attn: Department of Mechanical Engineering

Harvard University
Cambridge, Massachusetts
Attn: Prof. of Engineering Sciences & Applied Physics
Attn: Library

University of Wisconsin
P. O. Box 2127
Madison, Wisconsin
Attn: Prof. J. O. Hirschfelder

Dr. Antonio Ferri, Director
Guggenheim Aerospace Laboratories
New York University
181st St. and University Ave.
Bronx, New York

Cornell University
Graduate School of Aeronautical Engineering
Ithaca, New York
Attn: Dr. Shan-Fu Shen

AERODYNAMICS DEPARTMENT
EXTERNAL DISTRIBUTION LIST (A2)

No. of
Copies

Department of Aerospace & Mechanical
Engineering Sciences
University of California-San Diego
La Jolla, California 92037
Attn: Dr. P. A. Libby

University of New Mexico
Albuquerque, New Mexico
Attn: Dr. Theodore Sparks

Notre Dame University
Southbend, Indiana
Attn: Dr. John D. Nicolaides
Department of Aerospace Engineering

Security Classification

DOCUMENT CONTROL DATA - R&D

(Security classification of title, body of abstract and indexing annotation must be entered when the overall report is classified)

1. ORIGINATING ACTIVITY (Corporate author) U. S. Naval Ordnance Laboratory	2a. REPORT SECURITY CLASSIFICATION U 2b. GROUP

3. REPORT TITLE: Characteristics of the Turbulent Boundary Layer with Heat and Mass Transfer at M=6.7

4. DESCRIPTIVE NOTES (Type of report and inclusive dates)
Final

5. AUTHOR(S) (Last name, first name, initial)
Danberg, James E.

6. REPORT DATE 19 October 1964	7a. TOTAL NO. OF PAGES 113	7b. NO. OF REFS 65
8a. CONTRACT OR GRANT NO. RMGA-42-034/212-1/F009-10-001 b. PROJECT NO. c. d.	9a. ORIGINATOR'S REPORT NUMBER(S) NOLTR 64-99 9b. OTHER REPORT NO(S) (Any other numbers that may be assigned this report) ----------	

10. AVAILABILITY/LIMITATION NOTICES: (1) "Qualified requesters may obtain copies of this report from DDC."

11. SUPPLEMENTARY NOTES	12. SPONSORING MILITARY ACTIVITY Bureau of Naval Weapons

13. ABSTRACT: Transpiration from a porous surface into a turbulent boundary layer is a possible technique for protecting aerodynamic surfaces from the severe heating rates associated with hypersonic speeds. The effects of air transpiration and wall temperature on skin friction drag, heat transfer, and other pertinent boundary layer characteristics were determined from measurements on a porous flat plate in the U. S. Naval Ordnance Laboratory's Hypersonic Wind Tunnel No. 4 at a Mach number of 6.7.

The effects of heat and mass transfer on the distribution of Mach number, static and total temperature, and velocity were measured, from which various boundary layer parameters were determined such as: skin friction coefficient; Stanton number; total, momentum, displacement, and energy boundary layer thicknesses. Lowering the wall temperature decreased the total and displacement thicknesses and increased the momentum and energy thicknesses. All the boundary layer thicknesses increased approximately linearly with increasing injection rate.

Velocity distributions are adequately described by a Prandtl mixing length analysis in which the velocity profile is transformed into a form similar to the semi-logarithmic profile of incompressible flow. Unlike incompressible flow, the constant of integration of the mixing length velocity profile is found to increase with heat transfer rate and decrease with increasing mass transfer rate. These effects are related to changes in the laminar sublayer thicknesses.

DD FORM 1 JAN 64 1473

Security Classification

Security Classification

14. KEY WORDS	LINK A		LINK B		LINK C	
	ROLE	WT	ROLE	WT	ROLE	WT
Turbulent **Boundary Layer** **Heat and Mass Transfer** **Supersonic**						

INSTRUCTIONS

1. ORIGINATING ACTIVITY: Enter the name and address of the contractor, subcontractor, grantee, Department of Defense activity or other organization *(corporate author)* issuing the report.

2*a*. REPORT SECURITY CLASSIFICATION: Enter the overall security classification of the report. Indicate whether "Restricted Data" is included. Marking is to be in accordance with appropriate security regulations.

2*b*. GROUP: Automatic downgrading is specified in DoD Directive 5200.10 and Armed Forces Industrial Manual. Enter the group number. Also, when applicable, show that optional markings have been used for Group 3 and Group 4 as authorized.

3. REPORT TITLE: Enter the complete report title in all capital letters. Titles in all cases should be unclassified. If a meaningful title cannot be selected without classification, show title classification in all capitals in parenthesis immediately following the title.

4. DESCRIPTIVE NOTES: If appropriate, enter the type of report, e.g., interim, progress, summary, annual, or final. Give the inclusive dates when a specific reporting period is covered.

5. AUTHOR(S): Enter the name(s) of author(s) as shown on or in the report. Enter last name, first name, middle initial. If military, show rank and branch of service. The name of the principal author is an absolute minimum requirement.

6. REPORT DATE: Enter the date of the report as day, month, year; or month, year. If more than one date appears on the report, use date of publication.

7*a*. TOTAL NUMBER OF PAGES: The total page count should follow normal pagination procedures, i.e., enter the number of pages containing information.

7*b*. NUMBER OF REFERENCES: Enter the total number of references cited in the report.

8*a*. CONTRACT OR GRANT NUMBER: If appropriate, enter the applicable number of the contract or grant under which the report was written.

8*b*, 8*c*, & 8*d*. PROJECT NUMBER: Enter the appropriate military department identification, such as project number, subproject number, system numbers, task number, etc.

9*a*. ORIGINATOR'S REPORT NUMBER(S): Enter the official report number by which the document will be identified and controlled by the originating activity. This number must be unique to this report.

9*b*. OTHER REPORT NUMBER(S): If the report has been assigned any other report numbers *(either by the originator or by the sponsor)*, also enter this number(s).

10. AVAILABILITY/LIMITATION NOTICES: Enter any limitations on further dissemination of the report, other than those imposed by security classification, using standard statements such as:

(1) "Qualified requesters may obtain copies of this report from DDC."

(2) "Foreign announcement and dissemination of this report by DDC is not authorized."

(3) "U. S. Government agencies may obtain copies of this report directly from DDC. Other qualified DDC users shall request through _____."

(4) "U. S. military agencies may obtain copies of this report directly from DDC. Other qualified users shall request through _____."

(5) "All distribution of this report is controlled. Qualified DDC users shall request through _____."

If the report has been furnished to the Office of Technical Services, Department of Commerce, for sale to the public, indicate this fact and enter the price, if known.

11. SUPPLEMENTARY NOTES: Use for additional explanatory notes.

12. SPONSORING MILITARY ACTIVITY: Enter the name of the departmental project office or laboratory sponsoring *(paying for)* the research and development. Include address.

13. ABSTRACT: Enter an abstract giving a brief and factual summary of the document indicative of the report, even though it may also appear elsewhere in the body of the technical report. If additional space is required, a continuation sheet shall be attached.

It is highly desirable that the abstract of classified reports be unclassified. Each paragraph of the abstract shall end with an indication of the military security classification of the information in the paragraph, represented as *(TS)*, *(S)*, *(C)*, or *(U)*.

There is no limitation on the length of the abstract. However, the suggested length is from 150 to 225 words.

14. KEY WORDS: Key words are technically meaningful terms or short phrases that characterize a report and may be used as index entries for cataloging the report. Key words must be selected so that no security classification is required. Identifiers, such as equipment model designation, trade name, military project code name, geographic location, may be used as key words but will be followed by an indication of technical context. The assignment of links, roles, and weights is optional.

Security Classification

Naval Ordnance Laboratory, White Oak, Md.
(NOL technical report 64-99)
CHARACTERISTICS OF THE TURBULENT BOUNDARY LAYER WITH HEAT AND MASS TRANSFER AT M=6.7, by James E. Danberg. 19 Oct. 1964. 98p. illus., charts (Aerodynamics research report 228) BuWeps task RMGA-42-034/212-1/F009-10-001.

UNCLASSIFIED

Effects of air transpiration and wall temperature on turbulent boundary layer characteristics were measured on a porous flat plate at M=6.7. The velocity profile is described by a mixing length analysis, the velocity being in a form similar to the incompressible semi-logarithmic law. From this equation, the skin friction was calculated and found to agree with measurements. Heat transfer can be evaluated from Reynolds analogy, experimentally verified with and without air transpiration.

1. Boundary layer - Heat transfer
2. Boundary layer, Turbulent
3. Aerodynamics
I. Title
II. Danberg, James E.
III. Series
IV. Project

Abstract card is unclassified.

Naval Ordnance Laboratory, White Oak, Md.
(NOL technical report 64-99)
CHARACTERISTICS OF THE TURBULENT BOUNDARY LAYER WITH HEAT AND MASS TRANSFER AT M=6.7, by James E. Danberg. 19 Oct. 1964. 98p. illus., charts (Aerodynamics research report 228) BuWeps task RMGA-42-034/212-1/F009-10-001.

UNCLASSIFIED

Effects of air transpiration and wall temperature on turbulent boundary layer characteristics were measured on a porous flat plate at M=6.7. The velocity profile is described by a mixing length analysis, the velocity being in a form similar to the incompressible semi-logarithmic law. From this equation, the skin friction was calculated and found to agree with measurements. Heat transfer can be evaluated from Reynolds analogy, experimentally verified with and without air transpiration.

1. Boundary layer - Heat transfer
2. Boundary layer, Turbulent
3. Aerodynamics
I. Title
II. Danberg, James E.
III. Series
IV. Project

Abstract card is unclassified.

Naval Ordnance Laboratory, White Oak, Md.
(NOL technical report 64-99)
CHARACTERISTICS OF THE TURBULENT BOUNDARY LAYER WITH HEAT AND MASS TRANSFER AT M=6.7, by James E. Danberg. 19 Oct. 1964. 98p. illus., charts (Aerodynamics research report 228) BuWeps task RMGA-42-034/212-1/F009-10-001.

UNCLASSIFIED

Effects of air transpiration and wall temperature on turbulent boundary layer characteristics were measured on a porous flat plate at M=6.7. The velocity profile is described by a mixing length analysis, the velocity being in a form similar to the incompressible semi-logarithmic law. From this equation, the skin friction was calculated and found to agree with measurements. Heat transfer can be evaluated from Reynolds analogy, experimentally verified with and without air transpiration.

1. Boundary layer - Heat transfer
2. Boundary layer, Turbulent
3. Aerodynamics
I. Title
II. Danberg, James E.
III. Series
IV. Project

Abstract card is unclassified.

Naval Ordnance Laboratory, White Oak, Md.
(NOL technical report 64-99)
CHARACTERISTICS OF THE TURBULENT BOUNDARY LAYER WITH HEAT AND MASS TRANSFER AT M=6.7, by James E. Danberg. 19 Oct. 1964. 98p. illus., charts (Aerodynamics research report 228) BuWeps task RMGA-42-034/212-1/F009-10-001.

UNCLASSIFIED

Effects of air transpiration and wall temperature on turbulent boundary layer characteristics were measured on a porous flat plate at M=6.7. The velocity profile is described by a mixing length analysis, the velocity being in a form similar to the incompressible semi-logarithmic law. From this equation, the skin friction was calculated and found to agree with measurements. Heat transfer can be evaluated from Reynolds analogy, experimentally verified with and without air transpiration.

1. Boundary layer - Heat transfer
2. Boundary layer, Turbulent
3. Aerodynamics
I. Title
II. Danberg, James E.
III. Series
IV. Project

Abstract card is unclassified.

Naval Ordnance Laboratory, White Oak, Md.
(NOL technical report 64-99)
CHARACTERISTICS OF THE TURBULENT BOUNDARY LAYER WITH HEAT AND MASS TRANSFER AT M=6.7, by James E. Danberg. 19 Oct. 1964. 98p. illus., charts (Aerodynamics research report 228) BuWeps task RMGA-42-034/212-1/F009-10-001.

UNCLASSIFIED

Effects of air transpiration and wall temperature on turbulent boundary layer characteristics were measured on a porous flat plate at M=6.7. The velocity profile is described by a mixing length analysis, the velocity being in a form similar to the incompressible semi-logarithmic law. From this equation, the skin friction was calculated and found to agree with measurements. Heat transfer can be evaluated from Reynolds analogy, experimentally verified with and without air transpiration.

1. Boundary layer - Heat transfer
2. Boundary layer, Turbulent
3. Aerodynamics
I. Title
II. Danberg, James E.
III. Series
IV. Project

Abstract card is unclassified.

Naval Ordnance Laboratory, White Oak, Md.
(NOL technical report 64-99)
CHARACTERISTICS OF THE TURBULENT BOUNDARY LAYER WITH HEAT AND MASS TRANSFER AT M=6.7, by James E. Danberg. 19 Oct. 1964. 98p. illus., charts (Aerodynamics research report 228) BuWeps task RMGA-42-034/212-1/F009-10-001.

UNCLASSIFIED

Effects of air transpiration and wall temperature on turbulent boundary layer characteristics were measured on a porous flat plate at M=6.7. The velocity profile is described by a mixing length analysis, the velocity being in a form similar to the incompressible semi-logarithmic law. From this equation, the skin friction was calculated and found to agree with measurements. Heat transfer can be evaluated from Reynolds analogy, experimentally verified with and without air transpiration.

1. Boundary layer - Heat transfer
2. Boundary layer, Turbulent
3. Aerodynamics
I. Title
II. Danberg, James E.
III. Series
IV. Project

Abstract card is unclassified.

Naval Ordnance Laboratory, White Oak, Md.
(NOL technical report 64-99)
CHARACTERISTICS OF THE TURBULENT BOUNDARY LAYER WITH HEAT AND MASS TRANSFER AT M=6.7, by James E. Danberg. 19 Oct. 1964. 98p. illus., charts (Aerodynamics research report 228) BuWeps task RMGA-42-034/212-1/F009-10-001.

UNCLASSIFIED

Effects of air transpiration and wall temperature on turbulent boundary layer characteristics were measured on a porous flat plate at M=6.7. The velocity profile is described by a mixing length analysis, the velocity being in a form similar to the incompressible semi-logarithmic law. From this equation, the skin friction was calculated and found to agree with measurements. Heat transfer can be evaluated from Reynolds analogy, experimentally verified with and without air transpiration.

1. Boundary layer - Heat transfer
2. Boundary layer, Turbulent
3. Aerodynamics
I. Title
II. Danberg, James E.
III. Series
IV. Project

Abstract card is unclassified.

Naval Ordnance Laboratory, White Oak, Md.
(NOL technical report 64-99)
CHARACTERISTICS OF THE TURBULENT BOUNDARY LAYER WITH HEAT AND MASS TRANSFER AT M=6.7, by James E. Danberg. 19 Oct. 1964. 98p. illus., charts (Aerodynamics research report 228) BuWeps task RMGA-42-034/212-1/F009-10-001.

UNCLASSIFIED

Effects of air transpiration and wall temperature on turbulent boundary layer characteristics were measured on a porous flat plate at M=6.7. The velocity profile is described by a mixing length analysis, the velocity being in a form similar to the incompressible semi-logarithmic law. From this equation, the skin friction was calculated and found to agree with measurements. Heat transfer can be evaluated from Reynolds analogy, experimentally verified with and without air transpiration.

1. Boundary layer - Heat transfer
2. Boundary layer, Turbulent
3. Aerodynamics
I. Title
II. Danberg, James E.
III. Series
IV. Project

Abstract card is unclassified.

UNCLASSIFIED